Reply to reviewer #1:

We thank the reviewer for his positive evaluation of the submitted manuscript.

Reply to reviewer #3:

General reply:

We thank the reviewer for reading the manuscript and his/her constructive comments on the content and structure of the manuscript. The other reviewer rated the manuscript as publish as is. This spread in the assessment seems to underline that the manuscript investigates an interesting and controversial topic and derives substantial conclusions.

The authors have the impression that one of the major concerns raised by the reviewer about the novelty of the submitted manuscript are related to a misunderstanding of the work published previously in McCormack et al., 2017, who presented a first analysis of the mean winds focusing only on **boreal winter** dynamics around the SSW 2009/2010 and 2012/13. In this manuscript we present the first cross-comparison of mean winds with NAVGEM-HA and ground based meteor radars as well as a lidar using a full season, which presents a novelty in this respect. Further, the applied wave decomposition with a recently developed technique that is termed ASF throughout the manuscript, impacts the seasonal analysis with respect to each wave component compared to spectral analysis such like FFT or wavelet analysis, which typically use much longer windows to filter for atmospheric waves.

A major aim of this manuscript is also the focus on the phase variability of tides on seasonal and interday time scales and its relation to atmospheric dynamics. We also introduce a holographic analysis to account for the tidal phase variations, which was not yet included in the S-transform analysis shown in McCormack et al., 2017. Although some of the data was already published in McCormack et al., 2017, we present more details and new aspects of the NAVGEM-HA data set.

As a benchmark of the ASF and holographic analysis, together with the global fields from NAVGEM-HA we investigate in detail the postulated lunar tide enhancement due to the Pekeris resonance effect. Our analysis presents entirely new aspects on such data sets can be analyzed, which is a key aspect to study such intermittent and transient effects as the Pekeris resonance.

General comments:
The present manuscript compared the MLT winds obtained from meteor radar measurements at three mid-to-high latitude stations and those from NAVGEM-HA for the daily-mean, semidiurnal tides and their day-to-day variability during the SSW. It is shown that the NAVGEM-HA reproduces the observed winds reasonably well.

A major concern is that the novelty is not clear. Especially, the same type of comparison has been already made extensively by McCormack et al. (2017) including semidiurnal tides and their variability during SSW (the same cases) with the same datasets. Another major concern is that the manuscript is not well organized and sounds quite redundant for me. I sometimes get lost about what the authors are trying to suggest.

A small novelty of this study may be applying APF technique. And if so, I might recommend that the manuscript just focus on a subject of the day-to-day variability during SSW, although I do not find the relevant discussion (Sec. 5) written straightforward. For the discussion of Pekeris resonance, the authors resort on the results of Forbes and Zhang (2012); but it should be noted that the resonance period depends on the circulation pattern for each SSW and I would suspect that FZ2012 results cannot be applied so simply.

For the above reasons, I am afraid I feel this manuscript needs substantial revisions before the publication may be considered. Please see below for specific comments.

Major comments:

Comment:
1. I could not find what is a new finding for this study. McCormack et al. (2017) already made a comparison for the MLT winds between meteor radar measurements and NAVGEM-HA. They discussed the seasonality and day-to-day variability (during SSW) of semidiurnal tides. The present manuscript seems to emphasize a priority of ASF technique, but I do NOT think this technique is necessary at least for the analysis of seasonality (the variation with a relatively long time scale). In this context, I would barely guess that the discussion in Sec. 5.4 seems scientifically interesting; if so I might recommend the manuscript just concentrate on this subject, substantially reducing the rest part.

Reply:

McCormack et al., 2017 showed initial results of two **boreal winter seasons** of NAVGEM-HA and compare these three months with worldwide distributed meteor radars. The seasonality **was not included or discussed** given that there was no NAVGEM-HA data for a full year available at the time. Here we present the first time a seasonal cross-comparison of NAVGEM-HA and ground-based observations. However, for the sake of completeness the seasonal comparison also includes NAVGEM-HA outputs that was presented in McCormack et al., 2017. Further, the submitted manuscript emphasis the phase variability of tides and different tidal modes, which was not covered previously.

Comment:
2. Partly because of the issue #1, the manuscript is not well organized. Particularly I think Section 5 should only focus on scientific discussions about the results shown in Section 4. Sec. 5.1 should be briefly merged into Sec. 3 and Section 5.2 be into Sec. 2.3, because they are all related to the data quality and analysis methods. Section 5.3 can be entirely removed, because the description here is like an Introduction of tides and a brief summary of results, not providing any detailed scientific discussions.

Reply:

As suggested by the reviewer we restructured parts of the discussions as suggested. Thus, we removed some redundant paragraphs from the discussion or merged them with section 2 and 3. All paragraphs discussing the data quality and analysis are moved to the suggested sections. Repetitions were removed. The discussion of the mean winds and tide seasonal climatology is now more focused. We have to mention that most GCMs, although nudged to reanalysis, do not reproduce the seasonal wind pattern at the MLT nor do some models show the correct signs in the zonal mean winds compared to the observations presented here in. From linear theory, it is well-known that a biased mean zonal wind affects also the wave propagation and phase behavior. In so far, we kept a much shorter discussion of the climatologies in section 5.

Comment:
3. (L8-12 on p.7, L 3 on p.20) For the analysis, the authors assume that the vertical wavelengths of tides are much larger than 25 km. This may be true for semidiurnal tide but is not true for diurnal tide. The wavelength of the gravest propagating mode for the diurnal migrating tide is 25-30 km (the higher modes have shorter wavelengths; e.g., Chapman and Lindzen, 1970) and Davis et al. (2013) (cited by this manuscript) actually reported that the observed wavelengths were sometimes 20-30 km. In this sense, I am wondering whether the vertical retrieval kernel of 16 km damps a part of tides (esp. diurnal tides)? Also, is the averaging kernel applied also to NAVGEM-HA data for comparison?

Reply:

The reviewer brings up a good point that we carefully looked into this aspect in previous studies (Baumgarten and Stober, 2019). The ASF technique is not using a fixed vertical wavelength as cut off wavelength nor does the ASF use a vertical average to obtain the tides. The ASF constrains the smoothness of the phase behavior of the tide within the retrieval kernel, which means even a 7 km vertical wavelength tide would be nicely detected as long as the phase would not change dramatically (phase jumps are removed) within the 16 km average kernel.

Further, we have to note that comparison of Davis et al., 2013 was performed for low-latitude observations. A diurnal tidal mode with 7 km vertical wavelength is basically not observed at mid- and high-latitudes. Climatologies of the diurnal tide suggest that the amplitudes at mid- and high latitudes are much smaller compared to the semidiurnal tide and peak at around 100 km during the whole year, which is outside the altitude range of NAVGEM-HA so far. There is also a weak secondary maximum in the summer mesopause visible, but not of relevance for the study here.

Comment:
4. Section 5.4 might be potentially interesting, but the main conclusions are not clear for the present manuscript. For example, the authors first say that the semidiurnal amplitude is enhanced after SSW (L3 on p.14) and the observed phase is approaching that of Pekeris resonance (~M2?) (L21-22 on p.24), but later said (L1 on p.26) that there was no amplification of lunar tide; these descriptions seem contradicting and confusing. At the final paragraph (L2 on p.27) it is suddenly suggested that the day-to-day variability is attributed to zonal winds, but this seems just a speculation without any evidences. At the beginning of the discussion (L21 on p.23), the authors say “we want to disentangle these three aspects…”. I wonders what is the final conclusion in this context?

Reply:

The holographic analysis shows that the semidiurnal tide shows frequently a drift towards the 12.4 h period, which should fall into the Pekeris resonance according to Zhang and Forbes (2014) (see also reply below). Although the phase variability is drifting towards the period of the lunar tide no enhancement is visible in some cases. This becomes even more obvious when comparing the hologram to the lunar orbit. We looked into the lunar distance, the azimuth and elevation angle relative to our local and global references and found no correlation to our tidal analysis. There is no obvious connection between a phase drift of the semidiurnal tide and the lunar orbit. Now, one could argue that only during the SSW the thermal and dynamic structure satisfies the resonance condition as presented in the theory about the Pekeris resonance (see reference in Forbes and Zhang (2012)). However, our analysis shows that the enhancement after the SSW last longer (approx. 10 days) than the SSW itself (4 days) and there is a time delay of several days (3-5 days). So there is a mismatch of the duration of the enhancement and the time period that satisfies the resonance condition. Given that the ASF technique represents a more realistic true interday variability due to the short wind window length compared to many of the previous analysis, which were based on 21/24-day window analysis. Further, considering that the spectral line shape obtained from the global analysis remains symmetric, although the hologram shows that SW2 phase shift that approaches the 12.42 h period, but no shoulder or enhancement in the spectral domain becomes visible.

Comments:

5. For the Pekeris resonance, how is the resonance period determined? The resonance period depends on the background zonal wind and temperature each time. Forbes and Zhang (2012) examined the case for the January 2009. The present study considers the cases in the years 2010 and 2013, and so Forbes & Zhang's results cannot be simply applied.

Reply:

In fact, the reviewer made a good point only Forbes and Zhang (2012) actually computed the shift of the Pekeris resonance explicitly using the GSWM model for the SSW 2009. However, later **Zhang and Forbes (2014) argued somehow that we quote as it is difficult to express it much better. "**During the typical SSW years, e.g., 2006, 2009, or 2013, the *M*2 responses are significant with peak amplitudes at 25–30 K. Utilizing the Global-Scale Wave Model, *Forbes and Zhang* [2012] showed that *M*2 amplification during 2009 was due to a shifting of the Pekeris peak to *M*2's oscillation period at 12.42 h. It is reasonable to infer that during January of 2006 or 2013, the Pekeris frequency peak was also very close to 12.42 and with greater magnitude. The interesting thing is that almost every year, the *M*2 lunar tide has some degree of amplification that peaks at some day during January and February and lasts for 15–20 days. This is not surprising if we recall that the Pekeris peak is not very sharp but instead somewhat broad. Even if the Pekeris peak is not exactly at 12.42 h, part of its shape may also coincide with 12.42 h so that *M*2 gets amplified."

Although, we did not explicitly compute the resonance condition, the holographic analysis provides some indication of the resonance period, which is more or less defined by the time span of the red shift after the central day of the SSW. Further, we estimate the semidiurnal tidal wave properties with respect to the mean frequency and vertical wavelength (see appendix of revised manuscript). It turns out that before the SSW and during the enhancement a semidiurnal tide with about 50-60 km vertical wavelength is present. Only during the second phase of the SSW (after the central day), the mean frequency indicate a lunar period of about 12.42 h and a vertical wavelength of 200-400 km. However, it needs to be confirmed with models like the GSWM whether these changes point towards a lunar tide, or whether they are the result of the superposition of the non-migration, migrating and lunar tide. However, due to the much better temporal resolution of the ASF in combination with the holographic analysis such very transient and intermittent characteristics of the tidal variability can be studied.

Minor comments:

Comment:
1. L34 on p.6: What do you mean by “considering also a potential semidiurnal and terdiurnal tide”?

Reply:

We removed the word ‘potential’. As it is not needed, although the amplitude can become effectively zero.

Comment:
2. L1 on p.7: What do you mean by “regularization”? Do you mean that semidiurnal tide is fitted to the residual time series after removing the daily-mean and diurnal tide?

Reply:

Regularization is a mathematical expression to constrain fits adding other properties to the derived quantities or a priori knowledge. The most common regularization is the Tikhonov regularization for L2-norm functions. L1-norm regularizations are called Lasso-type.

Here we perform a regularization of the tidal waves considering large scales for the smaller windows. A classical harmonic fit of mean winds and the diurnal, semidiurnal and terdiurnal tide has 7 free parameters. Firstly, we use a window with more than 24 hours, which contains at least 24 measurements to fit the mean winds and diurnal tide. These values are than used as regularization for the smaller window adapted to the semidiurnal and terdiurnal tide. This shorter window contains only 12 points, however, as we have already knowledge of the mean wind and diurnal tide we don’t need to fit again for these parameters, but we can use them as boundary for the semidiurnal tidal fit and regularize the new fit. The result is that we have only 4 unknown in the adapted shorter window and we avoid an explicit computation of the residuals. Mathematically, we solve the Jacobien matrix as block diagonals using a Tikhonov regularization for the already determined parameters.

The algorithm is still under development and further releases are planned to include other type of constraints. The vertical regularization is implemented as second iteration step after we solved in a first guess using the temporal only ASF. Mainly to avoid to intense use of computational resources, as the matrices get soon large and more complicated.

Comment:
3. L10 on p.7: For the “16 km vertical retrieval kernel”, does this averaging(?) kernel put the same weights for the 16 km range? What kind of waves (wavelengths) would be effectively filtered with this kernel? (please also see Major comment #3).

Reply:

We apply a full error propagation of the statistical raw voltage fluctuations from the antenna expressed by a radial velocity error until the finally derived wind or tidal parameter. The retrieval is in more detail described in Stober et al., 2018 and Gudadze et al., 2019. All measurements within the retrieval kernel are weighted by their statistical uncertainty.

Comment:
4. L8 on p.11: It is said “the latter point (minimum in Nov.?) is not visible above Tavistock…” but for me, November minimum is clear at Tavistock.

Reply:

We rephrased the sentence. The comment only refered to the April semidiurnal tidal enhancement, which is visible at Tavistock, but is absent at Juliusruh and Andenes.

Comment:
5. L10 on p.12 “due to the coarser temporal resolution of the global data”: How can you reach this conclusion?

Reply:

We removed this sentence. The coarser temporal resolution is not dramatically impacting the phase and amplitude variations at seasonal scales. This is not of relevance for the conclusions.

Comment:
6. L10-11 on p.26: How are these two peaks explained vortex splitting event and planetary wave activity? Please describe more details.

Reply:

We expanded the discussion of the planetary wave and it affects the local measurements.

Comment:
7. L21-24 on p.28: I feel that this is just a speculation.

Reply:

We rephrase the statement. Tidal mean flow and mean flow tidal interactions are commonly discussed in the literature. Considering that tides also hold the polarization and dispersion relation of gravity waves for a dissipation free atmosphere based on the primitive equations (She et al., 2016), and, thus, the phase variability is explainable by changes in the mean flow. The seasonality of the mean zonal winds is also reflected by a seasonality of the phase behavior of the tide. In particular, the transitions times from winter to summer and from summer to winter including the asymmetry is reflected in the morphology of the phases. Apparently, the semidiurnal tide gains only significant amplitudes during eastward zonal winds and is less present during the westward wind phase.

Further, the tide seems to show an enhancement after a reversal from westward winds to eastward winds at the mesosphere.

However, in particular, the response of the semidiurnal tide on a global and local scale to SSWs seems to provide convincing evident that the wind and the thermal structure are highly relevant for the tidal structure at the MLT. From this perspective the statement seems to be not very speculative.

Comment:
8. Captions of Fig.3-12…: Please do not repeat the same sentences in captions.

Reply:

We replaced repeating captions with same as but for …

Comparative study between ground-based observations and NAVGEM-HA analysis data in the MLT region

Gunter Stober[1,2], Kathrin Baumgarten[2,3], John P. McCormack[4], Peter Brown[5,6], and Jerry Czarnecki[2]

[1]Institute of Applied Physics, Microwave Physics, University of Bern, Bern, Switzerland
[2]Leibniz-Institute of Atmospheric Physics at the University of Rostock, Kühlungsborn, Germany
[3]Fraunhofer Institute for Computer Graphics Research IGD, Rostock, Germany
[4]Space Science Division, Naval Research Laboratory, Washington DC
[5]Dept. of Physics and Astronomy, University of Western Ontario, London, Ontario, Canada N6A 3K7
[6]Western Institute for Earth and Space Exploration, University of Western Ontario, London, Ontario, N6A 5B7, Canada

Correspondence: gunter.stober@iap.unibe.ch

Abstract. Recent studies have shown that day-to-day variability of the migrating semidiurnal (SW2) solar tide within the mesosphere and lower thermosphere (MLT) is a key driver of anomalies in the thermosphere-ionosphere system. Here we study the variability in both the amplitude and phase of SW2 using meteor radar wind and lidar temperature observations at altitudes of 75-110 km as well as wind and temperature output from NAVGEM-HA, a high-altitude meteorological analysis system. Application of a new adaptive spectral filter technique to both local radar wind observations and global NAVGEM-HA analyses offers an important cross-validation of both data sets and makes it possible to distinguish between migrating and non-migrating tidal components, which is difficult using local measurements alone. Comparisons of NAVGEM-HA, meteor radar, and lidar observations over a 12-month period show that the meteorological analyses consistently reproduces the seasonal as well as day-to-day variability in mean winds, mean temperatures, and SW2 features from the ground-based observations. This study also examines in detail the day-to-day variability in SW2 during two sudden stratospheric warming, events that have been implicated in producing ionospheric anomalies. During this period, both meteor radar and NAVGEM-HA winds show a significant phase shift and amplitude modulation, but no signs of coupling to the lunar tide as previous studies have suggested. Overall, these findings demonstrate the benefit of combining global high altitude meteorological analyses with ground-based observations of the MLT region to better understand the tidal variability in the atmosphere.

1 Introduction

There is a growing need to understand the global wind field from the surface up to the lower thermosphere (0-100 km) and beyond as well as its day-to-day variability due to meteorological processes. Planetary waves and atmospheric tides are dominant drivers at the mesosphere and lower thermosphere (MLT) that provide a highly variable dynamical lower boundary to the thermospheric/ionospheric system, e.g. at the equatorial dynamo region at altitudes from 100 to 150 km (see, e.g., Akmaev, 2011, and references therein). The upward propagation of these drivers from their source regions near the surface into the MLT region is determined in large part by the global wind field. Accurate assessments of both daily and seasonal variability in winds and tidal modes has therefore become necessary for better understanding lower atmospheric forcing of the thermosphere/ionosphere system.

At mid- and polar latitudes planetary waves provide a significant contribution to the variability of the winter MLT and play a major role in vertical coupling processes between the different atmospheric layers. For example, during sudden stratospheric warmings (SSWs) (Matsuno, 1971; Andrews et al., 1987) the whole middle atmosphere (stratosphere/mesosphere) responds to sudden reversals of the zonal wind from eastward to westward and back to eastward accompanied by an increase of the stratospheric temperature and a mesospheric cooling (see, e.g. Chandran et al., 2014; Zülicke et al., 2018, , and references therin). SSWs are often studied using General Circulation Models (GCMs), which are either free-running (e.g., GAIA, WACCM, KMCM, Jin et al. (2012); Liu et al. (2010); Becker (2017); Zülicke et al. (2018)) or nudged to reanalysis fields (e.g., SD-WACCM, Marsh (2011); Stray et al. (2015); Limpasuvan et al. (2016)). Manney et al. (2008, 2009) characterized the SSW in 2006 as a vortex displacement and the SSW in 2009 as a vortex splitting event making use of global satellite observations (MLS-Microwave Limb Sounder) and data assimilated reanalysis mostly at the stratosphere and lower mesosphere. Matthias et al. (2013) investigated the role of planetary waves in the evolution of vortex splitting and displacement events combining satellite data and ground-based observations.

Atmospheric tides are generated in the troposphere and stratosphere mostly through the absorption of sunlight by water vapor and ozone (e.g., Lindzen, 1979). They have been studied theoretically (e.g., Chapman and Lindzen, 1970; Forbes, 1982; Wang et al., 2016) and from observations (e.g., Portnyagin et al., 1993; Merzlyakov et al., 2009; Oberheide et al., 2009, 2011, and references therein) for decades. More recent studies analyzed the response of the semidiurnal tide during SSWs using ground-based instruments and nudged GCM data or investigated the relative importance and impact of the semidiurnal lunar tide during SSWs with TIME-GCM and WACCM (Pedatella et al., 2012; Pedatella and Maute, 2015). However, atmospheric tides propagate from their source region up to the MLT through a constantly varying altitude dependent wind and temperature field, which significantly modifies the phase of the tides, depending on their vertical wavelength, as well as the vertical wavelength itself.

In this study, we compare local meteor radar (MR) wind observations as well as lidar temperature measurements with meteorological analyses produced with NAVGEM-HA (Navy Global Environmental Model - High Altitude), a data assimilation and modeling system that extends from the surface to the lower thermosphere. NAVGEM-HA fields were available from December 2009 to December 2010 and during the winter season 2012/13 starting in December 2012 until March 2013. Recent studies (Eckermann et al., 2018; McCormack et al., 2017) have presented initial cross-validation of the mesospheric winds from NAVGEM-HA for two winter seasons using worldwide distributed MR measurements. Here, we extend these initial comparisons to include seasonal mean winds (30-day median) from NAVGEM-HA and from three MRs at mid- to high latitudes for the year 2010. Time series of both NAVGEM-HA analysed winds and MR measurements are decomposed into daily mean winds, tides and GW residuals using a recently introduced analysis technique called adaptive spectral filter (ASF) (Stober et al., 2017; Pokhotelov et al., 2018; Wilhelm et al., 2019; Baumgarten and Stober, 2019). This technique is designed to extract daily mean winds and tidal variations on a day-to-day basis. In addition to MR measurements, we also present the first comparison between midlatitude temperature observations from a resonance lidar and NAVGEM-HA analysed temperatures for the 2010 period.

Meteorological analysis data, such as NAVGEM-HA, provide a much more realistic forcing of the upper atmosphere due to tides and mean winds compared to current versions of other comprehensive models. Chandran and Collins (2014) investigated SSW events using WACCM-SD nudged with reanalysis fields from the GEOS-5.2 reanalysis system up to an altitude of about 40 km. However, at altitudes above 70-80 km the nudged model started to substantially deviate from the observed wind climatologies (Wilhelm et al., 2019). In particular, the nudged model showed a wind reversal from eastward to westwards winds between 70-80 km, which is not confirmed from the wind climatologies. Such reversal of the zonal wind can be also found in other comprehensive models or mechanistic models (Smith, 2012; Becker, 2012). Liu (2016) shows a comparison among several GCMs indicating that there are substantial deviations at the mesosphere and upper atmosphere, although each of the GCMs was nudged up to the lower stratosphere (see also Pedatella et al. (2014) for more details). Only the GAIA model (Jin et al., 2012; Liu et al., 2014) showed during winter eastward winds at the MLT. Previously, the eCMAM model was also cross-validated with ground-based meteor radar observations to investigate mean winds and tides and their amplitude and phase behavior at equatorial latitudes (Du et al., 2007; Ward et al., 2010). They found a remarkably good agreement between the model and the local observations using 60-day running means underlining the value of such comparisons. The focus of the present study is to examine the degree of agreement between day-to-day and as well as seasonal variability in SW2 between a global meteorological analyses of the MLT region and ground-based observations as a means to, ultimately, better understand the origins of this variability.

Finally, we perform a detailed comparison of SW2 variability from both NAVGEM-HA and meteor radar observations during the SSWs in 2009/10 and 2012/13, focusing in particular on how the amplitude and phase of semidiurnal variability in both data sets responds to changes in the background wind. Overall, the results of these comparisons show very good agreement between NAVGEM-HA analysed winds and MR observations, highlighting the utility of combining global high altitude data assimilation products with ground-based observations of the MLT to lend new insight into the causes of semidiurnal tidal variability over daily to seasonal time scales. Such short time variations are essential for the understanding of the forcing from below of the thermosphere and ionosphere (Liu, 2016). Therefore, the paper is structured as follows. First, we describe the observations for winds and temperatures in the MLT region and the corresponding meteorological analysis data in Section 2. Section 3 provides a detailed explanation of the methodology used for the data analysis. Section 4 presents the results for the climatology, comparing mean winds simultaneously seen in the meteor radar data at different locations with the NAVGEM-HA analysis data accompanied with available temperature measurements from a resonance lidar at one mid-latitude location. The results are also discussed for the semidiurnal tide for the whole year (2010) as well as during the winter season in 2010 and 2013 in Section 5. Finally, the findings are summarized and a conclusion is given in Section 6.

2 Data description

2.1 Wind observations

In this study, we compare the 3-hourly global synoptic wind and temperature analyses from NAVGEM-HA with meteor radar observations collected at three different latitudes in Andenes (69° N, 11° E) in Norway, Juliusruh (54.3° N, 13° E) in Germany and Tavistock (CMOR- Canadian Meteor Orbit Radar) (43.2° N, 80.7° W) in Canada. All three meteor radars use the same software for meteor detection and classification as described in Hocking et al. (2001). All systems were almost continuously in operation for the analyzed periods. Only the Andenes system shows some data gaps, mainly due to the more extreme weather conditions in Northern Norway, which caused some damage to the antennas and from time to time a power outage. A more detailed description of the CMOR radar can be found in Brown et al. (2008). A summary of the Juliusruh and Andenes MR is found in Stober et al. (2012) and Wilhelm et al. (2017).

MLT winds are obtained with a temporal resolution of 1 hour and a vertical resolution of 2 km using the wind retrieval algorithm presented in Stober et al. (2018), which is a further development of the wind analysis presented in Hocking et al. (2001). The wind analysis contains a full error propagation of the statistical uncertainties and a physical error model based on the vertical and temporal shear as spatio-temporal Laplace filter for each wind component. Contrary to many other meteor radar wind analysis, the algorithm also solves for the vertical wind velocity. The obtained mean vertical velocities show values of a few cm/s and are mainly used as quality control for successful convergence of the wind fit. In the present study, we use 4 meteors as a minimum for a successful wind fit.

2.2 Temperature observations

At Kühlungsborn (54° N, 12° E), around 118 km southwest of the meteor radar at Juliusruh, a resonance lidar was in operation until 2012 to observe temperatures in the MLT region. The potassium lidar measures the Doppler broadening of the 770 nm potassium D1 resonance line by scanning with a narrow band Alexandrite ring laser. The system is fully daylight capable. Further details can be found in von Zahn and Höffner (1996); Fricke-Begemann et al. (2002).

The extent of the potassium layer in the atmosphere limits the range of heights at which temperatures can be determined. In this work, temperatures are determined for heights between 80 and 105 km. The integration time of the data used here is 1 h with a shift of 15 min. The vertical resolution is 1 km. In addition to the resonance lidar, also a Rayleigh-Mie-Raman (RMR) lidar was operated during the night at the same location until 2013. This lidar used the second harmonic output of a Nd:YAG laser at 532 nm. The temperatures are calculated under the assumption of hydrostatic equilibrium from the Rayleigh backscatter which is proportional to the atmospheric air density (Hauchecorne and Chanin, 1980). The initial temperature value for integration is taken from the resonance lidar (Alpers et al., 2004). The temperatures from the RMR lidar cover an altitude range between 22 and 90 km. But as the focus of this study is on the MLT region, we use these temperatures only above 70 km.

Here, daily mean temperatures as a composite between 2003 and 2012 are used to describe the mean temperature field during the year in the MLT region. A full description of the seasonal variation has been published in Gerding et al. (2008).

2.3 NAVGEM-HA meteorological analyses

NAVGEM-HA is a high-altitude numerical weather prediction (NWP) system extending from the surface to $\sim$116 km altitude that provides atmospheric winds, temperatures and constituent information. It is based on the operational system described in Hogan et al. (2014), which combines the NAVGEM global spectral forecast model with a hybrid four-dimensional variational (4DVAR) data assimilation algorithm (Kuhl et al., 2013).

In addition to standard operational meteorological observations in the troposphere and stratosphere, NAVGEM-HA assimilates satellite-based observations of temperature, ozone and water vapor in the stratosphere, mesosphere and lower thermosphere (McCormack et al., 2017). The NAVGEM-HA output is on a 1° latitude and longitude grid, respectively. The temporal resolution of the data output fields is 3 hours. NAVGEM-HA uses a fixed top level pressure of $6 \cdot 10^{-5}$ hPa (e.g., McCormack et al., 2017; Eckermann et al., 2018, and references therein), which corresponds to an approximate altitude of 116 km. However, at the upper three model levels, an enhanced diffusion is applied to reduce the effects of wave reflection. These layers effectively act as a "sponge layer" and are not included in the data analysis. The forecast model component of NAVGEM-HA incorporates the same implicit fourth-order horizontal diffusion of vorticity, divergence, and virtual potential temperature used in its predecessor system (NOGAPS-ALPHA) to suppress growth of unrealistic variances near the truncation scale, as described in McCormack et al. (2015). Default values for the diffusion result in an effective e-folding time of 24 hours at the highest wavenumber (here T119). In the top 3 model levels the diffusion is ramped up to produce an effective e-folding of 2 hours at the top level. In the 74-level version of NAVGEM-HA used in this study, this region of enhanced diffusion (sponge layer) covers levels with $p <$ 1.e-3 hPa or 95 km in pressure-altitude.

In an initial validation study, McCormack et al. (2017) used NAVGEM-HA output interpolated to geometric altitudes up to 95 km for the mean winds and up to 90 km for the wave analysis. In the present study, vertical profiles of NAVGEM-HA analyzed winds and temperatures are converted from the model vertical grid in geopotential altitude to a geometric altitude grid as done in Eckermann et al. (2009) up to 94 km altitude. Above this level, NAVGEM-HA vertical resolution degrades significantly, as the vertical grid spacing increases from $\sim$3 km near 80 km altitude to more than 5 km near 100 km altitude. To date, NAVGEM-HA winds and tides up to 90 km altitude have been shown to be in good agreement with both ground-based MR observations, as reported in McCormack et al. (2017), Eckermann et al. (2018), and Laskar et al. (2019), and with independent satellite-based wind observations as reported in Dhadly et al. (2018). The present study extends these initial validation studies to include, for the first time, validation with two independent ground-based data sets over a 12-month period.

In this study we use a fixed geometric altitude grid (based on the World Geodetic System 84 model) with a maximum altitude of 94 km and 2 km vertical resolution at the MLT to match the meteor radar data. We convert the geopotential altitudes of NAVGEM-HA to geometric altitudes. However, we note that the geopotential altitude of the highest usable output level, neglecting the sponge layer effects noted above, has a geometric altitude between 92 to 89 km. As a consequence tidal amplitudes above 90 km altitude should not be considered as geophysical and are caused by the extrapolation to the geometric altitude grid and sponge layer effects. Further, the vertical constraint implemented in the ASF amplifies this effect even more. At mesospheric altitudes, NAVGEM-HA assimilates satellite measurements from TIMED and AURA satellites and radiances from the Defense Meteorological Satellite program (DMSP) (Eckermann et al., 2018). Systematic differences between the meteorological analysis and the ground-based wind and temperature data herein may have different origins. There could be intrinsic differences due to the model physics leading to such deviations or the assimilated data itself may show some systematic differences in relation to the observations used for the comparison. Further, considering that the *true* state of the atmosphere of temperature and winds remains elusive, it is hard to determine which of the observational techniques provides a better representation of this *true* state. Thus, it is essential to assess some of the systematic differences, which can arise due to the methodology employed for the comparison e.g., does applying different diagnostics or different spatio-temporal sampling of the instruments make a large difference. Validation and assessment of potential biases between the SABER temperatures and ground-based lidar measurements can be found in Xu et al. (2006); Dawkins et al. (2018). A cross comparison of the MLS and SABER temperatures is presented in Schwartz et al. (2008). A detailed description of how the data assimilation in NAVGEM-HA treats the temperature biases between both satellites is given in Eckermann et al. (2018).

Another important point affecting the comparison is the availability of the assimilated data. Above 90 km less satellite observations can be assimilated. Further, it has to be noted that the spatial coverage of the assimilated SABER temperatures varies due to the yaw cycle of the spacecraft, which changes every 60 days the observing geometry providing a variable latitudinal coverage. From 52° S to 52° N the satellite collects constant measurements whereas the higher latitudes depend on the yaw cycle and alternates between up to 82° S or 82° N latitudinal coverage. This yaw cycle pattern may affect the quality of NAVGEM-HA analyses at Juliusruh and Andenes.

3 Local and global diagnostics

One of the challenges comparing different data sets is the use of a common diagnostic to ensure that all observations and the meteorological analysis data are treated in the same way. In particular, observational data can be more difficult to be analyzed due to data gaps or uneven temporal sampling. Atmospheric tidal and planetary wave amplitudes are often obtained from Fourier based techniques (e.g., Stockwell et al., 1996; Torrence and Compo, 1998). In the case of unevenly sampled data Lomb-Scargle periodigrams are used (Lomb, 1976; Scargle, 1982), which provide a amplitude/power spectrum and a significance level, but without a phase information. For observational data, it is also very common to derive the tidal information of amplitude and phase with a least-square fit (Lima et al., 2007) or by a multiple regression analysis assuming, for instance, a circular polarization for the semidiurnal tide (Jacobi et al., 2008).

A commonly used approach to extract tides is a harmonic analysis:

$$u,v,T = u_0,v_0,T_0 + \sum_{n=1}^{3} a_n \sin(\frac{2\pi}{P_n}\cdot t) + b_n \cos(\frac{2\pi}{P_n}\cdot t) \;\; ; \tag{1}$$

here u, v, T are the zonal, the meridional wind and the temperature, a_n and b_n are the tidal Fourier coefficients, $P_n = 24, 12, 8$ stands for the tidal periods in hours and t is the time of the observation either in UTC or local time, whatever is preferred. Harmonic tidal analysis work well for time series of several days or months, but assumes a constant mean background wind, tidal amplitude, and phase for the selected period. Recent studies of mean winds and tides using meteor radar, lidar and satellite observations indicate that tides have a fairly intermittent amplitude and phase character (Stober et al., 2017; Baumgarten et al., 2018; Baumgarten and Stober, 2019; Dhadly et al., 2018).

The adaptive spectral filter (ASF) aims to be a simple and general diagnostic to decompose time series in 1-D (temporal filter) (Stober et al., 2017) or 2-D (temporal-spatial filter) (Baumgarten and Stober, 2019). The technique is based on least-squares and, hence, applicable to unevenly sampled data and no additional zero-padding needs to be applied for data gaps as long as sufficient observations are available in the remaining adapted time window. Another benefit of the least-squares implementation is given in the error propagation to the derived quantities through the covariance matrix. The term 'adaptive' in this context relates, similar to the wavelet technique, that the window length adapts to the number of wave cycles for each frequency component that is fitted. The MR and NAVGEM-HA time series are decomposed into daily mean winds, diurnal tide, semidiurnal tide, terdiurnal tide and gravity wave residuum using the ASF.

The ASF uses a sliding window and fits each tidal component applying a scaling factor of 1.3 accounting for the number of wave cycles and no de-trending is applied. The scaling factor determines the window length that is used for the fitting for each frequency component. Here we applied a window length of 31 hours for the diurnal tide, whereas the semidiurnal tide is determined using a 16 hour window and so forth for the terdiurnal tide. At first, the daily mean wind and the diurnal tidal (amplitude and phase) components are determined considering also a semidiurnal and terdiurnal tide. In the next step, the semidiurnal tide is fitted using a regularization by the previously determined daily mean wind and diurnal tide and adapting the window length. The same procedure is repeated for the terdiurnal tide respectively. Due to the short window length, the bandwidth for each tidal component is rather wide and may also include some gravity wave contributions. It turns out that just applying temporal filtering leads to some contamination of the obtained tidal amplitudes and phases due to inertia gravity waves with short (less than 10 km) vertical wavelengths (see appendix A). However, there are also some studies from polar latitudes using lidar and radar observations from McMurdo/Scott base (77.8° S, 166.7° E) and from Syowa Station (39.6° E, 69.0° S) indicating the presence of gravity waves with vertical wavelengths of 22-23 km (Chen et al., 2013) or periods close to the semidiurnal tide (Shibuya et al., 2017). However, Davis et al. (2013) has shown that the diurnal and semidiurnal tide typically has vertical wavelengths larger than 20 km. Hence, we constrain our tidal amplitudes and phases by assuming that the phase of the diurnal and semidiurnal tide only gradually changes with altitude using a 16 km vertical retrieval kernel. The mean winds are constrained by a 10 km vertical retrieval kernel to avoid issues during the summer wind reversal from westward winds to eastward winds.

We optimized these vertical wavelength values considering the results of previous studies using meteor radars investigating the vertical wavelengths of tides (Yu et al., 2013; Davis et al., 2013; Fritts et al., 2019). These earlier studies showed that the vertical wavelengths for most of the tidal modes are much larger than >25 km. Only Yu et al. (2013) found for some Hough modes vertical wavelengths shorter than <25 km. To avoid a potential contamination of shorter tidal wavelengths in our vertical retrieval kernel, we did not implement a hard cut off vertical wavelength. Instead, we just constrain the smoothness of the vertical tidal phase within the averaging kernel and even allow a gradual change.

The vertical regularization constraint is an essential feature of the ASF compared to many other diagnostic techniques based on wavelet or Fourier methods. Previous studies based on lidar observations (e.g., Ehard et al., 2015; Baumgarten et al., 2017, and reference therin) already investigated how the potential gravity wave energy changes with the applied filtering. Temporal filters tend to underestimate inertia gravity waves due to their long periods combined with short vertical wavelengths, whereas vertical filters are designed to eliminate the tidal contribution due to their large vertical wavelengths. As a consequence, this filter underestimates gravity waves with comparatively large vertical wavelengths. The ASF is much less prone to such biases due to the combination of spatio-temporal information for the specific waves. Since NAVGEM-HA produces global wind and temperature fields, we can extract tides as global waves and separate migrating and non-migrating tidal modes. Migrating tides are the DW1 (diurnal westward wave number 1), SW2 (semidiurnal westward wave number 2) and TW3 (terdiurnal westward wave number 3); all other tidal modes are non-migrating tidal components (e.g., Forbes et al., 2008; Miyoshi et al., 2017, and references therein). The migrating and non-migrating tidal components are obtained using the following function;

$$u,v,T = u_0,v_0,T_0 + \sum_{s=-3}^{3}\sum_{i=1}^{3}\Big(a_{si}\cdot\sin(s\cdot\lambda - \frac{2\pi}{P_i}\cdot t) + b_{si}\cdot\cos(s\cdot\lambda - \frac{2\pi}{P_i}\cdot t)\Big) + further\ waves \quad , \tag{2}$$

where s is the zonal wave number (negative eastward, positive westward), λ denotes the longitude at a fixed latitude circle, P_i are the periods of the diurnal, semidiurnal and terdiurnal tide and a_{si} and b_{si} are the Fourier coefficients for each wave number s and period P_i. The zonal mean zonal and meridional wind and the zonal mean temperature are given by u_0,v_0,T_0. The function also includes longer period waves such as the quasi two day wave (QTDW) with wave number s=1,2,3 and stationary planetary waves with wave number s=1,2,3 (Baumgarten and Stober, 2019; Schranz et al., 2019).

Daily mean tides for all the components are obtained by using a 3-day window around a central day, which is sufficient to still see some day-to-day variability and to determine potential phase drifts of each tidal component. The global tidal phase for all tidal components is referenced to the Prime meridian (Greenwich). Although NAVGEM-HA provides validated wind and temperature products from ∼18 km up to ∼94 km altitude, we focus our comparison to the MLT region and mostly to the available MR observations. A detailed discussion of the QTDW or planetary waves is beyond the scope of this paper and we leave these for other studies.

4 Results

In the first two parts of the results, we show the mean state of the atmosphere during the year in the MLT region using winds and temperatures from observations and NAVGEM-HA data. Next, the seasonal variation of the semidiurnal tidal component derived with the adaptive spectral filter is presented for each location. In addition to this, the analysis is also done for two examples of sudden stratospheric warming in the winter 2009/2010 and 2012/2013 to determine how well the observed variations in the MLT winds correspond to the NAVGEM-HA analysis data as well as to determine the day-to-day variability of the semidiurnal tide.

4.1 Mean winds

Fig. 1 shows the time variation of the zonal and meridional winds at the three locations Andenes, Juliusruh and Tavistock, from hourly meteor radar observations (left column), and the corresponding 3-hourly NAVGEM analyzed winds (center column) for the same location and each latitude as zonal mean values (right column). Daily mean winds are calculated and small scale variations such as tides and gravity waves are removed by the adaptive spectral filter and planetary waves are effectively filtered using a 30-day running median. The climatologies are based on the same time periods for MR winds and NAVGEM-HA and include December 2009 until December 2010 with periodic boundary conditions. In general, there is a good agreement of the seasonal wind pattern between the meteor radar wind observations and the NAVGEM-HA data. At all three locations, the zonal wind observations show the typical eastward winds in winter and the prominent wind reversal in spring. In particular, the seasonal asymmetry of the spring transition as well as the the gradual change of the summer wind reversal altitude seen in the meteor radar winds is well-reproduced in the NAVGEM-HA analyses.

During summer, a strong transition between westward and eastward winds occurs between 80 and 90 km altitude. The transition height decreases from high to midlatitudes. Above 90 km altitude, the eastward jet reaches wind velocities of about 40 m/s for all stations. The meridional winds during winter are typically northward, while they are southward during the summer. Similar behavior is seen in the NAVGEM-HA analysis data, but here the magnitude of the winds is to some extent larger compared to the meteor radar observations. Although the general morphology of the seasonal pattern is well captured in NAVGEM-HA, there are some differences in the wind reversal altitudes in summer in both wind components, which would affect the gravity wave breaking altitudes and, hence, the altitude of the resulting momentum deposition.

Furthermore, the altitude where the zonal wind reverses during summer decreases not as much with latitude as indicated from the meteor radar observations for the different locations. Some differences occur between the NAVGEM-HA locally analyzed winds compared to the zonal averaged NAVGEM-HA analyzed winds for each latitude of the meteor radar stations. Short-term variations during winter are much more visible in the locally analyzed winds, this is especially true for the meridional wind case.

4.2 Mean temperatures

Until now, only NAVGEM-HA wind products have been extensively validated with independent ground-based measurements. To extend this validation to MLT temperatures, we next perform a similar comparison using NAVGEM-HA temperature analyses and a co-located potassium lidar instrument at Kühlungsborn. The composite daily mean lidar temperatures over the period 2003-2012 are shown in Fig. 2 together with the NAVGEM-HA analyzed temperatures between 2009 and 2010. Both data sets show the same seasonal temperature pattern with the lowest temperatures during summer. The mesopause, where the lowest

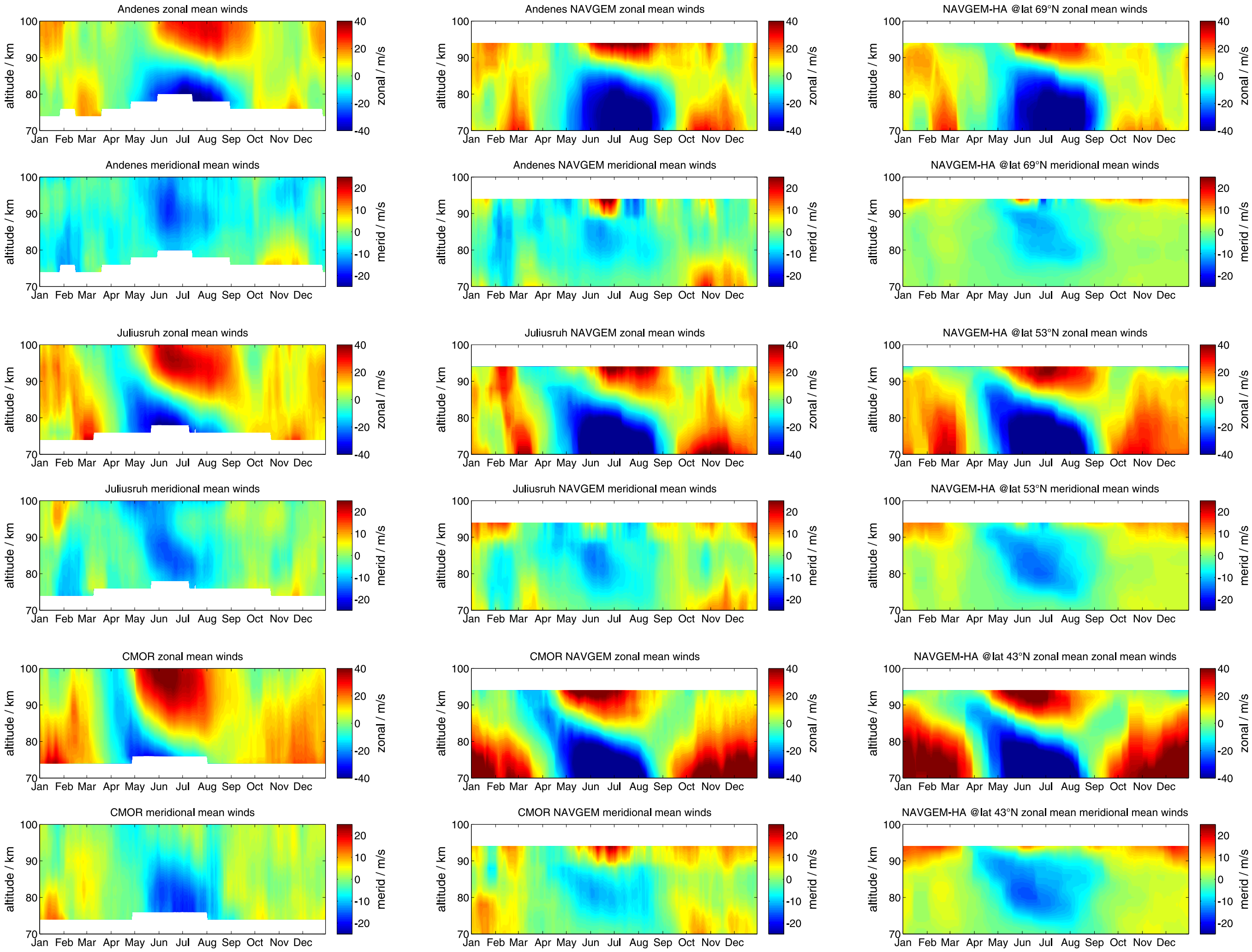

Figure 1. Comparison of mean winds above Andenes, Juliusruh and Tavistock (CMOR) using a 30-day running median with periodic boundary condition using the same dates for NAVGEM-HA and the meteor radar observations. The left panel shows the meteor radar observations. The central panel shows the NAVGEM-HA analysis fields for the same locations and periods. The right panel displays the zonal mean zonal and meridional winds for each latitude.

temperatures occur during the year, is estimated from the lidar data and found around 88 km in summer and just above 100 km in winter. For the NAVGEM-HA analyzed temperatures the altitude of the mesopause is in nearly the same altitude range. In general, the temperature values are in very good agreement with each other, although we note that the temperatures observed by lidar near 70 km are larger than the NAVGEM-HA temperature. At the upper edge of the NAVGEM-HA data, there is also a temperature enhancement during summer, which is not seen in the lidar data.

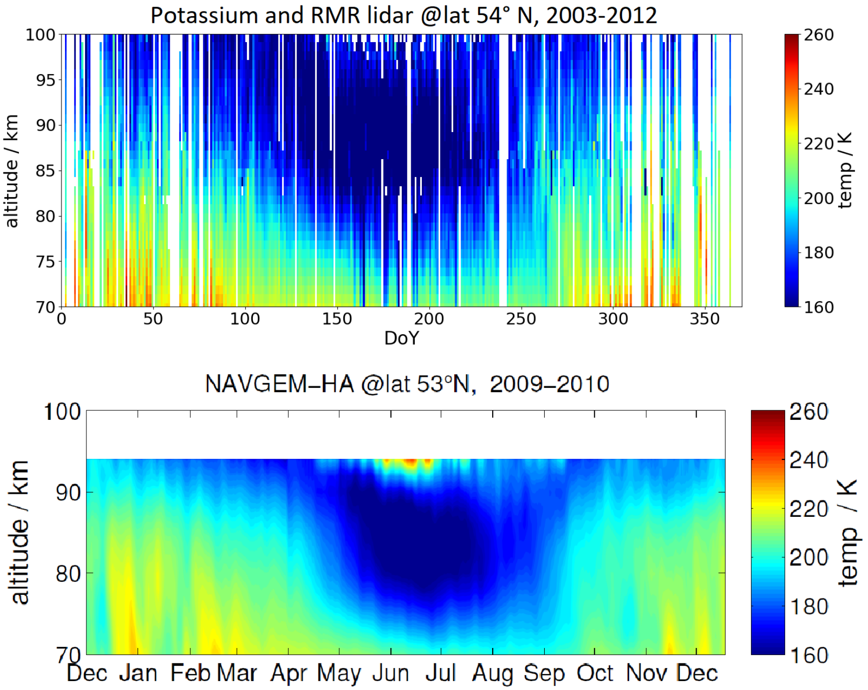

Figure 2. Comparison of mean temperatures above Kühlungsborn. The upper panel shows the temperatures derived from the potassium lidar. The lower panel shows the NAVGEM-HA analysis field for the same location.

4.3 Semidiurnal tides

In this section, we investigate the seasonal variation of the semidiurnal wind tide based on the calculation with the adaptive spectral filter. This component is the most dominant tidal component at the MLT and the latitudes analyzed herein (Chapman and Lindzen, 1970). The results for the semidiurnal tidal amplitude and phase for the stations at Andenes, Juliusruh and Tavistock are shown in Fig. 3, 4, and 5, respectively. Every data set is compared to the NAVGEM analyzed tidal fields from a local as well as from a global perspective as already done for the mean winds and temperatures.

The observations from all stations indicate a clear winter amplitude maximum. A second maximum is also evident during September. The amplitudes are smallest during November and April. Only Tavistock exhibits a significant semidiurnal tidal amplitude for April compared to the meteor radars at higher latitudes, and we note that the tidal amplitudes above Tavistock are also even stronger during fall than during winter. Compared to the other locations the winter maximum above Tavistock is less pronounced. In general, the amplitudes during winter are strongest for midlatitudes (Juliusruh).

The NAVGEM-HA analyzed amplitudes reveal the same temporal variability over the year as from the observations. Above an altitude of 90 km, the amplitudes from NAVGEM-HA show a significant increase which is not seen in the observations. This was also visible in the temperature data of NAVGEM-HA compared to the lidar data.

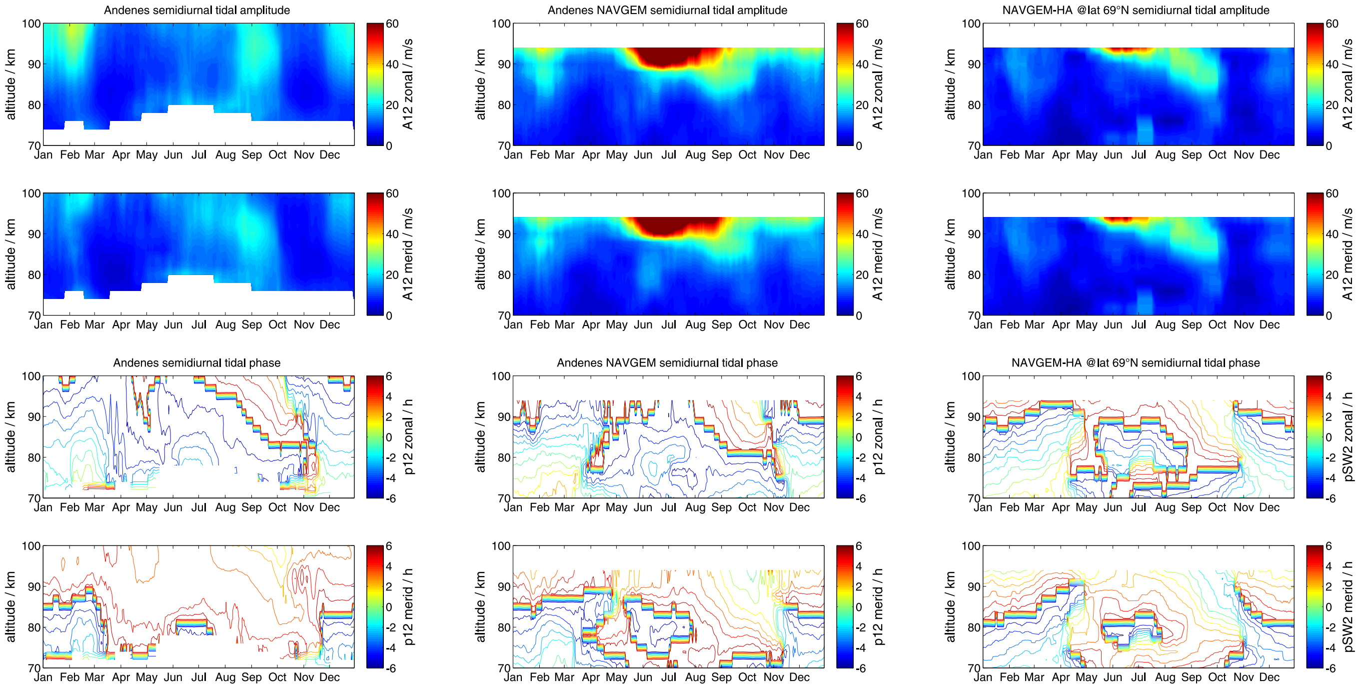

Figure 3. Comparison of semidiurnal seasonal zonal and meridional amplitude (upper two rows) and phase (lower two rows) tidal climatology using a 30-day running median with periodic boundary condition. The left panels show the meteor radar observations above Andenes (69° N, 11° E). The central panels show the NAVGEM-HA analysis fields for the same period. The right panels visualize the zonal mean tidal amplitude and phase of the SW2. The label A12 and p12 corresponds to the semidiurnal amplitude and phase using the local diagnostic.

In addition to the amplitudes of the semidiurnal tides, the annual phase behavior of those tides was also calculated using the spectral adaptive filter. In general, for every location, the phase of the semidiurnal tide is drifting and variable over the year. During winter the phases are continuously changing, at the beginning of March, the phase shows a sudden jump, which is evident in every location of the observations and the meteorological analysis. This behavior reverses during October/November, exactly when the atmospheric circulation reverses again from summer to winter conditions. A similar phase progression is visible from the NAVGEM-HA locally analyzed data as well as from the global fields.

4.4 Day-to-day variability during a sudden stratospheric warming

Having established that NAVGEM-HA wind and temperature analyses capture many of the salient features in the seasonal variation of both meteor radar wind and lidar temperature observations, we now examine the shorter-term variations in both data sets. Specifically, we examine the day-to-day variability of the mean winds, the semidiurnal tidal amplitudes and phases from the meteor radar winds during the sudden stratospheric warming (SSW) that took place in 2010 and 2013 in comparison to NAVGEM-HA analyzed data from a local perspective as well as from a global view. To do so, we apply the same ASF analysis procedure to both meteor radar and NAVGEM-HA data at a high latitude (Andenes) and midlatitude (Juliusruh) location.

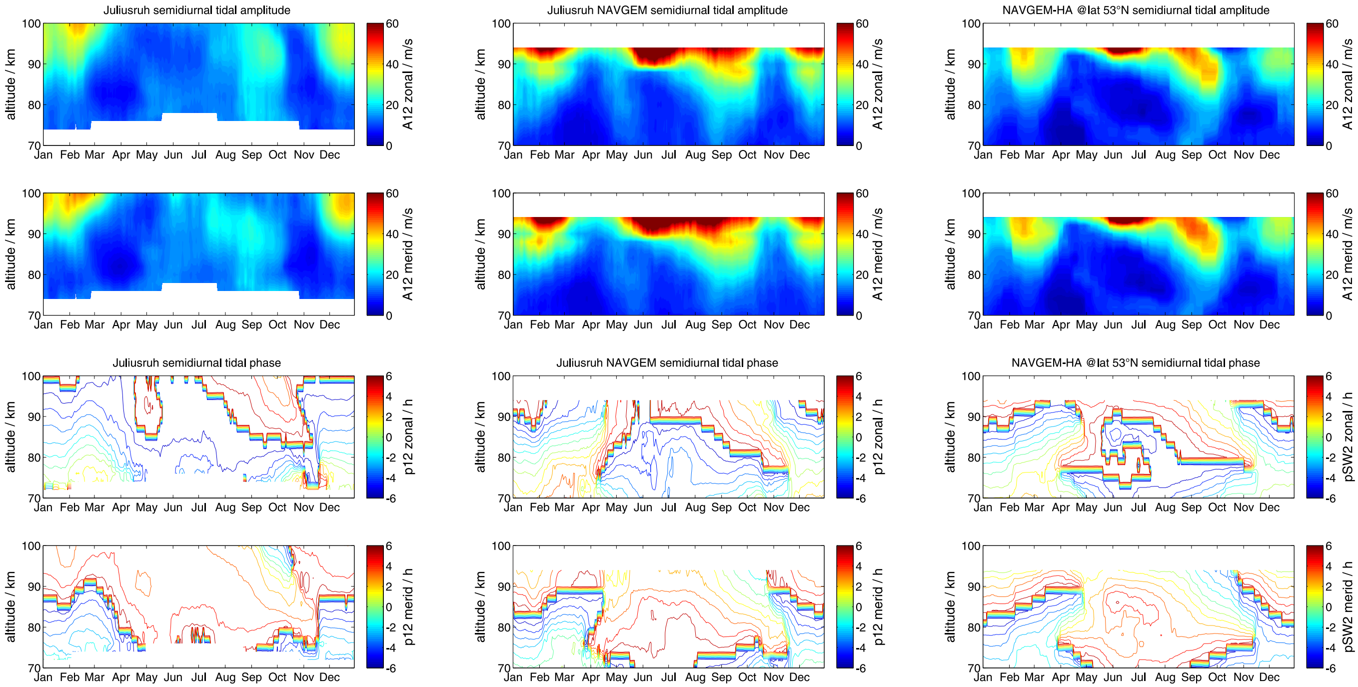

Figure 4. Same as Fig. 3, but for Juliusruh.

4.4.1 Winter season 2009/2010

During the winter in 2009/2010, a major sudden stratospheric warming occurred at the end of January when the polar vortex was markedly displaced from the pole (Stober et al., 2012) and then separated into two unequally strong lobes (e.g., Dörnbrack et al., 2012; Jones Jr. et al., 2018). Following previous studies involving NAVGEM-HA, we mark the onset of the SSW as occurring on 27th January (McCormack et al., 2017). Mean winds, the semidiurnal tidal amplitude and phase are shown in Fig. 6 from the meteor radar observations above Andenes as well as for the corresponding locally analyzed NAVGEM-HA data. In Fig. 7 the same results are shown for the station at midlatitudes above Juliusruh. Stronger changes in the winds are visible for Juliusruh than for Andenes. Even the semidiurnal amplitudes are stronger at midlatitudes, which agrees with the stronger seasonal variation of the semidiurnal tidal amplitude above Juliusruh. After the onset of the sudden stratospheric warming, the semidiurnal tidal amplitudes show an enhancement at the beginning of February, which is visible at both stations and in both wind components.

The semidiurnal tidal phases show a large day-to-day variability during the winter period, which is in general stronger at high latitudes than at midlatitudes. After the central date of the sudden stratospheric warming, the tidal phase shows a sudden increase which lasts only a few days. After these days, the phase shows a recovery where they become more stable again just as before the sudden stratospheric warming.

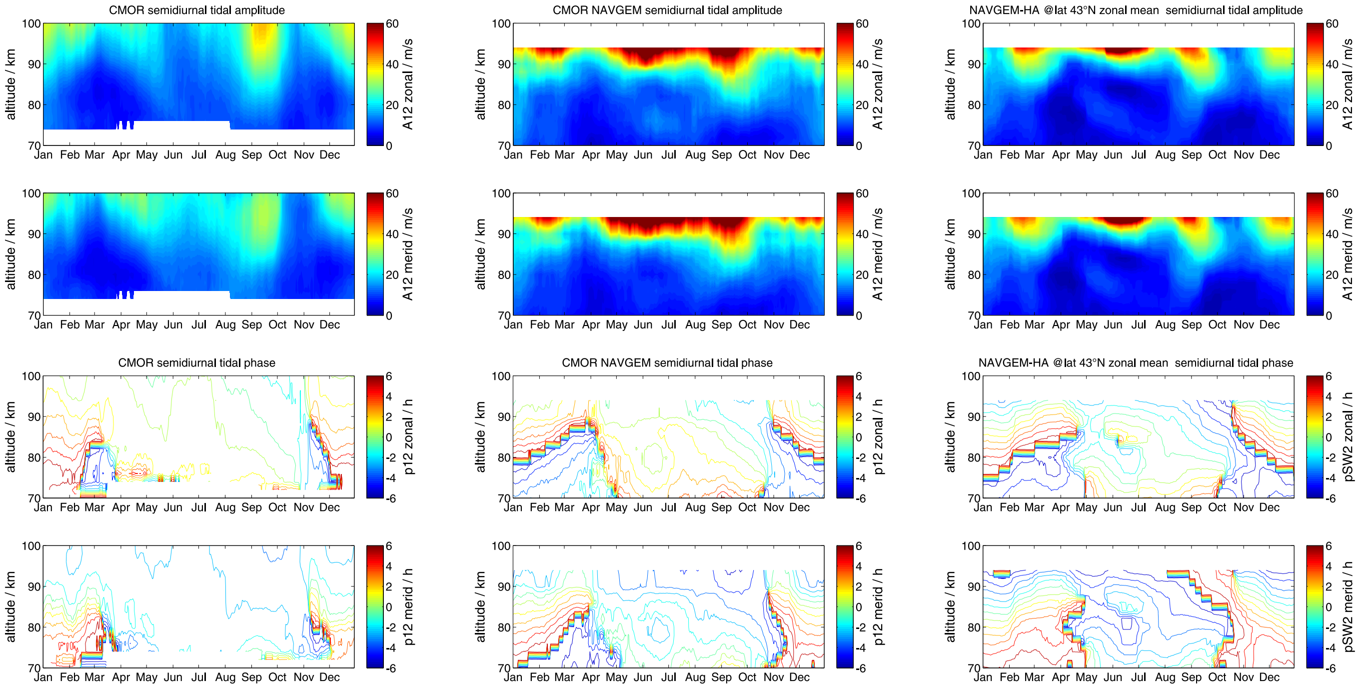

Figure 5. Same as Fig. 3, but for CMOR.

The NAVGEM-HA analyzed winds exhibit the same short-term variability during the 2009/2010 winter at both stations for the winds as well as for the semidiurnal tide. Even the phase enhancement after the central date of the SSW is remarkably well reflected by the NAVGEM-HA data. Some differences occur above an altitude of 85 km, where NAVGEM-HA data reveals larger magnitudes in the winds as well as larger amplitudes for the semidiurnal tide as previously seen. Fig. 8 shows global NAVGEM-HA results for both Andenes and Juliusruh station locations. The global analyzed NAVGEM-HA data indicates much less variability during the winter compared to the locally analyzed data. But the central date of the SSW is more easily identified in the winds than it was the case for the locally analyzed winds. However, the main features for the semidiurnal tide stay the same. The amplitudes show an increase after the central date of the SSW and the phases reveal a change for a few days at both locations. In contrast to the locally analyzed data, the phases from the global NAVGEM-HA fields slowly change during the winter. But in general, the agreement with the MR observations is still good.

4.4.2 Winter season 2012/2013

The winter season in 2012/2013 was also characterized by a major sudden stratospheric warming. In this case, the onset of the SSW occurred on 7th of January using again the definition presented in McCormack et al. (2017). During the SSW the vortex was split into two lobes (Coy and Pawson, 2015). Again, mean winds, the semidiurnal tidal amplitudes and phases are shown

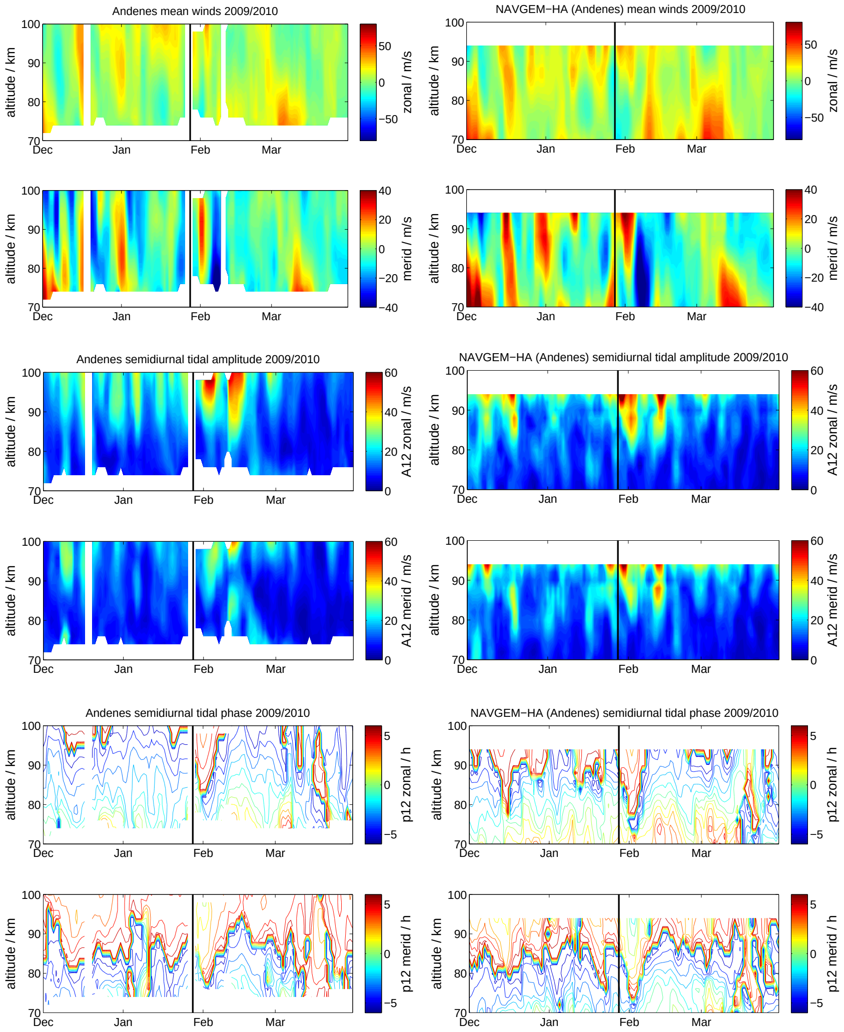

Figure 6. Comparison of meteor radar observations and NAVGEM-HA above Andenes during the winter 2009/10 for daily mean zonal and meridional winds (upper two panels), semidiurnal tidal zonal and meridional amplitude (middle panels) and semidiurnal tidal phases (lower two panels). The label A12 and p12 corresponds to the semidiurnal amplitude and phase using the local diagnostic.

in Fig. 9 and Fig. 10 for high latitudes and midlatitudes, respectively.

In this winter season, the mean zonal winds at high latitudes are stronger, especially after the SSW, than at midlatitudes, which is opposite to that seen in the winter season 2009/2010. The mean meridional winds are similar in strength for both

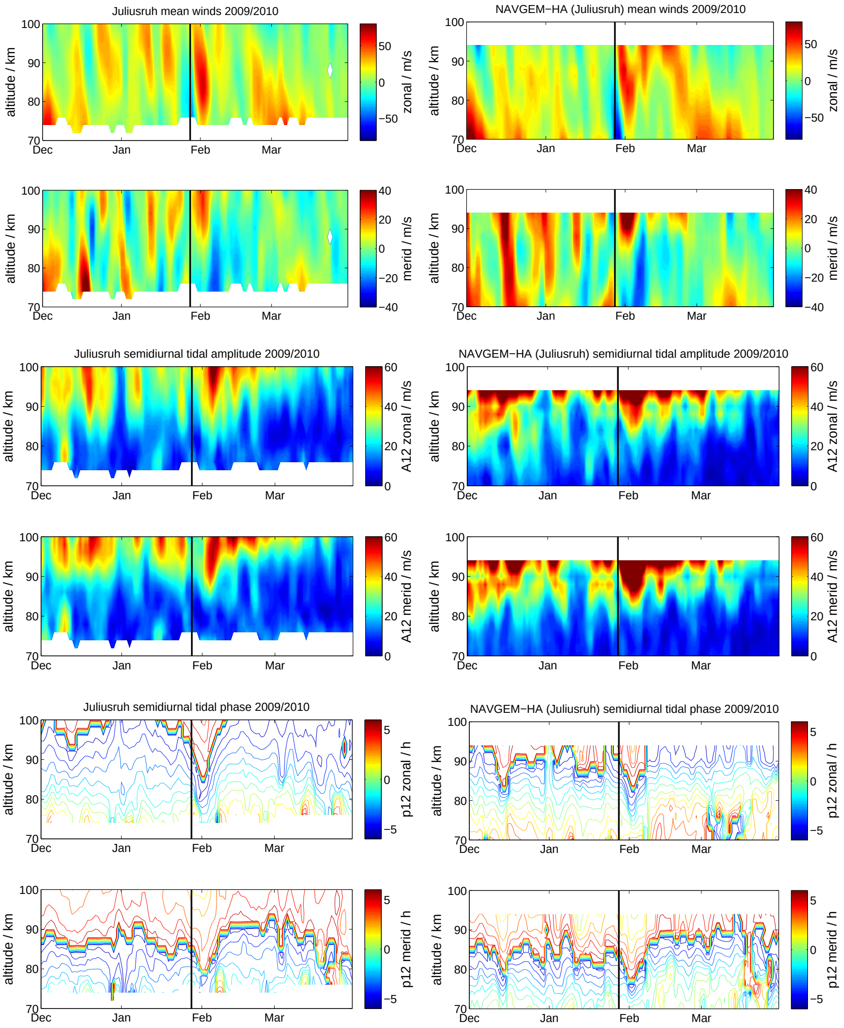

Figure 7. The same as Fig. 6, but for Juliusruh.

stations. Nevertheless, the semidiurnal tide shows again stronger amplitudes at the midlatitude station than at high latitudes. At Andenes, we see a distinct increase of the amplitudes after the SSW, which was already seen in the winter season 2009/2010, while in general at Juliusruh a larger tidal activity is visible. Here, before and during the central date of the SSW the tidal amplitudes decrease in the first place due to the strong changing winds. Afterward, the semidiurnal tidal amplitudes increase again stronger than during the whole winter.

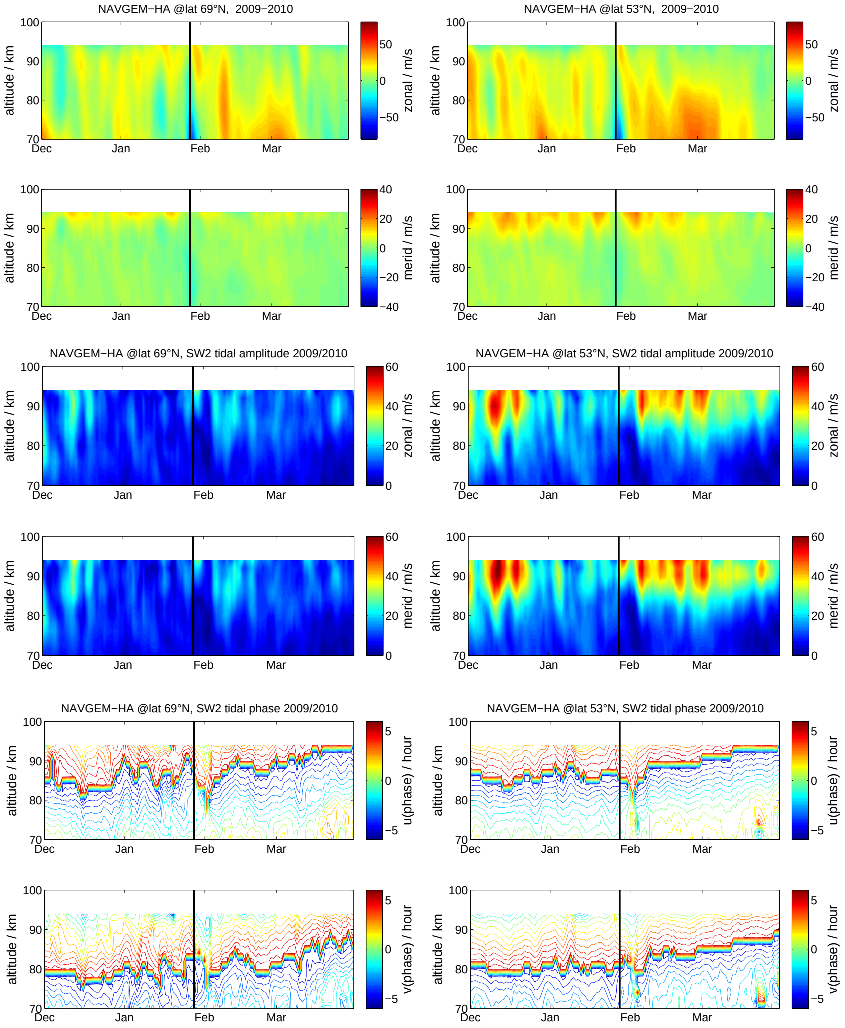

Figure 8. Comparison of global NAVGEM-HA above Andenes and Juliusruh during the winter 2009/10 for daily zonal mean zonal and meridional winds (upper two panels), zonal mean semidiurnal tidal zonal and meridional amplitude (middle panels) and zonal mean semidiurnal tidal phases (lower two panels).

The semidiurnal tidal phases show again a large variability during the whole time. A few days after the central date of the sudden stratospheric warming a sudden increase of the phase is visible in the same way as for the winter 2009/2010. The locally analyzed NAVGEM-HA data reveal structures during this winter period similar to those from the observations. Evident from every data set, the mean winds, as well as the amplitudes, are slightly overestimated in NAVGEM-HA. The NAVGEM-HA analyzed tidal phases exhibit also a sudden change after the SSW, but not as strong as from the observations, but this might be due to a general more disturbed winter period compared to the year 2009/2010. The globally analyzed data from NAVGEM-HA are shown in Fig. 11. As was the case for the 2009/2010 winter, in this winter season the winds from a global perspective are much stronger and uniformly distributed over the winter months, except for the wind reversal during the SSW, which is visible at the beginning of January.

5 Discussion

5.1 NAVGEM-HA and MR mean wind and temperature climatology

The comparison of the NAVGEM-HA mean winds and the meteor radar climatologies at Andenes, Juliusruh and CMOR is remarkable up to an altitude of 94 km. The assimilation of satellite-based middle atmospheric temperature and constituent observations enables NAVGEM-HA to capture the main features of the seasonal wind climatologies such as the weak eastward winds during the winter, the asymmetry of the seasonal pattern between the spring and autumn wind reversals as well as the gradual descent of the summer wind reversal between the mesospheric westward winds and the higher altitude thermospheric eastward jet. Our analysis shows that the initial good agreement reported during the winter months in McCormack et al. (2017) extends to seasonal time scales, and providing further cross-validation of the NAVGEM-HA winds with globally distributed and available meteor radar wind observations.

The MLT mean wind climatology is still afflicted with a high degree of uncertainty when comparing different GCMs, although nudged to the same reanalysis data sets. Pedatella et al. (2014) compared several GCMs and showed that not even the sign of the mean wind seems to agree between the models at the MLT. Further, the seasonal morphology at mid- and high-latitudes was not well-reproduced by some models compared to the climatologies published from meteor radars (Portnyagin et al., 2004; Wilhelm et al., 2019). In particular, the seasonal asymmetry of the zonal wind circulation from the winter to the summer conditions and back to the winter regime seems to be problematic for the GCMs. Comparing the seasonal morphology of the zonal and meridional winds between NAVGEM-HA and other comprehensive GCMs, such as WACCM or SD-WACCM (Smith, 2012; Chandran and Collins, 2014), and the meteor radar and lidar data indicate a much better agreement for the meteorological analysis for altitudes beyond 80 km. Similar results have been found by comparing meteor radar winds to free running mechanistic GCM (Pokhotelov et al., 2018). Previous studies comparing eCMAM with ground-based meteor radar observations at low latitudes and on seasonal time-scales revealed a similar good agreement for mean winds and diurnal tidal amplitude and phases (Du et al., 2007; Ward et al., 2010). The good agreement between NAVGEM-HA and ground-based wind observations shown in Section 4 indicate that global data assimilation products in the MLT can provide a valuable benchmark for evaluating the performance of “whole-atmosphere” GCMs extending into the thermosphere. These products could improve understanding of the large discrepancies among different models noted above by offering insight regarding where these models deviate most from a validated high-altitude meteorological analyses.

The general thermal structure and seasonal climatology are also well-reproduced in NAVGEM-HA for the lidar observations presented in Fig. 2 at the mid-latitude station of Kuehlungsborn. The meteorological analyses captures the seasonal course of

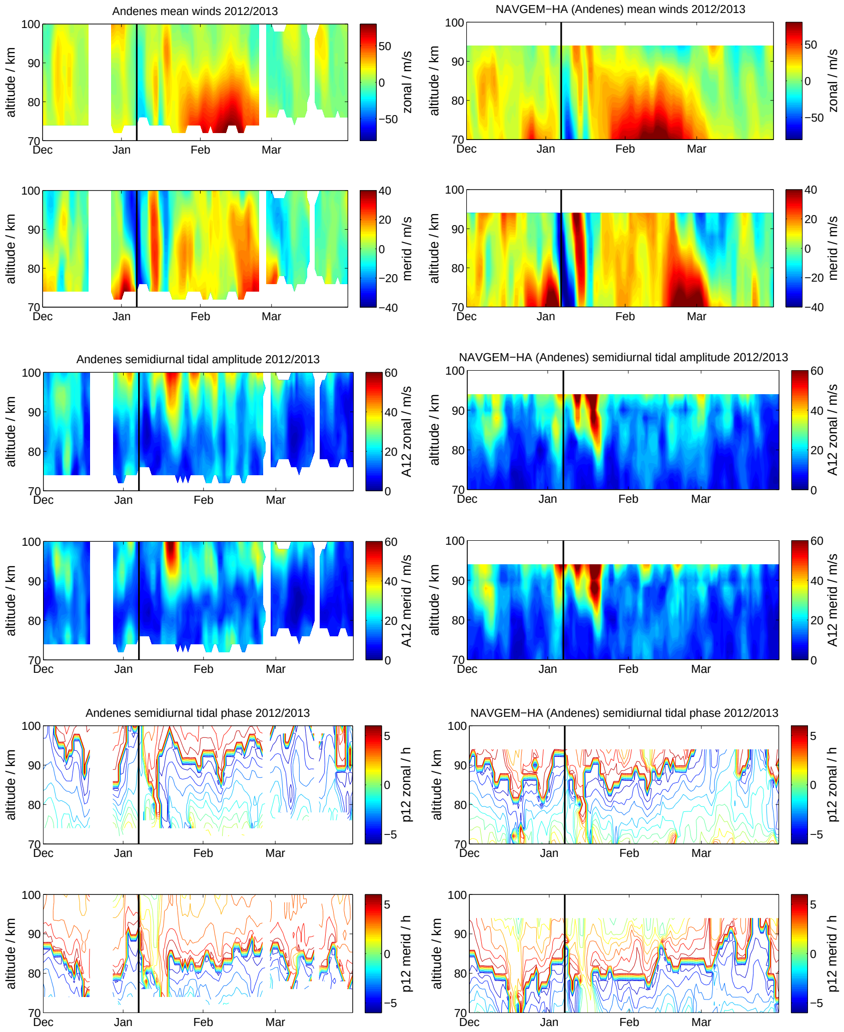

Figure 9. Comparison of meteor radar observations and NAVGEM-HA above Andenes during the winter 2012/13 for daily mean zonal and meridional winds (upper two panels), semidiurnal tidal zonal and meridional amplitude (middle panels) and semidiurnal tidal phases (lower two panels).The label A12 and p12 corresponds to the semidiurnal amplitude and phase using the local diagnostic.

the altitude variation of the mesopause. Further, we identified a small offset between the lidar and the NAVGEM-HA temperatures. The analysis data has a tendency towards slightly warmer temperatures compared to the resonance lidar. These slightly higher temperatures in NAVGEM-HA may also explain the higher wind magnitudes relative to the MR observations.

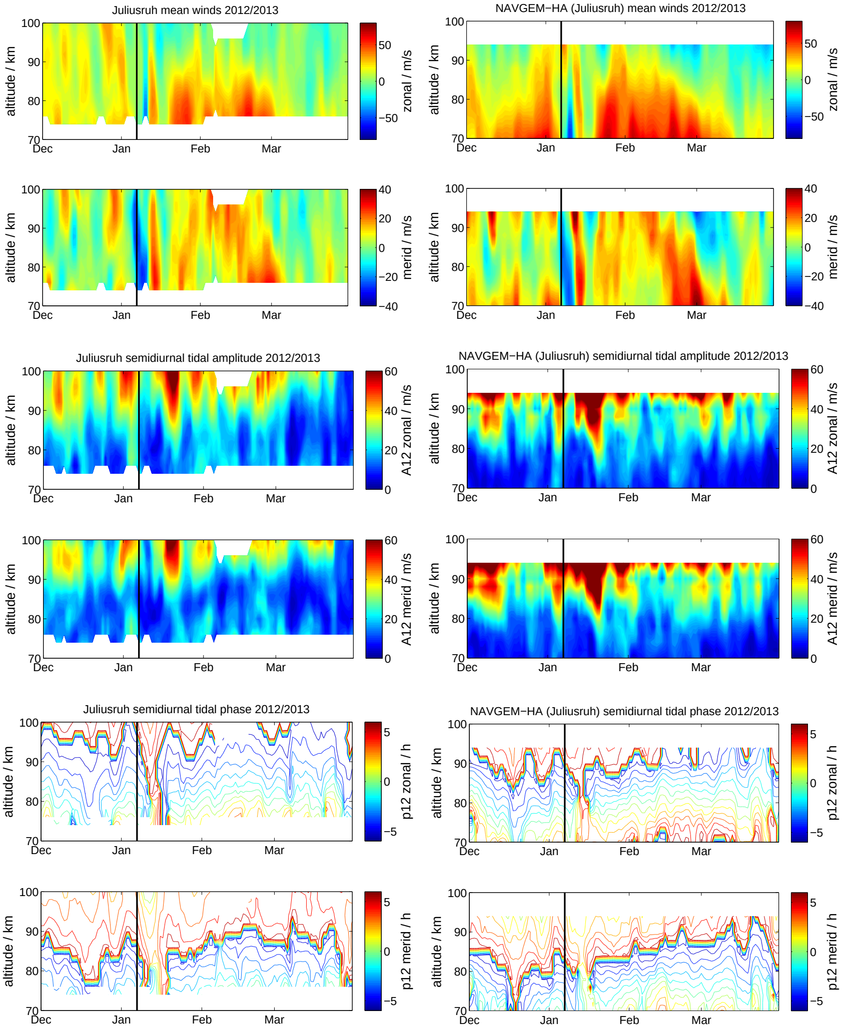

Figure 10. The same as Fig. 9, but for Juliusruh.

5.2 NAVGEM-HA and MR mean wind semidiurnal tidal comparison

At MLT heights, tidal amplitudes grow large and contribute significantly to the daily variability of the zonal and meridional winds. At mid- and polar latitudes, the semidiurnal tide is the most prominent tidal wave in the MLT that can be observed throughout the course of the year (Portnyagin et al., 2004; Pokhotelov et al., 2018; Wilhelm et al., 2019).

In principle, local observations (single measurements) can not distinguish between migrating and non-migrating tidal com-

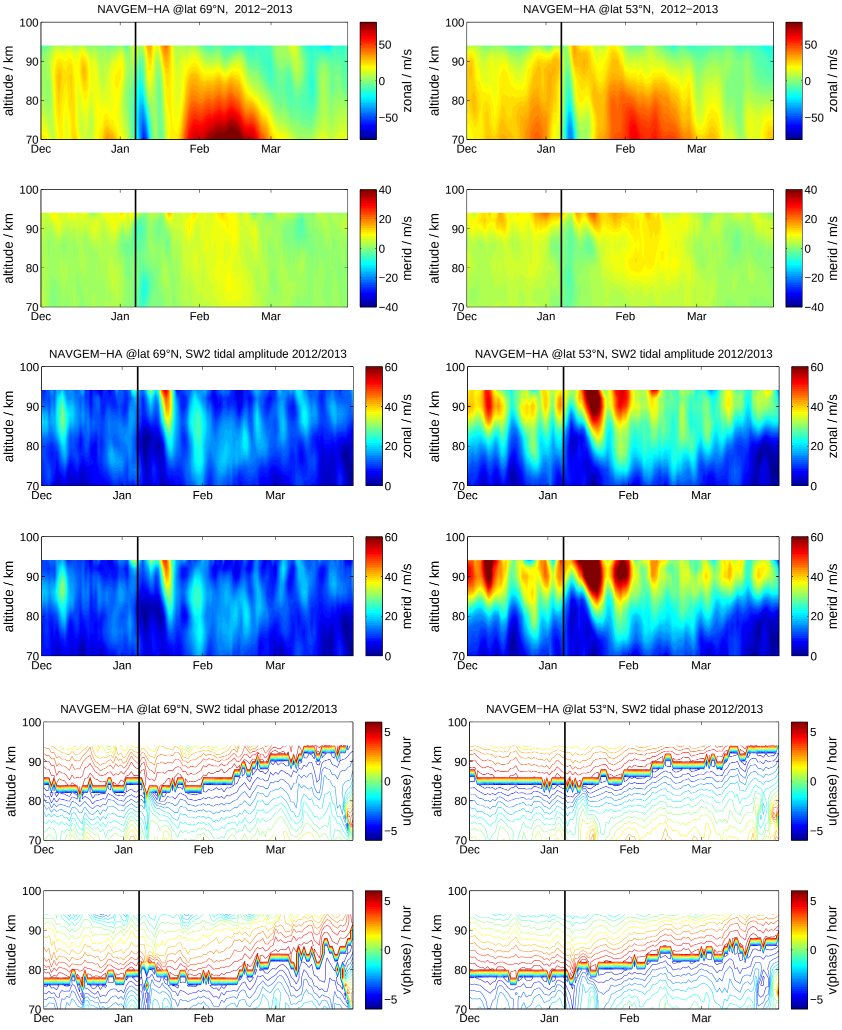

Figure 11. Comparison of global NAVGEM-HA above Juliusruh (left column) and Andenes (right column) during the winter 2012/13 for daily zonal mean zonal and meridional winds (upper two panels), zonal mean semidiurnal tidal zonal and meridional amplitude (middle panels) and zonal mean semidiurnal tidal phases (lower two panels).

ponents and only observe a total tide. Earlier studies (e.g., Portnyagin et al., 2004) have investigated the global nature of the diurnal and semidiurnal tide at polar latitudes using a chain of radars at approximately 70° N. They found very good agreement between monthly tidal amplitudes and phases for all stations along the latitudinal circle. Recently, there have been some attempts to separate migrating and non-migrating tides using globally distributed chains of meteor radars (He et al., 2018) assuming theoretical tidal wave fields consisting of migrating and non-migrating components. However, due to the small number of meteor radars at the latitudinal circles, the analysis still contains a high degree of ambiguity.

Combining the benefits of high resolution local measurements with global meteorological analysis data solves this problem. The comparison of the semidiurnal tidal climatology reveals that NAVGEM-HA reproduces the seasonal morphology of the tidal amplitudes for both wind components up to an altitude of 90 km applying the ASF tidal diagnostic. The local ASF diagnostic shows remarkable agreement between the global tidal analysis of the migrating SW2 tide in magnitude and phase. The non-migrating semidiurnal components show only very small and often negligible amplitudes. The agreement of the phase of the SW2 tide between the global and local measurements seem to be better at lower latitudes of CMOR and Juliusruh compared to Andenes.

? performed a similar validation of the tidal amplitude and phase behavior using the extended Canadian Middle Atmosphere Model (eCMAM) at low latitudes. However, they used much longer windows of 60-days to compute average amplitudes and phases. They also found the seasonal change of the tidal phase and remarkable good agreement between the ground-based lidar and radar data and the model. The comparison of NAVGEM-HA and the meteor radar indicates that tidal phase are variable on the seasonal scale showing already significant shifts and drifts within a week. Previously, for local observations this phase variability was assumed to be the result of a superposition of migrating and non-migrating tidal modes. However, comparing the global tidal fit obtained from NAVGEM-HA of the SW2 tide reflects this behavior as well. These continuous phase changes have severe implications for the analysis of tides at mid- and high latitudes from satellites, which usually requires to average over several weeks to cover all local times.

5.3 NAVGEM-HA and MR winds and tidal day-to-day variability and lunar tides during SSW events

Besides comparing mean winds, we also investigated the day-to-day variability of the semidiurnal tide during two winter seasons with a major SSW event at the mid-latitude location Juliusruh and polar latitudes above Andenes. In 2010 there was a vortex displacement event (e.g., Stober et al., 2012; Matthias et al., 2013), which was already validated by a cross comparison of the mean winds and waves in McCormack et al. (2017) using several worldwide-distributed meteor radars. The second SSW event occurred during winter 2012/13 and evolved as a vortex splitting event (e.g., Xu and San Liang, 2017).

Daily mean winds and tidal amplitudes were diagnosed by the ASF. The meteorological analysis of NAVGEM-HA reproduces the general day-to-day variability of winds and even shows a high level of agreement for individual planetary waves passing over the stations. In particular, the timing of the SSW event itself with the zonal wind reversal and the formation of an elevated stratopause is well-captured. Similar to the zonal and meridional wind climatologies, the meteorological analysis tends to show higher magnitudes of the wind speeds. Previous comparison of wind observations to model data, such as ECMWF or MERRA2, were limited to a maximum altitude of approximately 70-75 km and below (Rüfenacht et al., 2018) and, thus, we omit here any further detailed discussion.

Another very important aspect of this study is the phase variability on a day-to-day basis. The ASF provides information on the phase stability of tides with basically the same resolution as the original measurement time series. Very often tidal phases are assumed to be stable over long periods of up to several months in the analysis. However, for instance, the TIMED satellite requires 60-days to cover all local times due to its orbit geometry (Zhang et al., 2006; Oberheide et al., 2011). Our results indicate that during an SSW the phase of the SW2 tide is significantly altered on a global scale as well as on a regional or local scale as the dynamics of the middle atmosphere change (e.g., Manney et al., 2009; Matthias et al., 2012). Fuller-Rowell et al. (2016) discussed three possible mechanisms to understand these changes of the tide; Fuller-Rowell et al. (2010); Jin et al. (2012) attributed the change of the migrating tidal phase to changes of the mean winds in the middle atmosphere, whereas Pedatella and Forbes (2010) suggested non-migrating tides as a source of the SW2 phase variability. Other studies favor an amplification of the lunar tide during an SSW (Fejer et al., 2010; Forbes and Zhang, 2012).

We discuss these three aspects using the results obtained from the ASF decomposition of the local and global measurements and meteorological analysis data. Fejer et al. (2010) investigated vertical plasma drifts above Jicamarca and found a drift in local time of the semidiurnal oscillation, which was attributed to the lunar tide assuming that all other tidal waves remained stationary and monochromatic. Later Forbes and Zhang (2012) proposed that the lunar tide enhancement is a result of the Pekeris resonance effect that is shifted towards the lunar tide period M2 of 12.42 h due to changes in the mean zonal winds caused by the SSW. They tested the proposed physical mechanism on satellite observations from SABER, CHAMP and GRACE and the steady state Global-Scale-Wave-Model (GSWM) for a case study and the SSW in 2009. To separate the lunar tide from the semidiurnal SW2 tide, they used a window of 24-days to ensure sufficient frequency resolution and assumed monochromatic and stationary tidal waves within the window. Later, Zhang and Forbes (2014) claimed that the lunar tides seem to enhance during nearly every SSW event arguing that the Pekeris resonance has a rather broad peak and, thus, the resonance conditions are satisfied for all SSW events. Although, Forbes and Zhang (2012) pointed out that a very specific thermal and dynamic structure is required to satisfy the resonance condition.

In the following, we investigate the phase variability of the semidurnal tide introducing a holographic analysis for the SSW 2012/13 and discuss a potential connection to the Pekeris resonance (Zhang and Forbes, 2014). The day-to-day variability, obtained from the ASF, indicates that the tidal phase are not stable with time and show significant interday variability, which appears to be related to changes in the zonal wind in the middle atmosphere driven by the polar vortex and planetary waves. Considering that a time dependent phase corresponds to a frequency shift, it is possible to convert this temporal phase variability into a period change and, hence, to estimate the spectral line shape of the tide or to derive a holographic representation of the temporal evolution on a day to day basis.

The hologram is derived considering that the tide can be represented by a cosine wave with amplitude A (e.g., semidiurnal tide), a mean frequency w and a time dependent phase $\phi(t)$;

$$A(t) = A\cos(wt + \phi(t)) \quad . \tag{3}$$

Although the true functional form of the time dependent phase might be unknown, we can express this function as a Taylor series at a certain point in time t;

$$\phi(t) = \phi_0 + \frac{d\phi}{dt} \cdot t + ... \tag{4}$$

Truncating the Taylor series at the first order and inserting them in eq. 3 leads to;

$$A(t) = A\cos(wt + \phi_0 + \frac{d\phi}{dt} \cdot t) \ . \tag{5}$$

Rearranging the terms according to their time dependence leads to;

$$A(t) = A\cos((w + \frac{d\phi}{dt}) \cdot t + \phi_0) \ . \tag{6}$$

It is now straight forward to numerically obtain the time dependent phase change $d\phi/dt$ using a central differences approach in the complex domain.

In Fig. 12 we show a holographic reconstruction based on the ASF decomposition of the semidiurnal tide. This technique only assumes monochromaticity within the adopted window length (less than a day for the semidiurnal tide) and, thus, captures non-stationary processes on an interday basis. The hologram shows that during the SSW event in 2012/13 the phase behavior of the semidiurnal tide itself is shifted to the period range that is expected for the lunar tide M2 (solid white line) and N2 (dashed white line). Further, we overlayed the lunar orbit as elevation angle for the geographic location of Juliusruh to search for a potential connection of the semidiurnal phase variability and the moon position on the sky. The hologram for the global diagnostic is shown in Fig. 13. The main differences in the holograms between the local MR observations and the global tidal fields from NAVGEM-HA are attributed to the decomposition of the global fields into migrating and non-migrating tides. As shown in the appendix B there is an excitation of the non-migrating tides SW1 and SW3, which leads to the differences in the holographic reconstruction. The local diagnostic shows the superposition of all tidal components. However, the global diagnostic also indicates the frequency shifts of the SW2 tide to periods that can match the predicted Pekeris lunar tide resonances. However, as indicated by the white lines, these phase shifts happen frequently during a winter season and are neither correlated to the lunar orbit nor accompanied by a tide enhancement. The effect of the SSW is visible in both holograms up to 10 days after the onset of the SSW, which is also the time delay corresponding to the amplification of the semidiurnal tide after the SSW. Moreover, Forbes and Zhang (2012) reported a delay of 5-7 days between the occurrence of the lunar tide amplification and the central day of the SSW event. This delay of approx. 5-7 days is consistent with the holographic analysis, which also shows that the frequency/period shift towards the lunar tide frequency/period (M2 and N2) occurs after the SSW event (central day), at the beginning of the formation of an elevated stratopause or when the polar vortex begins to restore, however, well before the semidiurnal tide enhancement. This time span also corresponds to the response time of the semidiurnal tide to a transient forcing, which was estimated to be between 6-10 days (Vial et al., 1991) for comparisons to steady state models. An SSW is also associated by a large exchange of air masses between mid- and polar latitudes, which leads to a significant enhancement of the ozone volume mixing ratio inside the polar cap (Schranz et al., 2019), and, thus, provides a potential source to increase the tidal forcing of the semidiurnal tide. Further, this strong meridional coupling also provides a sufficient strong response to explain the low latitude response to the SSW.

Many recent studies have investigated lunar tides with window lengths that are long enough to ensure an unambiguous frequency resolution to separate the lunar tide from the semidiurnal tide, which requires at least 21-days or more (e.g., Forbes

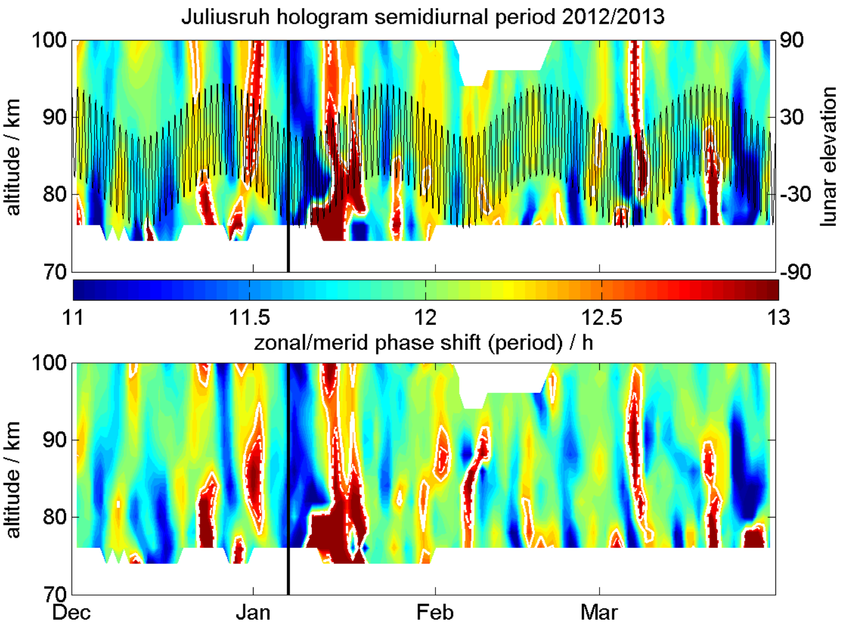

Figure 12. Holographic reconstruction of the semidiurnal tidal phase variability. The hologram shows the periods using a time variable phase, which is equivalent to a frequency shift or change in period. The white contour lines indicate the lunar tide M2 (12.42 h) (solid line) and N2 (12.66 h) (dashed line). The lunar orbit as elevation angle (-90° to 90°) for Juliusruh is plotted as black solid line.

and Zhang, 2012; Chau et al., 2015; Conte et al., 2017; He et al., 2018; Siddiqui et al., 2018, and reference therein). The ASF analysis indicates that there is a considerable interday tidal variability in amplitude and phase, which poses a challenge to the signal processing. Such intermittent behavior suggests that long windows (longer than even a day) might lead to spurious results, and do not allow a separation of the different waves from each other. The zonal wind reversal and accompanied cooling at the MLT during a SSW last only for a few days (much shorter than the typical window length used for the lunar tides) and cause significant changes in zonal mean wind at mid- and polar latitudes altering the propagation conditions for the tides. As a consequence, such a long window would not allow one to capture SSW effects, which themselves cause changes in the semidiurnal tide. Thus, if one does not notice that an SSW occurred, one cannot know whether the 12.42 h tide is lunar or a semidiurnal tide that was altered by the SSW.

These shortcomings are also mentioned and discussed in (Forbes and Zhang, 2012; Zhang and Forbes, 2014). They fitted the lunar tide, for instance, on the residuals of SABER measurements after removing the semidiurnal tide by a 12-day running mean, which still is too long given the huge phase variability of the tide. The caveats of the steady state model GSWM are also discussed in Forbes and Zhang (2012). In particular, the steady state assumption seems to be not fully met during an SSW recalling the results from Vial et al. (1991) as the whole event lasts only 3-4 days at the MLT. We also investigated the non-migrating tidal components (see appendix B) derived from NAVGEM-HA winds. It appears that only the SW1 and SW3

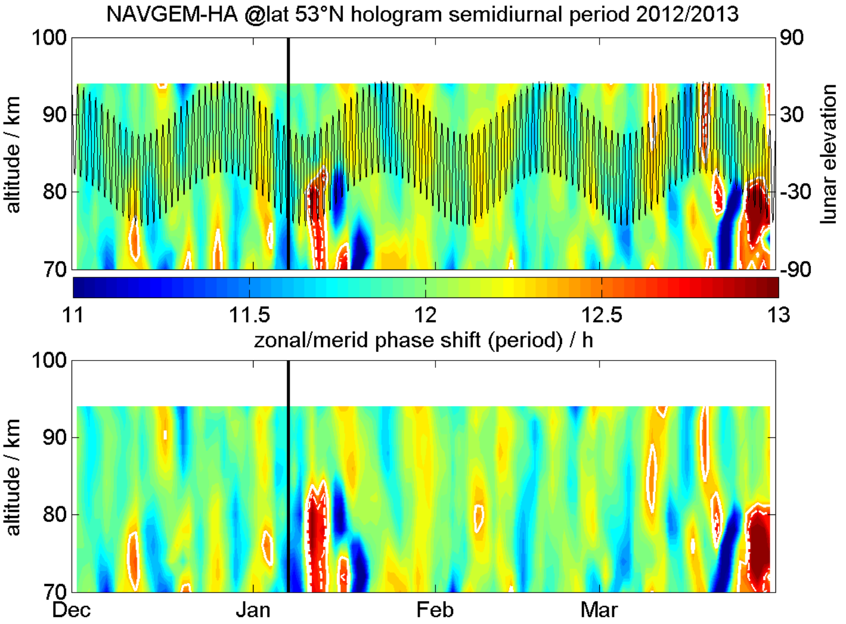

Figure 13. The same as Fig. 12, but for the global tidal analysis of the SW2

.

tides show a response to the SSW event depending on the latitude and how the SSW evolved. This is consistent with previous studies (Du et al., 2007; Liu et al., 2010). The SE1, SE2, SE3 and S0 semidiurnal tides show much smaller amplitudes and are negligible compared to the SW2 tide, in particular, at polar latitudes. Another interesting aspect when comparing the migrating and non-migrating tides from NAVGEM-HA is the winter seasonal phase behavior of the SW2 tide. The phase of the tide drifts by several hours between December to March, which correlates to the mean wind morphology. Apparently, the change of the phase of the semidiurnal tide may not be explained by a superposition of migrating and non-migrating tides. However, this needs to be examined in more detail and is beyond the scope of this paper.

The next aspect we did investigate is a potential correlation between the phase shifts from the holographic analysis and the lunar orbit. Thus, the lunar azimuth, elevation and lunar distance was checked, whether there exists a connection with the SSW events. Holographic analysis of the S2 phase shifts shows frequently periods close to the the M2 tide, indicated by the white contour lines, but no obvious correlation to the lunar position or the other orbital parameters. This behavior is also found for the global hologram.

Finally, we examined the properties of the semidiurnal tide with respect to the frequency and vertical wavelength at the MLT before and during the SSW as well as during the amplitude enhancement after the SSW. The vertical wavelength of the semidiurnal tide was about 50-60 km before the SSW at altitudes between 74-100 km. The same vertical wavelength was observed during the tide enhancement. During the SSW event the vertical wavelength suddenly increased to 150-600 km at Juliusruh

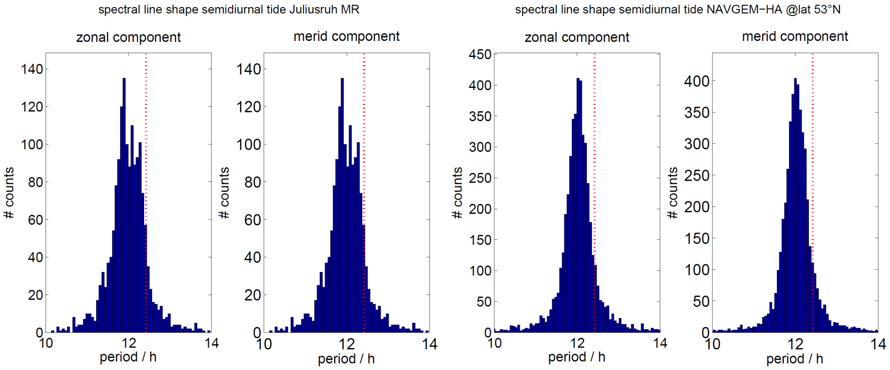

Figure 14. Histograms for the zonal and meridional frequency shift due to a temporal variable phase derived from the holograms. The left two panels show the local meteor radar observations at Juliusruh and the right two panels the global diagnostic inferred from NAVGEM-HA.

and then decreased just as suddenly after the wind reversal, but before the tide enhancement. The global zonal mean diagnostic exhibit similar vertical wavelengths before and after the SSW, but the sudden response in vertical wavelength due to the SSW was less pronounced. However, the hologram also shows that the mean period of the S2/SW2 tide before the SSW and during the tide enhancement is centered around 12.0 h. This does not indicate a lunar tide enhancement, which would require a 12.42 h period. Only during the SSW event itself do the increase in vertical wavelength and the shift of the period towards the M2 period together point to a lunar tide signature that could be interpreted as Pekeris resonance. However, this needs to be investigated with comprehensive models to account for the complex dynamics associated with a SSW.

Previous analysis of the lunar tide facilitating multi-year observations from meteor radars by Sandford et al. (2006) showed that the signal is much weaker compared to the total S2 tide. Their spectral analysis also confirms that tides show some spectral broadening. Such a line broadening is also found in our holographic analysis.

Fig. 14 shows the histograms of the frequency distributions obtained from the holograms. The left two panels are computed from the meteor radar observations at Juliusruh (zonal and meridional) and the right two panels from the global diagnostic using NAVGEM-HA at the same latitude (zonal and meridional, respectively). The spectral line shape seems to agree from their general morphology, in particular, the line width. The vertical dashed line denotes the period of the lunar tide M2, which lies in the natural line width of the SW2 tide. However, the peak of the spectral line obtained from the meteor radar observations at Juliusruh shows two side peaks that can be associated to the vortex splitting event and are related to the planetary wave activity during the winter 2012/13. Due to instrumental effects the number of measurements is not equally distributed over the winter season leading to an apparent double peak structure. The same plot obtained from NAVGEM-HA at the Juliusruh location shows a fully symmetric spectral line shape similar to the global diagnostic. During the vortex displacement event in the winter season 2009/10 the spectral line at Juliusruh is entirely symmetric similar to the global diagnostic for both cases. The global diagnostic is not prone to this type of effect as all longitudes are included in the analysis and, hence, these particularities average out. In the case of lunar tide amplification the global diagnostic should reveal a shoulder at the M2 period or asymmetry around the dashed vertical line, which seems to be not present.

Similar to previous studies (Fuller-Rowell et al., 2010, 2016), we attribute the day-to-day variability of the semidiurnal tidal amplitudes and phases to changes of the zonal winds in the middle atmosphere altering the vertical propagation conditions. Although atmospheric tides are global scale waves, their vertical propagation depends on the regional meteorological situation. As a consequence, the observed period or phase at the MLT can be altered. Due to the long horizontal wavelength of the semidiurnal tide, a change in the wind pattern in the middle atmosphere manifests as changes in phase for a single station measurement accompanied by a change of the vertical wavelength of the tide. The holographic reconstruction shows that the day-to-day variability of phase is equivalent to a Doppler shifting of the intrinsic tidal frequency, which causes the line broadening at the MLT.

6 Conclusions

In this study, we cross-validate NAVGEM-HA meteorological analyses with ground-based meteor radar and lidar observations at mid- and high latitudes. For the validation, we performed a detailed analysis of mean winds and temperatures and atmospheric tides using a recently developed tool called adaptive spectral filter (ASF), which is designed to capture the intermittent tidal behavior and provide vector information for mean winds and tides for climatologies. We present a comparison of mean winds, temperatures and the semidiurnal wind tide and its phase behavior and a detailed discussion of the day-to-day variability of the semidiurnal tide during two SSW events in 2009/10 and 2012/13 combining global and local diagnostics. We discussed our results in the context of previous studies, in particular, on the lunar tide amplification during SSWs and have outlined potential issues due to the day-to-day semidiurnal tidal variability. The agreement between MR/lidar climatologies and NAVGEM-HA analysis data is remarkably good compared to the seasonal wind and temperature pattern of comprehensive models. NAVGEM-HA tends to show slightly higher wind speeds and temperatures compared to the ground-based instruments. NAVGEM-HA reproduces the seasonal asymmetry of the zonal wind at mid- and high latitudes. The temperature and wind fields in NAVGEM-HA are realistic compared to ground-based sensors up to an altitude of 90 km (geometric altitude). However, our comparison also confirms that the availability of satellites observations for the data assimilation in NAVGEM-HA has an impact on the overall agreement. Further, the meteorological analysis reflects the seasonal phase behavior of the semidiurnal tide, which is constantly changing. These continuous phase changes are important and need to be considered when analyzing satellite observations or spectral analysis using long windows.

NAVGEM-HA reflects the day-to-day variability of the wind and semidiurnal tide amplitude and phase behavior during SSW events. The combination of NAVGEM-HA meteorological analysis data and ground-based observations allowed us to develop new diagnostics to retrieve atmospheric information and to investigate physical processes. The cross-validation suggests that the global fields of NAVGEM-HA provide a realistic boundary to nudge other GCMs coupling the middle atmosphere to the upper atmosphere. In particular, the good agreement of the tidal phases is an essential quality benchmark for the lower forcing of the thermosphere and ionosphere through atmospheric tides. The day-to-day tidal variability (amplitude and phase) of the semidiurnal tide is associated to changes in the wind pattern in the middle atmosphere altering the vertical propagation conditions of the tide. This is in agreement with previous studies by Fuller-Rowell et al. (2010); Jin et al. (2012); Fuller-Rowell et al. (2016). Further, we did investigate a potential lunar tide amplification through the Pekeris resonance effect as proposed by Forbes and Zhang (2012); Zhang and Forbes (2014). The ASF and holographic analysis permit to determine the different phases of the SSW 2012/13 and the tidal response in much more detail with respect to the timing. The tidal enhancement after the SSW, which was in many previous studies termed to be a lunar tidal enhancement, shows essentially a period around 12.0 h (see holograms) and has the same vertical wavelength of about 50-60 km than the semidiurnal tide before the SSW. The global diagnostic also confirms a wavenumber 2 structure. Further, there are no signs of a coupling and phase relation to the lunar orbit during this time. However, during the SSW there occurs a phase shift of the semidiurnal tide towards the 12.42 h period and the dynamical and thermal structure could be suitable to shift the Pekeris resonance towards a period of 12.42 h as well, as outlined in Forbes and Zhang (2012); Zhang and Forbes (2014). The increased vertical wavelength of about 150-400 km and the time span of 3-5 days during this phase of the SSW might be the result of the resonance and may indicate the presence of a lunar tidal mode, but this needs to be confirmed by tidal modelling and is beyond the discussion herein. However, the amplitude of this tidal mode is still much smaller than a typical semidiurnal tide, but might be larger than the average lunar amplitude of about 1-4 m/s (Sandford et al., 2006). Holographic analysis provide a new method to investigate the frequency behavior using short windows in the time domain, but keeping a localized measurement of the frequency resolution. Further, we were able to provide a quantitative spectral measurement of the spectral variability for the semidiurnal tide, which pointed out that the lunar tide (M2) lies well withing the spectral line shape. This has now some implications for epoch analysis of the lunar tide from local observations. The holograms show that there are frequently shifts of the semidiurnal tide towards the M2 (12.42 h) that are disconnected to the lunar orbit, which means the lunar tide can hardly be inferred from such an analysis without additional information, for instance, the vertical wavelength of the lunar tide. In this work we have demonstrated the value of meteorological analysis data from NAVGEM-HA to investigate the day-to-day variability of tides in a global context and for local meteor radar observations. Such data sets are essential for nudging thermospheric and ionospheric models for space weather applications. Further, we emphasized that new analysis techniques are required to infer the tidal variability or to separate lunar tides from the semidiurnal tide. Holographic reconstructions and spectral line models for atmospheric tides might be part of such a solution.

Data availability. The meteor radar can be obtained from Gunter Stober upon request from the Leibniz-Institute for Atmospheric Physics. The NAVGEM-HA data used in this study can be obtained from (https://map.nrl.navy.mil/map/pub/nrl/navgem/iap). The lidar observations are available upon request from Kathrin Baumgarten.

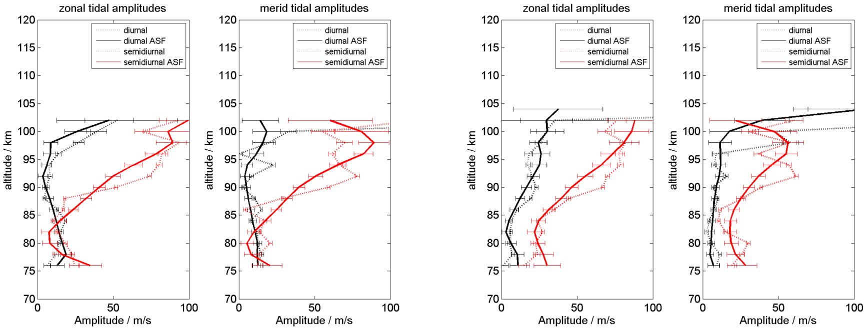

Figure A1. Here we show observations from 1st February 2010 and the Juliusruh meteor radar. The dashed lines indicate the tidal solution applying only temporal fitting and solid line shows the ASF solution with vertical regularization for the diurnal and semidiurnal tide.

Appendix A: Comparison of ASF with and without vertical regularization

Here we provide two examples comparing a tidal amplitude fit for the zonal and meridional component using the 1D ASF and the 2D ASF with vertical regularization to demonstrate how a potential contamination of gravity waves with short vertical wavelengths is reduced. The time difference between the left two panels and the right two panels is 6 hours.

Appendix B: Tidal components from global NAVGEM-HA analyzed winds

In addition to the semidiurnal tide locally observed from the meteor radar as well as from NAVGEM analyzed winds here we provide the results for the westward- and eastward-propagating non-migrating semidiurnal tidal components (SW1, SW3, SE1, SE2, SE3) as well as for the stationary semidiurnal tide (S0) during the winter 2009/2010 and 2012/2013 for the stations at Andenes and Juliusruh from the global fields of NAVGEM-HA.

Appendix C: Vertical wavelength from MR and NAVGEM-HA

Vertical wavelengths were derived from the vertical profiles of the phases of the semidiurnal tidal fit for every day. In the case of the meteor radar the fit is performed at altitudes between 74-100 km. The NAVGEM-HA data was analyzed in the altitude range from 70-90 km. However, as we estimate the vertical wavelengths from a rather thin atmospheric layer at the MLT, the uncertainty of the obtained wavelengths scales with the wavelength itself. There is a tendency that the uncertainties are larger for wavelengths beyond 250 km.

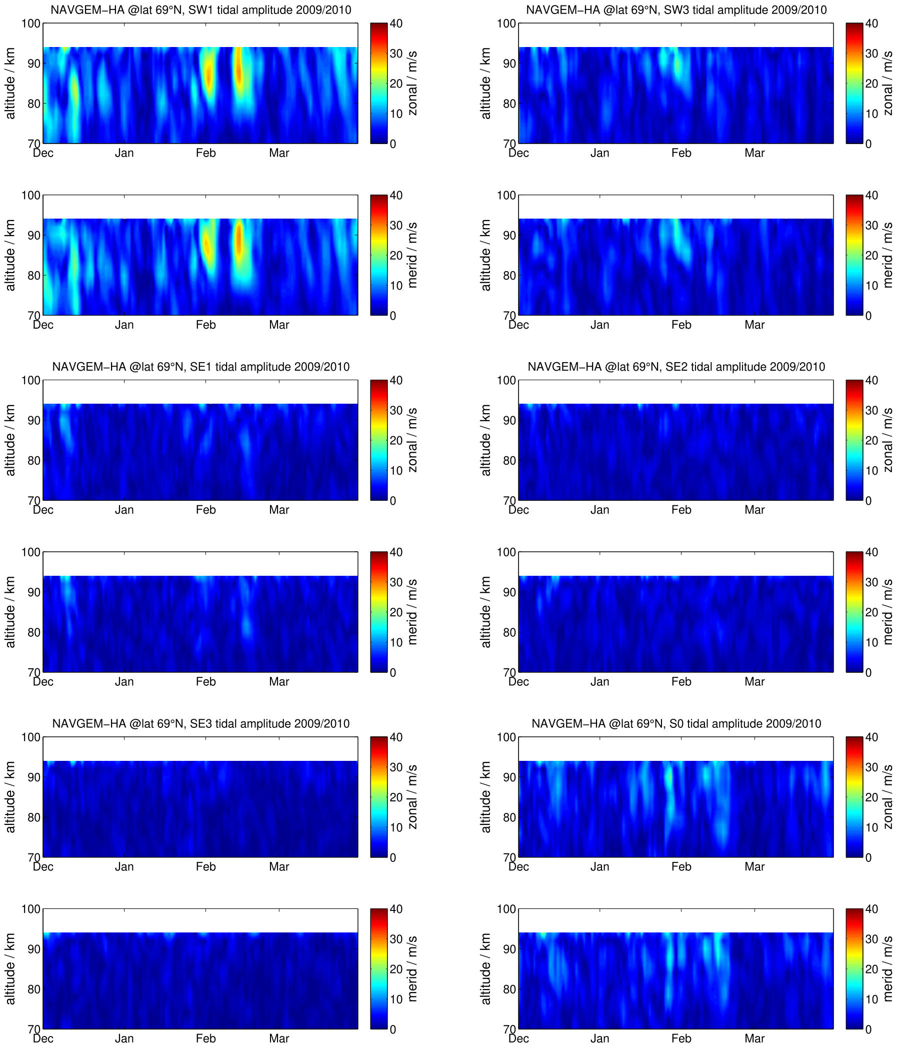

Figure B1. Non-migrating tides derived from global NAVGEM-HA winds above Andenes during the winter 2009/10 for SW1 and SW3 (upper two panels), SE1 and SE2 (middle panels), and SE3 and S0 (lower two panels) tidal components.

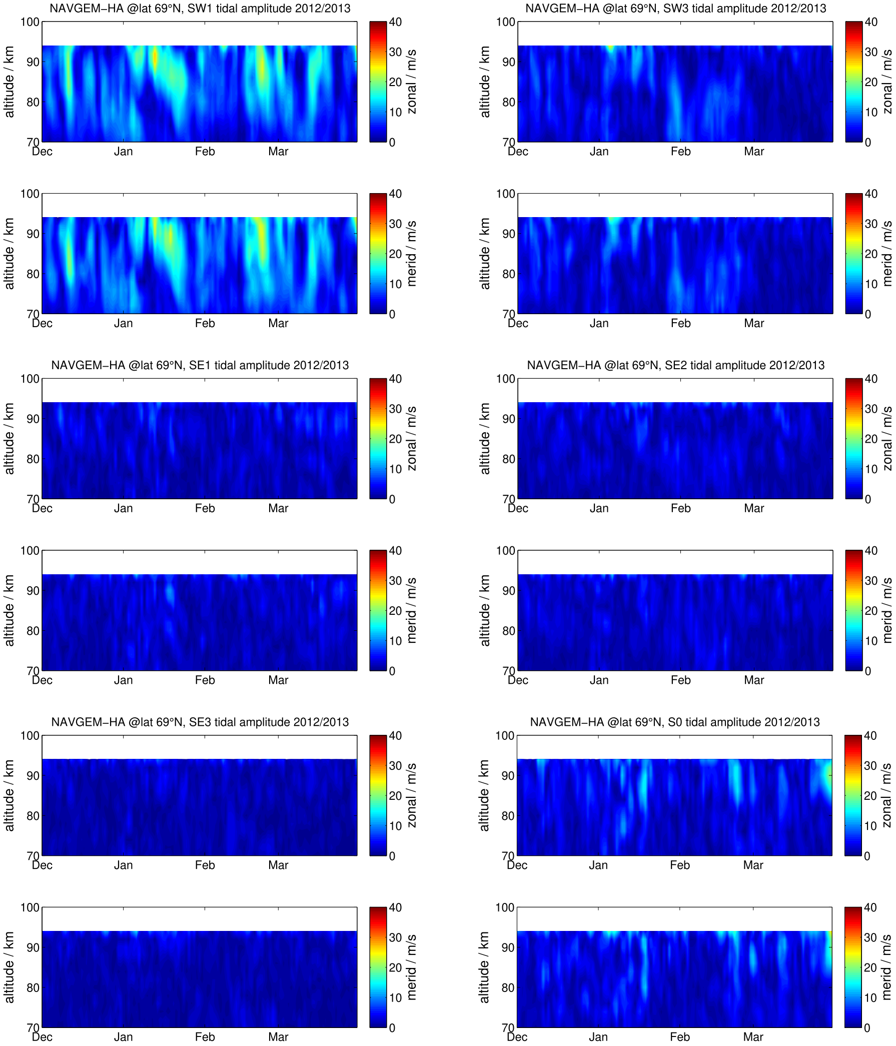

Figure B2. The same as Fig. 13 but for the winter 2012/2013.

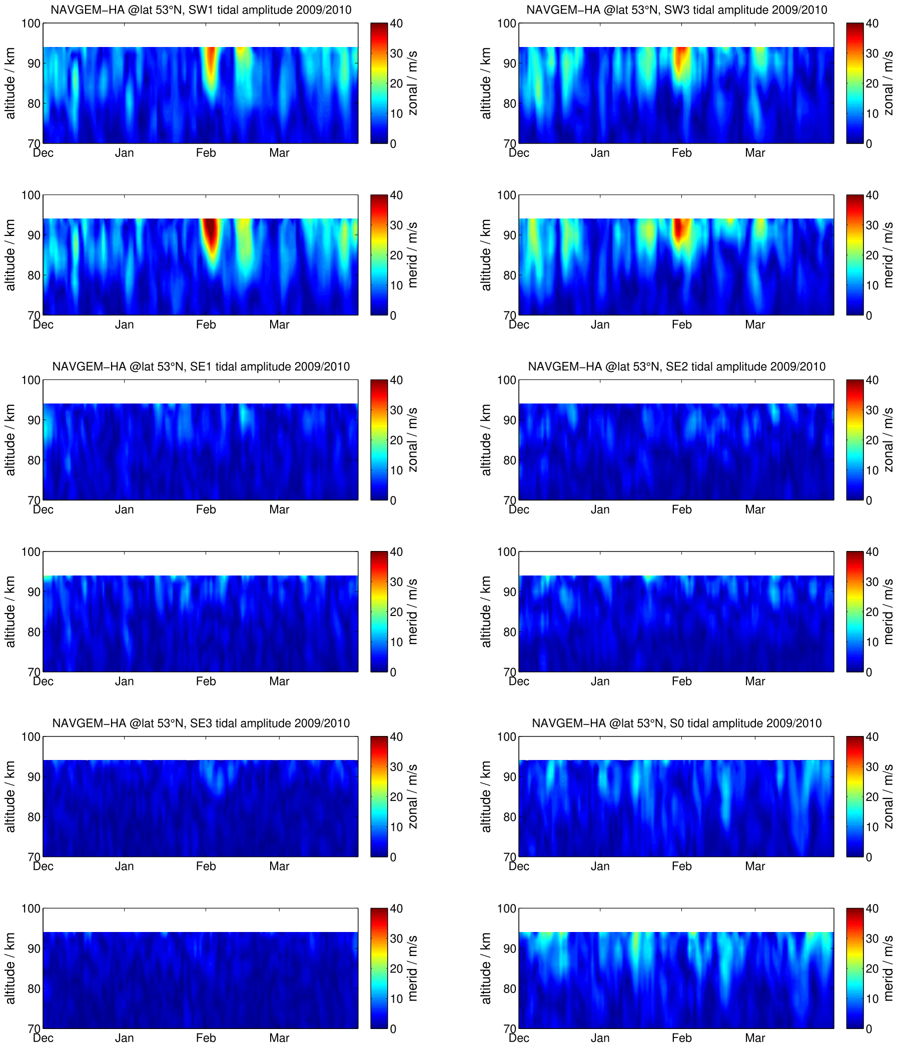

Figure B3. The same as Fig. 13 but above Juliusruh and for the winter 2009/2010.

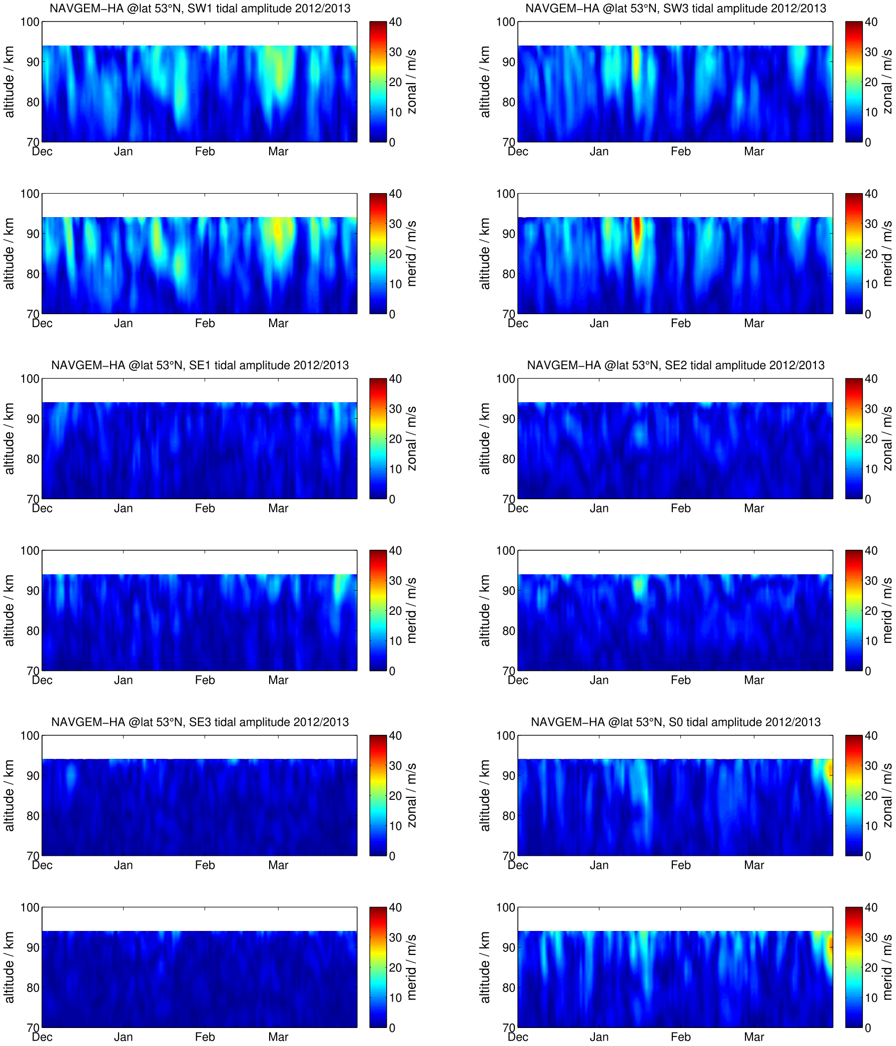

NAVGEM–HA @lat 53°N, SW1 tidal amplitude 2012/2013

NAVGEM–HA @lat 53°N, SW3 tidal amplitude 2012/2013

NAVGEM–HA @lat 53°N, SE1 tidal amplitude 2012/2013

NAVGEM–HA @lat 53°N, SE2 tidal amplitude 2012/2013

NAVGEM–HA @lat 53°N, SE3 tidal amplitude 2012/2013

NAVGEM–HA @lat 53°N, S0 tidal amplitude 2012/2013

Figure B4. The same as Fig. 13 but above Juliusruh and for the winter 2012/2013.

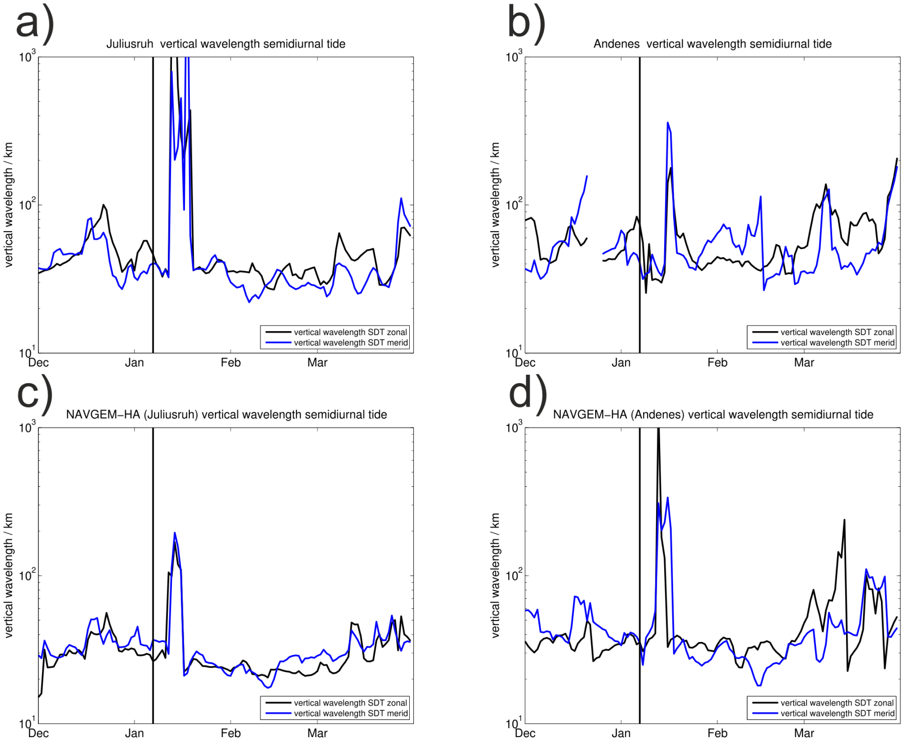

Figure C1. Time series of the vertical wavelength of the semidiurnal tide at Juliusruh and Andenes. The upper two panels a) and b) denote the meteor radar observations for both locations. The lower panels c) and d) are obtained from NAVGEM-HA.

Author contributions. The manuscript is edited and discussed with all authors. The conceptual idea of the manuscript was developed by Gunter Stober, Kathrin Baumgarten and John McCormack. The meteor radar data analysis is performed by Gunter Stober. Kathrin Baumgarten computed partly the lidar temperatures and analyzed both lidar data sets. Peter Brown contributed with the CMOR radar data, read and edited the manuscript and helped with the discussions. Jerry Czarnecki provided support in the data analysis and helped discussing the results.

Acknowledgements. This work is supported by the University of Bern Institute of Applied Physics and the Oeschger Center for Climate Change Research. Kathrin Baumgarten is supported by the Deutsche Forschungsgemeinschaft (DFG; German Research Foundation) under project LU1174/8-1 (PACOG) of the research unit FOR1898 within the Research Unit MS-GWaves. The work at the Naval Research Laboratory was supported by the Chief of Naval research and by a grant of computer time from the High Performance Computing Modernization Program. We gratefully acknowledge Michael Gerding, Michael Priester and Torsten Köpnick for the maintenance and operation of the lidar systems at IAP as well as all students for helping in lidar operation. We appreciate the support from Josef Höffner in computing the resonance lidar temperatures. We acknowledge the technical support of the IAP technicians in the operation of the meteor radars.

References

Akmaev, R. A.: WHOLE ATMOSPHERE MODELING: CONNECTING TERRESTRIAL AND SPACE WEATHER, Reviews of Geophysics, 49, https://doi.org/10.1029/2011RG000364, https://agupubs.onlinelibrary.wiley.com/doi/abs/10.1029/2011RG000364, 2011.

Alpers, M., Eixmann, R., Fricke-Begemann, C., Gerding, M., and Höffner, J.: Temperature lidar measurements from 1 to 105 km altitude using resonance, Rayleigh, and rotational Raman scattering, Atmos. Chem. Phys., 4, 793–800, 2004.

Andrews, D., Holton, J., and Leovy, C.: Middle Atmosphere Dynamics, International Geophysics, Elsevier Science, https://books.google.de/books?id=N1oNurYZefAC, 1987.

Baumgarten, K. and Stober, G.: On the evaluation of the phase relation between temperature and wind tides based on ground-based measurements and reanalysis data in the middle atmosphere, Annales Geophysicae, 37, 581–602, https://doi.org/10.5194/angeo-37-581-2019, https://www.ann-geophys.net/37/581/2019/, 2019.

Baumgarten, K., Gerding, M., and Lübken, F.-J.: Seasonal variation of gravity wave parameters using different filter methods with daylight lidar measurements at midlatitudes, Journal of Geophysical Research: Atmospheres, 122, 2683–2695, https://doi.org/10.1002/2016JD025916, https://agupubs.onlinelibrary.wiley.com/doi/abs/10.1002/2016JD025916, 2017.

Baumgarten, K., Gerding, M., Baumgarten, G., and Lübken, F.-J.: Temporal variability of tidal and gravity waves during a record long 10-day continuous lidar sounding, Atmospheric Chemistry and Physics, 18, 371–384, https://doi.org/10.5194/acp-18-371-2018, https://www.atmos-chem-phys.net/18/371/2018/, 2018.

Becker, E.: Dynamical Control of the Middle Atmosphere, Space Science Reviews, 168, 283–314, https://doi.org/10.1007/s11214-011-9841-5, http://dx.doi.org/10.1007/s11214-011-9841-5, 2012.

Becker, E.: Mean-Flow Effects of Thermal Tides in the Mesosphere and Lower Thermosphere, Journal of the Atmospheric Sciences, 74, 2043–2063, https://doi.org/10.1175/JAS-D-16-0194.1, https://doi.org/10.1175/JAS-D-16-0194.1, 2017.

Brown, P., Weryk, R., Wong, D., and Jones, J.: A meteoroid stream survey using the Canadian Meteor Orbit Radar: I. Methodology and radiant catalogue, Icarus, 195, 317–339, https://doi.org/https://doi.org/10.1016/j.icarus.2007.12.002, http://www.sciencedirect.com/science/article/pii/S0019103507005994, 2008.

Chandran, A. and Collins, R. L.: Stratospheric sudden warming effects on winds and temperature in the middle atmosphere at middle and low latitudes: a study using WACCM, Annales Geophysicae, 32, 859–874, https://doi.org/10.5194/angeo-32-859-2014, https://www.ann-geophys.net/32/859/2014/, 2014.

Chandran, A., Collins, R., and Harvey, V.: Stratosphere-mesosphere coupling during stratospheric sudden warming events, Advances in Space Research, 53, 1265–1289, https://doi.org/https://doi.org/10.1016/j.asr.2014.02.005, http://www.sciencedirect.com/science/article/pii/S0273117714000933, 2014.

Chapman, S. and Lindzen, R.: Atmospheric Tides: Thermal and Gravitational, Gordon and Breach, https://books.google.de/books?id=9kSRJaLJ9EEC, 1970.

Chau, J. L., Hoffmann, P., Pedatella, N. M., Matthias, V., and Stober, G.: Upper mesospheric lunar tides over middle and high latitudes during sudden stratospheric warming events, Journal of Geophysical Research: Space Physics, 120, 3084–3096, https://doi.org/10.1002/2015JA020998, https://agupubs.onlinelibrary.wiley.com/doi/abs/10.1002/2015JA020998, 2015.

Chen, C., Chu, X., McDonald, A. J., Vadas, S. L., Yu, Z., Fong, W., and Lu, X.: Inertia-gravity waves in Antarctica: A case study using simultaneous lidar and radar measurements at McMurdo/Scott Base (77.8°S, 166.7°E), Journal of Geophysical Research: Atmospheres, 118, 2794–2808, https://doi.org/10.1002/jgrd.50318, https://agupubs.onlinelibrary.wiley.com/doi/abs/10.1002/jgrd.50318, 2013.

Conte, J. F., Chau, J. L., Stober, G., Pedatella, N., Maute, A., Hoffmann, P., Janches, D., Fritts, D., and Murphy, D. J.: Climatology of semidiurnal lunar and solar tides at middle and high latitudes: Interhemispheric comparison, Journal of Geophysical Research: Space Physics, 122, 7750–7760, https://doi.org/10.1002/2017JA024396, https://agupubs.onlinelibrary.wiley.com/doi/abs/10.1002/2017JA024396, 2017.

Coy, L. and Pawson, S.: The Major Stratospheric Sudden Warming of January 2013: Analyses and Forecasts in the GEOS-5 Data Assimilation System, Monthly Weather Review, 143, 491–510, https://doi.org/10.1175/MWR-D-14-00023.1, https://doi.org/10.1175/MWR-D-14-00023.1, 2015.

Davis, R. N., Du, J., Smith, A. K., Ward, W. E., and Mitchell, N. J.: The diurnal and semidiurnal tides over Ascension Island (8° S, 14° W) and their interaction with the stratospheric quasi-biennial oscillation: studies with meteor radar, eCMAM and WACCM, Atmospheric Chemistry and Physics, 13, 9543–9564, https://doi.org/10.5194/acp-13-9543-2013, https://www.atmos-chem-phys.net/13/9543/2013/, 2013.

Dawkins, E. C. M., Feofilov, A., Rezac, L., Kutepov, A. A., Janches, D., Hoeffner, J., Chu, X., Lu, X., Mlynczak, M. G., and Russell, J.: Validation of SABER v2.0 Operational Temperature Data With Ground-Based Lidars in the Mesosphere-Lower Thermosphere Region (75-105 km), Journal of Geophysical Research: Atmospheres, 123, 9916–9934, https://doi.org/10.1029/2018JD028742, https://doi.org/10.1029/2018JD028742, 2018.

Dhadly, M. S., Emmert, J. T., Drob, D. P., McCormack, J. P., and Niciejewski, R. J.: Short-Term and Interannual Variations of Migrating Diurnal and Semidiurnal Tides in the Mesosphere and Lower Thermosphere, Journal of Geophysical Research: Space Physics, 123, 7106–7123, https://doi.org/10.1029/2018JA025748, https://agupubs.onlinelibrary.wiley.com/doi/abs/10.1029/2018JA025748, 2018.

Dörnbrack, A., Pitts, M. C., Poole, L. R., Orsolini, Y. J., Nishii, K., and Nakamura, H.: The 2009–2010 Arctic stratospheric winter – general evolution, mountain waves and predictability of an operational weather forecast model, Atmospheric Chemistry and Physics, 12, 3659–3675, https://doi.org/10.5194/acp-12-3659-2012, https://www.atmos-chem-phys.net/12/3659/2012/, 2012.

Du, J., Ward, W., Oberheide, J., Nakamura, T., and Tsuda, T.: Semidiurnal tides from the extended Canadian Middle Atmosphere Model (CMAM) and comparisons with TIMED Doppler interferometer (TIDI) and meteor radar observations, Journal of Atmospheric and Solar-Terrestrial Physics, 69, 2159 – 2202, https://doi.org/https://doi.org/10.1016/j.jastp.2007.07.014, http://www.sciencedirect.com/science/article/pii/S1364682607002234, vertical Coupling in the Atmosphere/Ionosphere System, 2007.

Eckermann, S. D., Hoppel, K. W., Coy, L., McCormack, J. P., Siskind, D. E., Nielsen, K., Kochenash, A., Stevens, M. H., Englert, C. R., Singer, W., and Hervig, M.: High-altitude data assimilation system experiments for the northern summer mesosphere season of 2007, Journal of Atmospheric and Solar-Terrestrial Physics, 71, 531 – 551, https://doi.org/https://doi.org/10.1016/j.jastp.2008.09.036, http://www.sciencedirect.com/science/article/pii/S1364682608002575, global Perspectives on the Aeronomy of the Summer Mesopause Region, 2009.

Eckermann, S. D., Ma, J., Hoppel, K. W., Kuhl, D. D., Allen, D. R., Doyle, J. A., Viner, K. C., Ruston, B. C., Baker, N. L., Swadley, S. D., Whitcomb, T. R., Reynolds, C. A., Xu, L., Kaifler, N., Kaifler, B., Reid, I. M., Murphy, D. J., and Love, P. T.: High-Altitude (0-100 km) Global Atmospheric Reanalysis System: Description and Application to the 2014 Austral Winter of the Deep Propagating Gravity Wave Experiment (DEEPWAVE), Monthly Weather Review, 146, 2639–2666, https://doi.org/10.1175/MWR-D-17-0386.1, https://doi.org/10.1175/MWR-D-17-0386.1, 2018.

Ehard, B., Kaifler, B., Kaifler, N., and Rapp, M.: Evaluation of methods for gravity wave extraction from middle-atmospheric lidar temperature measurements, Atmospheric Measurement Techniques, 8, 4645–4655, https://doi.org/10.5194/amt-8-4645-2015, https://www.atmos-meas-tech.net/8/4645/2015/, 2015.

Fejer, B. G., Olson, M. E., Chau, J. L., Stolle, C., Lühr, H., Goncharenko, L. P., Yumoto, K., and Nagatsuma, T.: Lunar-dependent equatorial ionospheric electrodynamic effects during sudden stratospheric warmings, Journal of Geophysical Research: Space Physics, 115, https://doi.org/10.1029/2010JA015273, https://agupubs.onlinelibrary.wiley.com/doi/abs/10.1029/2010JA015273, 2010.

Forbes, J. M.: Atmospheric tides: 1. Model description and results for the solar diurnal component, Journal of Geophysical Research: Space Physics, 87, 5222–5240, https://doi.org/10.1029/JA087iA07p05222, https://agupubs.onlinelibrary.wiley.com/doi/abs/10.1029/JA087iA07p05222, 1982.

Forbes, J. M. and Zhang, X.: Lunar tide amplification during the January 2009 stratosphere warming event: Observations and theory, Journal of Geophysical Research: Space Physics, 117, https://doi.org/10.1029/2012JA017963, https://agupubs.onlinelibrary.wiley.com/doi/abs/10.1029/2012JA017963, 2012.

Forbes, J. M., Zhang, X., Palo, S., Russell, J., Mertens, C. J., and Mlynczak, M.: Tidal variability in the ionospheric dynamo region, Journal of Geophysical Research: Space Physics, 113, https://doi.org/10.1029/2007JA012737, https://agupubs.onlinelibrary.wiley.com/doi/abs/10.1029/2007JA012737, 2008.

Fricke-Begemann, C., Alpers, M., and Höffner, J.: Daylight rejection with a new receiver for potassium resonance temperature lidars, Opt. Lett., 27, 1932–1934, https://doi.org/10.1364/OL.27.001932, http://ol.osa.org/abstract.cfm?URI=ol-27-21-1932, 2002.

Fritts, D. C., Miller, A. D., Kjellstrand, C. B., Geach, C., Williams, B. P., Kaifler, B., Kaifler, N., Jones, G., Rapp, M., Limon, M., Reimuller, J., Wang, L., Hanany, S., Gisinger, S., Zhao, Y., Stober, G., and Randall, C. E.: PMC Turbo: Studying Gravity Wave and Instability Dynamics in the Summer Mesosphere Using Polar Mesospheric Cloud Imaging and Profiling From a Stratospheric Balloon, Journal of Geophysical Research: Atmospheres, 124, 6423–6443, https://doi.org/10.1029/2019JD030298, https://agupubs.onlinelibrary.wiley.com/doi/abs/10.1029/2019JD030298, 2019.

Fuller-Rowell, T., Wu, F., Akmaev, R., Fang, T.-W., and Araujo-Pradere, E.: A whole atmosphere model simulation of the impact of a sudden stratospheric warming on thermosphere dynamics and electrodynamics, Journal of Geophysical Research: Space Physics, 115, https://doi.org/10.1029/2010JA015524, https://agupubs.onlinelibrary.wiley.com/doi/abs/10.1029/2010JA015524, 2010.

Fuller-Rowell, T. J., Fang, T.-W., Wang, H., Matthias, V., Hoffmann, P., Hocke, K., and Studer, S.: Impact of Migrating Tides on Electrodynamics During the January 2009 Sudden Stratospheric Warming, chap. 14, pp. 163–174, American Geophysical Union (AGU), https://doi.org/10.1002/9781118929216.ch14, https://agupubs.onlinelibrary.wiley.com/doi/abs/10.1002/9781118929216.ch14, 2016.

Gerding, M., Höffner, J., Lautenbach, J., Rauthe, M., and Lübken, F.-J.: Seasonal variation of nocturnal temperatures between 1 and 105 km altitude at 54° N observed by lidar, Atmospheric Chemistry and Physics, 8, 7465–7482, https://doi.org/10.5194/acp-8-7465-2008, https://www.atmos-chem-phys.net/8/7465/2008/, 2008.

Hauchecorne, A. and Chanin, M. L.: Density and Temperature Profiles obtained by Lidar between 35 and 70 km, Geophys. Res. Lett., 7, 565–568, 1980.

He, M., Chau, J. L., Stober, G., Li, G., Ning, B., and Hoffmann, P.: Relations Between Semidiurnal Tidal Variants Through Diagnosing the Zonal Wavenumber Using a Phase Differencing Technique Based on Two Ground-Based Detectors, Journal of Geophysical Research: Atmospheres, 123, 4015–4026, https://doi.org/10.1002/2018JD028400, https://agupubs.onlinelibrary.wiley.com/doi/abs/10.1002/2018JD028400, 2018.

Hocking, W., Fuller, B., and Vandepeer, B.: Real-time determination of meteor-related parameters utilizing modern digital technology, Journal of Atmospheric and Solar-Terrestrial Physics, 63, 155 – 169, https://doi.org/http://dx.doi.org/10.1016/S1364-6826(00)00138-3, http://www.sciencedirect.com/science/article/pii/S1364682600001383, radar applications for atmosphere and ionosphere research - PIERS 1999, 2001.

Hogan, T. F., Liu, M., Ridout, J. A., Peng, M. S., Whitcomb, T. R., Ruston, B. C., Reynolds, C. A., Eckermann, S. D., Moskaitis, J. R., Baker, N. L., McCormack, J. P., Viner, K. C., McLay, J. G., Flatau, M. K., Xu, L., Chen, C., and Chang, S. W.: The Navy Global Environmental Model, Oceanography, 27, https://doi.org/10.5670/oceanog.2014.73, 2014.

Jacobi, C., Hoffmann, P., and Kürschner, D.: Trends in MLT region winds and planetary waves, Collm (52° N, 15° E), Annales Geophysicae, 26, 1221–1232, https://doi.org/10.5194/angeo-26-1221-2008, https://www.ann-geophys.net/26/1221/2008/, 2008.

Jin, H., Miyoshi, Y., Pancheva, D., Mukhtarov, P., Fujiwara, H., and Shinagawa, H.: Response of migrating tides to the stratospheric sudden warming in 2009 and their effects on the ionosphere studied by a whole atmosphere-ionosphere model GAIA with COSMIC and TIMED/SABER observations, Journal of Geophysical Research: Space Physics, 117, https://doi.org/10.1029/2012JA017650, https://agupubs.onlinelibrary.wiley.com/doi/abs/10.1029/2012JA017650, 2012.

Jones Jr., M., Drob, D. P., Siskind, D. E., McCormack, J. P., Maute, A., McDonald, S. E., and Dymond, K. F.: Evaluating Different Techniques for Constraining Lower Atmospheric Variability in an Upper Atmosphere General Circulation Model: A Case Study During the 2010 Sudden Stratospheric Warming, Journal of Advances in Modeling Earth Systems, 10, 3076–3102, https://doi.org/10.1029/2018MS001440, https://agupubs.onlinelibrary.wiley.com/doi/abs/10.1029/2018MS001440, 2018.

Kuhl, D., Rosmond, T., Bishop, C., McLay, J., and Baker, N.: Comparison of hybrid ensemble/4DVar and 4DVar within the NAVDAS-AR data assimilation framework, Mon. Wea. Rev., 141, 2740–2758, https://doi.org/10.1175/MWR-D-12-00182.1, 2013.

Laskar, F. I., McCormack, J. P., Chau, J. L., Pallamraju, D., Hoffmann, P., and Singh, R. P.: Interhemispheric Meridional Circulation During Sudden Stratospheric Warming, Journal of Geophysical Research: Space Physics, 124, 7112–7122, https://doi.org/10.1029/2018JA026424, https://agupubs.onlinelibrary.wiley.com/doi/abs/10.1029/2018JA026424, 2019.

Lima, L. M., Paulino, A. R. S., Medeiros, A. F., Buriti, R. A., Batista, P. P., Clemesha, B. R., and Takahashi, H.: First observation of the diurnal and semidiurnal ocillation in the mesospheric winds over São João do Cariri-PB, Brazil, Revista Brasileira de Geofísica, 25, 35–41, http://www.scielo.br/scielo.php?script=sci_arttext&pid=S0102-261X2007000600005&nrm=iso, 2007.

Limpasuvan, V., Orsolini, Y. J., Chandran, A., Garcia, R. R., and Smith, A. K.: On the composite response of the MLT to major sudden stratospheric warming events with elevated stratopause, Journal of Geophysical Research: Atmospheres, 121, 4518–4537, https://doi.org/10.1002/2015JD024401, https://agupubs.onlinelibrary.wiley.com/doi/abs/10.1002/2015JD024401, 2016.

Lindzen, R. S.: Atmospheric Tides, Annual Review of Earth and Planetary Sciences, 7, 199–225, https://doi.org/10.1146/annurev.ea.07.050179.001215, https://doi.org/10.1146/annurev.ea.07.050179.001215, 1979.

Liu, H., Miyoshi, Y., Miyahara, S., Jin, H., Fujiwara, H., and Shinagawa, H.: Thermal and dynamical changes of the zonal mean state of the thermosphere during the 2009 SSW: GAIA simulations, Journal of Geophysical Research: Space Physics, 119, 6784–6791, https://doi.org/10.1002/2014JA020222, https://agupubs.onlinelibrary.wiley.com/doi/abs/10.1002/2014JA020222, 2014.

Liu, H.-L.: Variability and predictability of the space environment as related to lower atmosphere forcing, Space Weather, 14, 634–658, https://doi.org/10.1002/2016SW001450, https://agupubs.onlinelibrary.wiley.com/doi/abs/10.1002/2016SW001450, 2016.

Liu, H.-L., Wang, W., Richmond, A. D., and Roble, R. G.: Ionospheric variability due to planetary waves and tides for solar minimum conditions, Journal of Geophysical Research: Space Physics, 115, https://doi.org/10.1029/2009JA015188, https://agupubs.onlinelibrary.wiley.com/doi/abs/10.1029/2009JA015188, 2010.

Lomb, N. R.: Least-squares frequency analysis of unequally spaced data, Astrophysics and Space Science, 39, 447–462, https://doi.org/10.1007/BF00648343, http://dx.doi.org/10.1007/BF00648343, 1976.

Manney, G. L., Krüger, K., Pawson, S., Minschwaner, K., Schwartz, M. J., Daffer, W. H., Livesey, N. J., Mlynczak, M. G., Remsberg, E. E., Russell III, J. M., and Waters, J. W.: The evolution of the stratopause during the 2006 major warming: Satellite data and assimilated meteorological analyses, Journal of Geophysical Research: Atmospheres, 113, https://doi.org/10.1029/2007JD009097, https://agupubs.onlinelibrary.wiley.com/doi/abs/10.1029/2007JD009097, 2008.

Manney, G. L., Schwartz, M. J., Krüger, K., Santee, M. L., Pawson, S., Lee, J. N., Daffer, W. H., Fuller, R. A., and Livesey, N. J.: Aura Microwave Limb Sounder observations of dynamics and transport during the record-breaking 2009 Arctic stratospheric major warming, Geophysical Research Letters, 36, https://doi.org/10.1029/2009GL038586, https://agupubs.onlinelibrary.wiley.com/doi/abs/10.1029/2009GL038586, 2009.

Marsh, D. R.: Chemical–Dynamical Coupling in the Mesosphere and Lower Thermosphere, pp. 3–17, Springer Netherlands, Dordrecht, https://doi.org/10.1007/978-94-007-0326-1_1, https://doi.org/10.1007/978-94-007-0326-1_1, 2011.

Matsuno, T.: A Dynamical Model of the Stratospheric Sudden Warming, Journal of the Atmospheric Sciences, 28, 1479–1494, https://doi.org/10.1175/1520-0469(1971)028<1479:ADMOTS>2.0.CO;2, https://doi.org/10.1175/1520-0469(1971)028<1479:ADMOTS>2.0.CO;2, 1971.

Matthias, V., Hoffmann, P., Rapp, M., and Baumgarten, G.: Composite analysis of the temporal development of waves in the polar {MLT} region during stratospheric warmings, Journal of Atmospheric and Solar-Terrestrial Physics, 90 - 91, 86 – 96, https://doi.org/http://dx.doi.org/10.1016/j.jastp.2012.04.004, recent Progress in the Vertical Coupling in the Atmosphere-Ionosphere System, 2012.

Matthias, V., Hoffmann, P., Manson, A., Meek, C., Stober, G., Brown, P., and Rapp, M.: The impact of planetary waves on the latitudinal displacement of sudden stratospheric warmings, Annales Geophysicae, 31, 1397–1415, https://doi.org/10.5194/angeo-31-1397-2013, http://www.ann-geophys.net/31/1397/2013/, 2013.

McCormack, J., Hoppel, K., Kuhl, D., de Wit, R., Stober, G., Espy, P., Baker, N., Brown, P., Fritts, D., Jacobi, C., Janches, D., Mitchell, N., Ruston, B., Swadley, S., Viner, K., Whitcomb, T., and Hibbins, R.: Comparison of mesospheric winds from a high-altitude meteorological analysis system and meteor radar observations during the boreal winters of 2009-2010 and 2012-2013, Journal of Atmospheric and Solar-Terrestrial Physics, 154, 132 – 166, https://doi.org/http://dx.doi.org/10.1016/j.jastp.2016.12.007, http://www.sciencedirect.com/science/article/pii/S1364682616303182, 2017.

McCormack, J. P., Eckermann, S. D., and Hogan, T. F.: Generation of a Quasi-Biennial Oscillation in an NWP Model Using a Stochastic Gravity Wave Drag Parameterization, Monthly Weather Review, 143, 2121–2147, https://doi.org/10.1175/MWR-D-14-00208.1, https://doi.org/10.1175/MWR-D-14-00208.1, 2015.

Merzlyakov, E., Jacobi, C., Portnyagin, Y., and Solovjova, T.: Structural changes in trend parameters of the MLT winds based on wind measurements at Obninsk (55°N, 37°E) and Collm (52°N, 15°E), J. of Atmospheric and Solar-Terrestrial Physics, 71, 1547–1557, https://doi.org/https://doi.org/10.1016/j.jastp.2009.05.013, http://www.sciencedirect.com/science/article/pii/S1364682609001461, long-Term Changes and Trends in the Atmosphere-Ionosphere System, 2009.

Miyoshi, Y., Pancheva, D., Mukhtarov, P., Jin, H., Fujiwara, H., and Shinagawa, H.: Excitation mechanism of non-migrating tides, J. of Atmospheric and Solar-Terrestrial Physics, 156, 24–36, https://doi.org/https://doi.org/10.1016/j.jastp.2017.02.012, http://www.sciencedirect.com/science/article/pii/S1364682616302711, 2017.

Oberheide, J., Forbes, J. M., Häusler, K., Wu, Q., and Bruinsma, S. L.: Tropospheric tides from 80 to 400 km: Propagation, interannual variability, and solar cycle effects, Journal of Geophysical Research: Atmospheres, 114, https://doi.org/10.1029/2009JD012388, https://agupubs.onlinelibrary.wiley.com/doi/abs/10.1029/2009JD012388, 2009.

Oberheide, J., Forbes, J. M., Zhang, X., and Bruinsma, S. L.: Climatology of upward propagating diurnal and semidiurnal tides in the thermosphere, Journal of Geophysical Research: Space Physics, 116, https://doi.org/10.1029/2011JA016784, https://agupubs.onlinelibrary.wiley.com/doi/abs/10.1029/2011JA016784, 2011.

Pedatella, N. M. and Forbes, J. M.: Evidence for stratosphere sudden warming-ionosphere coupling due to vertically propagating tides, Geophysical Research Letters, 37, https://doi.org/10.1029/2010GL043560, https://agupubs.onlinelibrary.wiley.com/doi/abs/10.1029/2010GL043560, 2010.

Pedatella, N. M. and Maute, A.: Impact of the semidiurnal lunar tide on the midlatitude thermospheric wind and ionosphere during sudden stratosphere warmings, Journal of Geophysical Research: Space Physics, 120, 10,740–10,753, https://doi.org/10.1002/2015JA021986, https://agupubs.onlinelibrary.wiley.com/doi/abs/10.1002/2015JA021986, 2015.

Pedatella, N. M., Liu, H.-L., and Richmond, A. D.: Atmospheric semidiurnal lunar tide climatology simulated by the Whole Atmosphere Community Climate Model, Journal of Geophysical Research: Space Physics, 117, https://doi.org/10.1029/2012JA017792, https://agupubs.onlinelibrary.wiley.com/doi/abs/10.1029/2012JA017792, 2012.

Pedatella, N. M., Fuller-Rowell, T., Wang, H., Jin, H., Miyoshi, Y., Fujiwara, H., Shinagawa, H., Liu, H.-L., Sassi, F., Schmidt, H., Matthias, V., and Goncharenko, L.: The neutral dynamics during the 2009 sudden stratosphere warming simulated by different whole atmosphere models, Journal of Geophysical Research: Space Physics, 119, 1306–1324, https://doi.org/10.1002/2013JA019421, https://agupubs.onlinelibrary.wiley.com/doi/abs/10.1002/2013JA019421, 2014.

Pokhotelov, D., Becker, E., Stober, G., and Chau, J. L.: Seasonal variability of atmospheric tides in the mesosphere and lower thermosphere: meteor radar data and simulations, Annales Geophysicae, 36, 825–830, https://doi.org/10.5194/angeo-36-825-2018, https://www.ann-geophys.net/36/825/2018/, 2018.

Portnyagin, Y., Forbes, J., Fraser, G., Vlncent, R., Avery, S., Lysenko, I., and Makarov, N.: Dynamics of the Antarctic and Arctic mesosphere and lower thermosphere regions II. The semidiurnal tide, J. of Atmospheric and Terrestrial Physics, 55, 843–855, https://doi.org/https://doi.org/10.1016/0021-9169(93)90025-T, http://www.sciencedirect.com/science/article/pii/002191699390025T, 1993.

Portnyagin, Y. I., Solovjova, T. V., Makarov, N. A., Merzlyakov, E. G., Manson, A. H., Meek, C. E., Hocking, W., Mitchell, N., Pancheva, D., Hoffmann, P., Singer, W., Murayama, Y., Igarashi, K., Forbes, J. M., Palo, S., Hall, C., and Nozawa, S.: Monthly mean climatology of the prevailing winds and tides in the Arctic mesosphere/lower thermosphere, Annales Geophysicae, 22, 3395–3410, https://doi.org/10.5194/angeo-22-3395-2004, https://www.ann-geophys.net/22/3395/2004/, 2004.

Rüfenacht, R., Baumgarten, G., Hildebrand, J., Schranz, F., Matthias, V., Stober, G., Lübken, F.-J., and Kämpfer, N.: Intercomparison of middle-atmospheric wind in observations and models, Atmospheric Measurement Techniques, 11, 1971–1987, https://doi.org/10.5194/amt-11-1971-2018, https://www.atmos-meas-tech.net/11/1971/2018/, 2018.

Sandford, D. J., Muller, H. G., and Mitchell, N. J.: Observations of lunar tides in the mesosphere and lower thermosphere at Arctic and middle latitudes, Atmospheric Chemistry and Physics, 6, 4117–4127, https://doi.org/10.5194/acp-6-4117-2006, https://www.atmos-chem-phys.net/6/4117/2006/, 2006.

Scargle, J. D.: Studies in astronomical time series analysis. II - Statistical aspects of spectral analysis of unevenly spaced data, Astrophysical Journal, 263, 835–853, 1982.

Schranz, F., Hagen, J., Stober, G., Hocke, K., Murk, A., and Kämpfer, N.: Small-scale variability of stratospheric ozone during the SSW 2018/2019 observed at Ny-Ålesund, Svalbard, Atmospheric Chemistry and Physics Discussions, 2019, 1–25, https://doi.org/10.5194/acp-2019-1093, https://www.atmos-chem-phys-discuss.net/acp-2019-1093/, 2019.

Schwartz, M., Lambert, A., Manney, G., Read, W., Livesey, N., Froidevaux, L., Ao, C., Bernath, P., Boone, C., Cofield, R., Daffer, W., Drouin, B., Fetzer, E., Fuller, R., Jarnot, R., Jiang, J., Jiang, Y., Knosp, B. W., Krüger, K., Li, J.-L., Mlynczak, M., Pawson, S., Russell, J., Santee, M., Snyder, W., Stek, P., Thurstans, R., Tompkins, A., Wagner, P., Walker, K., Waters, J. W., and Wu, D. L.: Validation of the Aura Microwave Limb Sounder temperature and geopotential height measurements, Journal of Geophysical Research: Atmospheres, 113, https://doi.org/10.1029/2007JD008783, http://dx.doi.org/10.1029/2007JD008783, d15S11, 2008.

Shibuya, R., Sato, K., Tsutsumi, M., Sato, T., Tomikawa, Y., Nishimura, K., and Kohma, M.: Quasi-12 h inertia–gravity waves in the lower mesosphere observed by the PANSY radar at Syowa Station (39.6° E, 69.0° S), Atmospheric Chemistry and Physics, 17, 6455–6476, https://doi.org/10.5194/acp-17-6455-2017, https://www.atmos-chem-phys.net/17/6455/2017/, 2017.

Siddiqui, T. A., Yamazaki, Y., Stolle, C., Lühr, H., Matzka, J., Maute, A., and Pedatella, N.: Dependence of Lunar Tide of the Equatorial Electrojet on the Wintertime Polar Vortex, Solar Flux, and QBO, Geophysical Research Letters, 45, 3801–3810, https://doi.org/10.1029/2018GL077510, https://agupubs.onlinelibrary.wiley.com/doi/abs/10.1029/2018GL077510, 2018.

Smith, A. K.: Global Dynamics of the MLT, Surveys in Geophysics, 33, 1177–1230, https://doi.org/10.1007/s10712-012-9196-9, https://doi.org/10.1007/s10712-012-9196-9, 2012.

Stober, G., Latteck, R., Rapp, M., Singer, W., and Zecha, M.: MAARSY - the new MST radar on Andøya: first results of spaced antenna and Doppler measurements of atmospheric winds in the troposphere and mesosphere using a partial array, Advances in Radio Science, 10, 291–298, https://doi.org/10.5194/ars-10-291-2012, http://www.adv-radio-sci.net/10/291/2012/, 2012.

Stober, G., Matthias, V., Jacobi, C., Wilhelm, S., Höffner, J., and Chau, J. L.: Exceptionally strong summer-like zonal wind reversal in the upper mesosphere during winter 2015/16, Annales Geophysicae, 35, 711–720, https://doi.org/10.5194/angeo-35-711-2017, https://www.ann-geophys.net/35/711/2017/, 2017.

Stober, G., Chau, J. L., Vierinen, J., Jacobi, C., and Wilhelm, S.: Retrieving horizontally resolved wind fields using multi-static meteor radar observations, Atmospheric Measurement Techniques, 11, 4891–4907, https://doi.org/10.5194/amt-11-4891-2018, https://www.atmos-meas-tech.net/11/4891/2018/, 2018.

Stockwell, R. G., Mansinha, L., and Lowe, R. P.: Localization of the complex spectrum: the S transform, IEEE Transactions on Signal Processing, 44, 998–1001, https://doi.org/10.1109/78.492555, 1996.

Stray, N. H., Orsolini, Y. J., Espy, P. J., Limpasuvan, V., and Hibbins, R. E.: Observations of planetary waves in the mesosphere-lower thermosphere during stratospheric warming events, Atmospheric Chemistry and Physics, 15, 4997–5005, https://doi.org/10.5194/acp-15-4997-2015, https://www.atmos-chem-phys.net/15/4997/2015/, 2015.

Torrence, C. and Compo, G. P.: A Practical Guide to Wavelet Analysis, Bull. Amer. Meteor. Soc., 79, 61–78, 1998.

Vial, F., Forbes, J. M., and Miyahara, S.: Some transient aspects of tidal propagation, Journal of Geophysical Research: Space Physics, 96, 1215–1224, https://doi.org/10.1029/90JA02181, https://agupubs.onlinelibrary.wiley.com/doi/abs/10.1029/90JA02181, 1991.

von Zahn, U. and Höffner, J.: Mesopause temperature profiling by potassium lidar, Geophysical Research Letters, 23, 141–144, https://doi.org/10.1029/95GL03688, https://agupubs.onlinelibrary.wiley.com/doi/abs/10.1029/95GL03688, 1996.

Wang, H., Boyd, J. P., and Akmaev, R. A.: On computation of Hough functions, Geoscientific Model Development, 9, 1477–1488, https://doi.org/10.5194/gmd-9-1477-2016, https://www.geosci-model-dev.net/9/1477/2016/, 2016.

Ward, W. E., Oberheide, J., Goncharenko, L. P., Nakamura, T., Hoffmann, P., Singer, W., Chang, L. C., Du, J., Wang, D.-Y., Batista, P., Clemesha, B., Manson, A. H., Riggin, D. M., She, C.-Y., Tsuda, T., and Yuan, T.: On the consistency of model, ground-based, and satellite observations of tidal signatures: Initial results from the CAWSES tidal campaigns, Journal of Geophysical Research: Atmospheres, 115, https://doi.org/10.1029/2009JD012593, https://agupubs.onlinelibrary.wiley.com/doi/abs/10.1029/2009JD012593, 2010.

Wilhelm, S., Stober, G., and Chau, J. L.: A comparison of 11-year mesospheric and lower thermospheric winds determined by meteor and MF radar at 69° N, Annales Geophysicae, 35, 893–906, https://doi.org/10.5194/angeo-35-893-2017, https://www.ann-geophys.net/35/893/2017/, 2017.

Wilhelm, S., Stober, G., and Brown, P.: Climatologies and long-term changes in mesospheric wind and wave measurements based on radar observations at high and mid latitudes, Annales Geophysicae, 37, 851–875, https://doi.org/10.5194/angeo-37-851-2019, https://www.ann-geophys.net/37/851/2019/, 2019.

Xu, F. and San Liang, X.: On the Generation and Maintenance of the 2012/13 Sudden Stratospheric Warming, Journal of the Atmospheric Sciences, 74, 3209–3228, https://doi.org/10.1175/JAS-D-17-0002.1, https://doi.org/10.1175/JAS-D-17-0002.1, 2017.

Xu, J., She, C. Y., Yuan, W., Mertens, C., Mlynczak, M., and Russell, J.: Comparison between the temperature measurements by TIMED/SABER and lidar in the midlatitude, Journal of Geophysical Research: Space Physics (1978–2012), 111, https://doi.org/10.1029/2005JA011439, https://doi.org/10.1029/2005JA011439, 2006.

Yu, Y., Wan, W., Ning, B., Liu, L., Wang, Z., Hu, L., and Ren, Z.: Tidal wind mapping from observations of a meteor radar chain in December 2011, Journal of Geophysical Research: Space Physics, 118, 2321–2332, https://doi.org/10.1029/2012JA017976, https://agupubs.onlinelibrary.wiley.com/doi/abs/10.1029/2012JA017976, 2013.

Zhang, X. and Forbes, J. M.: Lunar tide in the thermosphere and weakening of the northern polar vortex, Geophysical Research Letters, 41, 8201–8207, https://doi.org/10.1002/2014GL062103, https://agupubs.onlinelibrary.wiley.com/doi/abs/10.1002/2014GL062103, 2014.

Zhang, X., Forbes, J. M., Hagan, M. E., Russell III, J. M., Palo, S. E., Mertens, C. J., and Mlynczak, M. G.: Monthly tidal temperatures 20–120 km from TIMED/SABER, Journal of Geophysical Research: Space Physics, 111, https://doi.org/10.1029/2005JA011504, https://agupubs.onlinelibrary.wiley.com/doi/abs/10.1029/2005JA011504, 2006.

Zülicke, C., Becker, E., Matthias, V., Peters, D. H. W., Schmidt, H., Liu, H.-L., Ramos, L. d. l. T., and Mitchell, D. M.: Coupling of Stratospheric Warmings with Mesospheric Coolings in Observations and Simulations, Journal of Climate, 31, 1107–1133, https://doi.org/10.1175/JCLI-D-17-0047.1, https://doi.org/10.1175/JCLI-D-17-0047.1, 2018.

Comparative study between ground-based observations and NAVGEM-HA analysis data in the MLT region

Gunter Stober[1,2], Kathrin Baumgarten[2,3], John P. McCormack[4], Peter Brown[5,6], and Jerry Czarnecki[2]

[1]Institute of Applied Physics, Microwave Physics, University of Bern, Bern, Switzerland
[2]Leibniz-Institute of Atmospheric Physics at the University of Rostock, Kühlungsborn, Germany
[3]Fraunhofer Institute for Computer Graphics Research IGD, Rostock, Germany
[4]Space Science Division, Naval Research Laboratory, Washington DC
[5]Dept. of Physics and Astronomy, University of Western Ontario, London, Ontario, Canada N6A 3K7
[6]Western Institute for Earth and Space Exploration, University of Western Ontario, London, Ontario, N6A 5B7, Canada

Correspondence: gunter.stober@iap.unibe.ch

Abstract. ~~Atmospheric waves are a key driving mechanism for the circulation in the Earth's atmosphere. Such waves cover various spatial and temporal scales, e.g., planetary waves with periods of several days, atmospheric tides with periods of an integer fraction of a day and gravity waves with periods ranging from minutes to several hours. In particular, atmospheric tides gain large amplitudes at the Mesosphere/lower Thermosphere~~ Recent studies have shown that day-to-day variability of the migrating semidiurnal (SW2) solar tide within the mesosphere and lower thermosphere (MLT) ~~region. Recently the day-to-day tidal variability as driver of~~ is a key driver of anomalies in the thermosphere-ionosphere system~~has become an emerging topic~~. Here we study the ~~intermittent behavior of atmospheric tides by~~ variability in both the amplitude and phase of SW2 using meteor radar wind and lidar temperature observations at altitudes of ~~75 – 110 km accompanied with lidar measurements. The observations are compared to meteorological analyses~~ 75-110 km as well as wind and temperature output from NAVGEM-HA~~to infer how well the tidal variability on a daily to a seasonal basis is captured in the model. Therefore, a new diagnostic approach, a so-called~~, a high-altitude meteorological analysis system. Application of a new adaptive spectral filter ~~, is used to decompose the time series into a mean wind (zonal and meridional component) and temperature containing the planetary wave activity, atmospheric tides (diurnal, semi-diurnal and terdiurnal) as well as the gravity wave activity. By combining the local radar data with global analysis fields, we extract the relative contribution of the~~ technique to both local radar wind observations and global NAVGEM-HA analyses offers an important cross-validation of both data sets and makes it possible to distinguish between migrating and non-migrating ~~tides for the available data using a global version of the adaptive spectral filter. Our results indicate that the migrating semidiurnal (SW2) tide~~tidal components, which is ~~the dominant mode at mid- and high latitudes at the MLT, shows a large seasonal variability in amplitude and phase. The comparison~~ difficult using local measurements alone. Comparisons of NAVGEM-HA~~results with meteor radarobservations demonstrate~~, meteor radar, and lidar observations over a 12-month period show that the meteorological ~~analysis~~ analyses consistently reproduces the ~~mean seasonal behavior~~ seasonal as well as ~~the~~ day-to-day variability ~~. This is especially obvious during sudden stratospheric warmings, where the~~ in mean winds, mean temperatures, and SW2 ~~tide shows~~ features from the ground-based observations. This study also examines in detail the day-to-day variability in SW2 during two sudden stratospheric warming events that have

been implicated in producing ionospheric anomalies. During this period, both meteor radar and NAVGEM-HA winds show a significant phase shift and amplitude modulation~~. These findings show~~ , but no signs of coupling to the lunar tide as previous studies have suggested. Overall, these findings demonstrate the benefit of combining global high altitude ~~data assimilation products~~ meteorological analyses with ground-based observations of the MLT region to better understand the tidal variability in the atmosphere.

1 Introduction

There is a growing need to understand the global wind field from the surface up to the lower thermosphere (0-100 km) and beyond as well as its day-to-day variability due to meteorological processes. Planetary waves and atmospheric tides are dominant drivers at the mesosphere and lower thermosphere (MLT) that provide a highly variable dynamical lower boundary to the thermospheric/ionospheric system, e.g. at the equatorial dynamo region at altitudes from 100 to 150 km ~~(see, e.g. Akmaev, 2011, and references therein)~~(see, e.g., Akmaev, 2011, and references therein). The upward propagation of these drivers from their source regions near the surface into the MLT region is determined in large part by the global wind field. Accurate assessments of both daily and seasonal variability in winds and tidal modes has therefore become necessary for better understanding lower atmospheric forcing of the thermosphere/ionosphere system.

At mid- and polar latitudes planetary waves provide a significant contribution to the variability of the winter MLT and play a major role in vertical coupling processes between the different atmospheric layers. For example, during sudden stratospheric warmings (SSWs) (Matsuno, 1971; Andrews et al., 1987) the whole middle atmosphere (stratosphere/mesosphere) responds to sudden reversals of the zonal wind from eastward to westward and back to eastward accompanied by an increase of the stratospheric temperature and a mesospheric cooling (see, e.g. Chandran et al., 2014; Zülicke et al., 2018, , and references therin). SSWs are often studied using ~~Global~~ General Circulation Models (GCMs), which are either free-running (e.g., GAIA, WACCM, KMCM, Jin et al. (2012); Liu et al. (2010); Becker (2017); Zülicke et al. (2018)) or nudged to reanalysis fields (e.g., SD-WACCM, Marsh (2011); Stray et al. (2015); Limpasuvan et al. (2016)). Manney et al. (2008, 2009) characterized the SSW in 2006 as a vortex displacement and the SSW in 2009 as a vortex splitting event making use of global satellite observations (MLS-Microwave Limb Sounder) and data assimilated reanalysis mostly at the stratosphere and lower mesosphere. Matthias et al. (2013) investigated the role of planetary waves in the evolution of vortex splitting and displacement events combining satellite data and ground-based observations.

Atmospheric tides are generated in the troposphere and stratosphere mostly through the absorption of sunlight by water vapor and ozone ~~(e.g., Lindzen, 1979)~~(e.g., Lindzen, 1979). They have been studied theoretically ~~(e.g. Chapman and Lindzen, 1970; Forbes, 198~~

(e.g., Chapman and Lindzen, 1970; Forbes, 1982; Wang et al., 2016) and from observations ~~(e.g. Portnyagin et al., 1993; Merzlyakov et al~~ (e.g., Portnyagin et al., 1993; Merzlyakov et al., 2009; Oberheide et al., 2009, 2011, and references therein) for decades. More recent studies analyzed the response of the semidiurnal tide during SSWs using ground-based instruments and nudged GCM data or investigated the relative importance and impact of the semidiurnal lunar tide during SSWs with TIME-GCM and WACCM (Pedatella et al., 2012; Pedatella and Maute, 2015). However, atmospheric tides propagate from their source region up to the MLT through a constantly varying altitude dependent wind and temperature field, which significantly modifies the phase of the tides, depending on their vertical wavelength, as well as the vertical wavelength itself.

In this study, we compare local meteor radar (MR) wind observations as well as lidar temperature measurements with meteorological analyses produced with NAVGEM-HA (Navy Global Environmental Model - High Altitude), a data assimilation and modeling system that extends from the surface to the lower thermosphere. NAVGEM-HA fields were ~~availble~~ available from December 2009 to December 2010 and during the winter season 2012/13 starting in December 2012 until March 2013. Recent studies (Eckermann et al., 2018; McCormack et al., 2017) have presented initial cross-validation of the mesospheric winds from NAVGEM-HA for two winter seasons using worldwide distributed MR measurements. Here, we extend these initial comparisons to include seasonal mean winds (30-day median) from NAVGEM-HA and from three MRs at mid- to high latitudes for the year 2010. Time series of both NAVGEM-HA analysed winds and MR measurements are decomposed into daily mean winds, tides and GW residuals using a recently introduced analysis technique called adaptive spectral filter (ASF) (Stober et al., 2017; Pokhotelov et al., 2018; Wilhelm et al., 2019; Baumgarten and Stober, 2019). This technique is designed to extract daily mean winds and tidal variations on a day-to-day basis. In addition to MR measurements, we also present the first comparison between midlatitude temperature observations from a resonance lidar and NAVGEM-HA analysed temperatures for the 2010 period.~~Finally, we present a detailed comparison of two SSWs in 2009/10 and 2012/13 and outline how the semidiurnal tide responds to changes in the background wind concerning the tidal phase and amplitude. Overall, the results of these comparisons show very good agreement between NAVGEM-HA analysed winds and MR observations, highlighting the utility of combining global high altitude data assimilation products with ground-based observations of the MLT to better understand tidal variability over daily to seasonal time scales.~~

~~Further, we present a cross-comparison of mean winds and semidiurnal tidal day-to-day variability during two SSW events. Such short time variations are essential for the understanding of the forcing from below of the thermosphere and ionosphere (Liu, 2016).~~ Meteorological analysis data, such as NAVGEM-HA, provide a much more realistic forcing of the upper atmosphere due to tides and mean winds compared to current versions of other comprehensive models. ~~Chandran and Collins (2014)~~ Chandran and Collins (2014) investigated SSW events using WACCM-SD nudged with reanalysis fields from the GEOS-5.2 reanalysis system up to an altitude of about 40 km. However, at altitudes above 70-80 km the nudged model started to substantially deviate from the observed wind climatologies (Wilhelm et al., 2019). In particular, the nudged model showed a wind reversal from eastward to westwards winds between 70-80 km, which is not confirmed from the wind climatologies. Such reversal of the zonal wind can be also found in other comprehensive models or mechanistic models (Smith, 2012; Becker, 2012). ~~Liu (2016)~~ Liu (2016) shows a comparison among several GCMs indicating that there are substantial deviations at the mesosphere and upper atmosphere, although each of the GCMs was nudged up to the lower stratosphere (see also ~~Pedatella et al. (2014)~~ Pedatella et al. (2014) for more details). Only the GAIA model (Jin et al., 2012; Liu et al., 2014) showed during winter eastward winds at the MLT. Previously, the eCMAM model was also cross-validated with ground-based meteor radar observations to investigate mean winds and tides and their amplitude and phase behavior at equatorial latitudes (Du et al., 2007; Ward et al., 2010). They found a remarkably good agreement between the model and the local observations using 60-day running means underlining the value of such comparisons. The focus of the present study is to examine the degree of agreement between day-to-day and as well as seasonal variability in SW2 between a global meteorological analyses of the MLT region and ground-based observations as a means to, ultimately, better understand the origins of this variability. Finally, we perform a detailed comparison of SW2 variability from both NAVGEM-HA and meteor radar observations during the SSWs in 2009/10 and 2012/13, focusing in particular on how the amplitude and phase of semidiurnal variability in both data sets responds to changes in the background wind. Overall, the results of these comparisons show very good agreement between NAVGEM-HA analysed winds and MR observations, highlighting the utility of combining global high altitude data assimilation products with ground-based observations of the MLT to lend new insight into the causes of semidiurnal tidal variability over daily to seasonal time scales. Such short time variations are essential for the understanding of the forcing from below of the thermosphere and ionosphere (Liu, 2016). Therefore, the paper is structured as follows. First, we describe the observations for winds and temperatures in the MLT region and the corresponding meteorological analysis data in Section 2. Section 3 provides a detailed explanation of the methodology used for the data analysis. Section 4 presents the results for the climatology, comparing mean winds simultaneously seen in the meteor radar data at different locations with the NAVGEM-HA analysis data accompanied with available temperature measurements from a resonance lidar at one mid-latitude location. The results are also discussed for the semidiurnal tide for the whole year (2010) as well as during the winter season in 2010 and 2013 in Section 5. Finally, the findings are summarized and a conclusion is given in Section 6.

2 Data description

2.1 Wind observations

In this study, we compare the 3-hourly global synoptic wind and temperature analyses from NAVGEM-HA with meteor radar observations collected at three different latitudes in Andenes (69° N, 11° E) in Norway, Juliusruh (54.3° N, 13° E) in Germany and Tavistock (CMOR- Canadian Meteor Orbit Radar) (43.2° N, 80.7° W) in Canada. All three meteor radars use the same software for meteor detection and classification as described in Hocking et al. (2001). All systems were almost continuously in operation for the analyzed periods. Only the Andenes system shows some data gaps, mainly due to the more extreme weather conditions in Northern Norway, which caused some damage to the antennas and from time to time a power outage. A more detailed description of the CMOR radar can be found in Brown et al. (2008). A summary of the Juliusruh and Andenes MR is found in ~~Stober et al. (2012) and Wilhelm et al. (2017)~~Stober et al. (2012) and Wilhelm et al. (2017).

MLT winds are obtained with a temporal resolution of 1 hour and a vertical resolution of 2 km using the wind retrieval algorithm ~~as~~ presented in Stober et al. (2018), which is a further development of the wind analysis presented in Hocking et al. (2001). The wind analysis contains a full error propagation of the statistical uncertainties and a physical error model based on the vertical and temporal shear as spatio-temporal Laplace filter for each wind component. Contrary to many other meteor radar wind analysis, the algorithm also solves for the vertical wind velocity. The obtained mean vertical velocities show values of a few cm/s and are mainly used as quality control for successful convergence of the wind fit. In the present study, we use 4 meteors as a minimum for a successful wind fit.

2.2 Temperature observations

At Kühlungsborn (54° N, 12° E), around 118 km southwest of the meteor radar at Juliusruh, a resonance lidar was in operation until 2012 to ~~derive~~ observe temperatures in the MLT region. The potassium lidar measures the Doppler broadening of the 770 nm potassium D1 resonance line by scanning with a narrow band Alexandrite ring laser. The system is fully daylight capable. Further details can be found in von Zahn and Höffner (1996); Fricke-Begemann et al. (2002).

The extent of the potassium layer in the atmosphere limits the range of heights at which temperatures can be determined. In this work, temperatures are determined for heights between 80 and 105 km. The integration time of the data used here is 1 h with a shift of 15 min. The vertical resolution is 1 km. In addition to the resonance lidar, also a Rayleigh-Mie-Raman (RMR) lidar ~~is~~ was operated during the night at the same location until 2013. This lidar used the second harmonic output of a Nd:YAG laser at 532 nm. The temperatures are calculated under the assumption of hydrostatic equilibrium from the Rayleigh backscatter which is proportional to the atmospheric air density (Hauchecorne and Chanin, 1980). The initial temperature value for integration is taken from the resonance lidar (Alpers et al., 2004). The temperatures from the RMR lidar cover an altitude range between 22 and 90 km. But as the focus of this study is on the MLT region, we use these temperatures only above 70 km. Here, daily mean temperatures as a composite between 2003 and 2012 are used to describe the mean temperature field during the year in the MLT region. A full description of the seasonal variation has been published in Gerding et al. (2008).

2.3 NAVGEM-HA meteorological analyses

NAVGEM-HA is a high-altitude numerical weather prediction (NWP) system extending from the surface to ∼116 km altitude that provides atmospheric winds, temperatures and constituent information. It is based on the operational system described in Hogan et al. (2014), which combines the NAVGEM global spectral forecast model with a hybrid four-dimensional variational (4DVAR) data assimilation algorithm ~~Kuhl et al. (2013).~~ (Kuhl et al., 2013).

In addition to standard operational meteorological observations in the troposphere and stratosphere, NAVGEM-HA assimilates satellite-based observations of temperature, ozone and water vapor in the stratosphere, mesosphere and lower thermosphere (McCormack et al., 2017). The NAVGEM-HA output is on a 1° latitude and longitude grid, respectively. The temporal resolution of the data output fields is 3 hours. NAVGEM-HA uses a fixed top level pressure of $6 \cdot 10^{-5}$ hPa (e.g., McCormack et al., 2017; Eckermann et al., 2018, and references therein), which corresponds to an approximate altitude of 116 km. However, at the upper three model levels, an enhanced diffusion is applied to reduce the effects of wave reflection. These layers effectively act as a "sponge layer" and ~~should not be~~ are not included in the data analysis. The ~~NOGAPS-ALPHA model incorporates~~ forecast model component of NAVGEM-HA incorporates the same implicit fourth-order horizontal diffusion of vorticity, divergence, and virtual potential temperature used in its predecessor system (NOGAPS-ALPHA) to suppress growth of unrealistic variances near the truncation scale, as described in ~~McCormack et al. (2015)~~McCormack et al. (2015). Default values for the diffusion result in an effective e-folding time of 24 hours at the highest wavenumber (here T119). In the top 3 model levels the diffusion is ramped up to produce an effective e-folding of 2 hours at the top level. In the 74-level version of NAVGEM-HA used in this study, this region of enhanced diffusion (sponge layer) covers levels with $p <$ 1.e-3 hPa or 95 km in pressure-altitude.

~~McCormack et al. (2017) used for the initial validation~~ In an initial validation study, McCormack et al. (2017) used NAVGEM-HA output interpolated to geometric altitudes up to 95 km for the mean winds and ~~a maximum altitude of~~ up to 90 km for the wave analysis. ~~For comparison with the ground-based instruments~~In the present study, vertical profiles of NAVGEM-HA analyzed winds and temperatures are converted from the model vertical grid in geopotential altitude to a geometric altitude grid as done in Eckermann et al. (2009) ~~. The vertical resolution decreases with increasing altitude and is 3-5~~up to 94 km altitude. Above this level, NAVGEM-HA vertical resolution degrades significantly, as the vertical grid spacing increases from $\sim$3 km ~~between~~ near 80~~and~~ km altitude to more than 5 km near 100 km altitude. To date, NAVGEM-HA winds and tides up to 90 km altitude have been shown to be in good agreement with both ground-based MR observations, as reported in McCormack et al. (2017), Eckermann et al. (2018), and Laskar et al. (2019), and with independent satellite-based wind observations as reported in Dhadly et al. (2018). The present study extends these initial validation studies to include, for the first time, validation with two independent ground-based data sets over a 12-month period.

In this study we use a fixed geometric altitude grid (based on the World Geodetic System 84 model) with a maximum altitude of 94 km and 2 km vertical resolution at the MLT to match the meteor radar data. We convert the geopotential altitudes of NAVGEM-HA to geometric altitudes. However, we ~~have to~~ note that the geopotential altitude of the highest ~~model level, after removing~~ usable output level, neglecting the sponge layer effects noted above, has a geometric altitude between 92 to 89 km. As a consequence tidal amplitudes above 90 km altitude should not be considered as geophysical and are caused by the extrapolation to the geometric altitude grid and sponge layer effects. Further, the vertical constraint implemented in the ASF amplifies this effect even more. At mesospheric altitudes, NAVGEM-HA assimilates satellite measurements from TIMED and AURA satellites and radiances from the Defense Meteorological Satellite program (DMSP) (Eckermann et al., 2018). Systematic differences between the meteorological analysis and the ground-based wind and temperature data herein may have different origins. There could be intrinsic differences due to the model physics leading to such deviations or the assimilated data itself may show some systematic differences in relation to the observations used for the comparison. Further, considering that the *true* state of the atmosphere of temperature and winds remains elusive, it is hard to determine which of the observational techniques provides a better representation of this *true* state. Thus, it is essential to assess some of the systematic differences, which can arise due to the methodology employed for the comparison e.g., does applying different diagnostics or different spatio-temporal sampling of the instruments make a large difference. Validation and assessment of potential biases between the SABER temperatures and ground-based lidar measurements can be found in Xu et al. (2006); Dawkins et al. (2018). A cross comparison of the MLS and SABER temperatures is presented in Schwartz et al. (2008). A detailed description of how the data assimilation in NAVGEM-HA treats the temperature biases between both satellites is given in Eckermann et al. (2018) .

Another important point affecting the comparison is the availability of the assimilated data. Above 90 km less satellite observations can be assimilated. Further, it has to be noted that the spatial coverage of the assimilated SABER temperatures varies due to the yaw cycle of the spacecraft, which changes every 60 days the observing geometry providing a variable latitudinal coverage. From 52° S to 52° N the satellite collects constant measurements whereas the higher latitudes depend on the yaw cycle and alternates between up to 82° S or 82° N latitudinal coverage. This yaw cycle pattern may affect the quality of NAVGEM-HA analyses at Juliusruh and Andenes.

3 Local and global diagnostics

One of the challenges comparing different data sets is the use of a common diagnostic to ensure that all observations and the meteorological analysis data are treated in the same way. In particular, observational data can be more difficult to be ~~analyze~~ analyzed due to data gaps or uneven temporal sampling. Atmospheric tidal and planetary wave amplitudes are often obtained from Fourier based techniques ~~(e.g. Stockwell et al., 1996; Torrence and Compo, 1998)~~(e.g., Stockwell et al., 1996; Torrence and Compo, . In the case of unevenly sampled data Lomb-Scargle periodigrams are used ~~Lomb (1976); Scargle (1982)~~(Lomb, 1976; Scargle, 1982) , which provide a amplitude/power spectrum and a significance level, but without a phase information. For observational data, it is also very common to derive the tidal information of amplitude and phase with a least-square fit (Lima et al., 2007) or by a multiple regression analysis assuming, for instance, a circular polarization for the semidiurnal tide (Jacobi et al., 2008).

A commonly used approach to extract tides is a harmonic analysis:

$$u, v, T = u_0, v_0, T_0 + \sum_{n=1}^{3} a_n \sin(\frac{2\pi}{P_n} \cdot t) + b_n \cos(\frac{2\pi}{P_n} \cdot t) \quad ; \tag{1}$$

here u, v, T are the zonal, the meridional wind and the temperature, a_n and b_n are the tidal Fourier coefficients, $P_n = 24, 12, 8$ stands for the tidal periods in hours and t is the time of the observation either in UTC or local time, whatever is preferred. Harmonic tidal analysis work well for time series of several days or months, but assumes a constant mean background wind, tidal amplitude, and phase for the selected period. Recent studies of mean winds and tides using meteor radar, lidar and satellite observations indicate that tides have a fairly intermittent amplitude and phase character (Stober et al., 2017; Baumgarten et al., 2018; Baumgarten and Stober, 2019; Dhadly et al., 2018).

The adaptive spectral filter (ASF) aims to be a simple and general diagnostic to decompose time series in 1-D (temporal filter) (Stober et al., 2017) or 2-D (temporal-spatial filter) (Baumgarten and Stober, 2019). The technique is based on least-squares and, hence, applicable to unevenly sampled data and no additional zero-padding needs to be applied for data gaps as long as sufficient observations are available in the remaining adapted time window. Another benefit of the least-squares implementation is given in the error propagation to the derived quantities through the covariance matrix. The term ’adaptive’ in this context relates, similar to the wavelet technique, that the window length adapts to the number of wave cycles for each frequency component that ~~are~~ is fitted. The MR and NAVGEM-HA time series are decomposed into daily mean winds, diurnal tide, semidiurnal tide, terdiurnal tide and gravity wave residuum using the ASF.

The ASF uses a sliding window and fits each tidal component applying a scaling factor of 1.3 accounting for the number of wave cycles and no de-trending is applied. The scaling factor determines the window length that is used for the fitting for each frequency component. Here we applied a window length of 31 hours for the diurnal tide, whereas the semidiurnal tide is determined using a 16 hour window and so forth for the terdiurnal tide. At first, the daily mean wind and the diurnal tidal (amplitude and phase) components are determined considering also a ~~potential~~ semidiurnal and terdiurnal tide. In the next step, the semidiurnal tide is fitted using a regularization by the previously determined daily mean wind and diurnal tide and adapting the window length. The same procedure is repeated for the terdiurnal tide respectively. Due to the short window length, the bandwidth for each tidal component is rather wide and may also include some gravity wave contributions. It turns out that just applying temporal filtering leads to some contamination of the obtained tidal amplitudes and phases due to ~~inertial~~ inertia gravity waves with short (less than 10 km) vertical wavelengths (see appendix A). However, there are also some studies from polar latitudes using lidar and radar observations from McMurdo/Scott base (77.8° S, 166.7° E) and from Syowa Station (39.6° E, 69.0° S) indicating the presence of gravity waves with vertical wavelengths of 22-23~~km Chen et al. (2013)~~ km (Chen et al., 2013) or periods close to the semidiurnal tide ~~Shibuya et al. (2017)~~(Shibuya et al., 2017). However, Davis et al. (2013) has shown that the diurnal and semidiurnal tide typically has vertical wavelengths larger than 20 km. Hence, we constrain our tidal amplitudes and phases by assuming that the phase of the diurnal and semidiurnal tide only gradually ~~change~~ changes with altitude using a 16 km vertical retrieval kernel. The mean winds are constrained by a 10 km vertical retrieval kernel to avoid issues during the summer wind reversal from westward winds to eastward winds.

~~Atmospheric tides are a major driver of the short term variability of the lower thermosphere/ionosphere. The developed ASF technique provides a new tool to decompose time series to assess this short term variability from local and global data sets and allows a unified data analysis from observations and models or meteorological analysis such as NAVGEM-HA. The benefits of the method are :~~

- ~~data can contain data gaps (gaps have to be shorter than adapted window length)~~
- ~~applicable to unevenly sampled time series~~
- ~~full error propagation through covariance matrices~~
- ~~individual vertical regularization for each atmospheric parameter~~

~~The ASF technique aims , similar to the S-transform (Stockwell et al., 1996), to infer spectral information of intermittent signals. However, the S-transform is based on wavelet techniques and, thus, takes all the pros and cons of these methods.The main benefits~~ We optimized these vertical wavelength values considering the results of previous studies using meteor radars investigating the vertical wavelengths of tides (Yu et al., 2013; Davis et al., 2013; Fritts et al., 2019). These earlier studies showed that the vertical wavelengths for most of the tidal modes are much larger than >25 km. Only Yu et al. (2013) found for some Hough modes vertical wavelengths shorter than <25 km. To avoid a potential contamination of shorter tidal wavelengths in our vertical retrieval kernel, we did not implement a hard cut off vertical wavelength. Instead, we just constrain the smoothness of the vertical tidal phase within the averaging kernel and even allow a gradual change.

The vertical regularization constraint is an essential feature of the ASF ~~are given in the error, the possibility to use unevenly sampled time series with data gaps and most importantly to apply individual constrains to each fitted frequency component. Both methods should yield similar results for model data sets that obey the requirements mentioned above e. g. meteorological analysis like NAVGEM-HA (McCormack et al., 2017).~~

compared to many other diagnostic techniques based on wavelet or Fourier methods. Previous studies based on lidar observations (e.g., Ehard et al., 2015; Baumgarten et al., 2017, and reference therin) already investigated how the potential gravity wave energy changes with the applied filtering. Temporal filters tend to underestimate inertia gravity waves due to their long periods combined with short vertical wavelengths, whereas vertical filters are designed to eliminate the tidal contribution due to their large vertical wavelengths. As a consequence, this filter underestimates gravity waves with comparatively large vertical wavelengths. The ASF is much less prone to such biases due to the combination of spatio-temporal information for the specific waves. Since NAVGEM-HA produces global wind and temperature fields, we can extract tides as global waves and separate migrating and non-migrating tidal modes. Migrating tides are the DW1 (diurnal westward wave number 1), SW2 (semidiurnal westward wave number 2) and TW3 (terdiurnal westward wave number 3); all other tidal modes are non-migrating tidal components ~~(e.g., Forbes et al., 2008; Miyoshi et al., 2017, and references therin)~~(e.g., Forbes et al., 2008; Miyoshi et al., 2017, and references th
. The migrating and non-migrating tidal components are obtained using the following function;

$$u,v,T = u_0,v_0,T_0 + \sum_{s=-3}^{3}\sum_{i=1}^{3}\Big(a_{si}\cdot\sin(s\cdot\lambda - \frac{2\pi}{P_i}\cdot t) + b_{si}\cdot\cos(s\cdot\lambda - \frac{2\pi}{P_i}\cdot t)\Big) + further\ waves \quad , \qquad (2)$$

where s is the zonal wave number (negative eastward, positive westward), λ denotes the longitude at a fixed latitude circle, P_i are the periods of the diurnal, semidiurnal and terdiurnal tide and a_{si} and b_{si} are the Fourier coefficients for each wave number s and period P_i. The zonal mean zonal and meridional wind and the zonal mean temperature are given by u_0, v_0, T_0. The function also includes longer period waves such as the quasi two day wave (QTDW) with wave number s=1,2,3 and stationary planetary waves with wave number s=1,2,3 (Baumgarten and Stober, 2019; Schranz et al., 2019).

Daily mean tides for all the components are obtained by using a 3-day window around a central day, which is sufficient to still see some day-to-day variability and to determine potential phase drifts of each tidal component. The global tidal phase for all tidal components is referenced to the Prime meridian (Greenwich). Although NAVGEM-HA provides validated wind and temperature products from ∼18 km up to ∼94 km altitude, we focus our comparison to the MLT region and mostly to the available MR observations. A detailed discussion of the QTDW or planetary waves is beyond the scope of this paper and we leave these for other studies.

4 Results

In the first two parts of the results, we show the mean state of the atmosphere during the year in the MLT region using winds and temperatures from observations and NAVGEM-HA data. Next, the seasonal variation of the semidiurnal tidal component derived with the adaptive spectral filter is presented for each location. In addition to this, the analysis is also done for two examples of sudden stratospheric warming in the winter 2009/2010 and 2012/2013 to determine how well the observed variations in the MLT winds correspond to the NAVGEM-HA analysis data as well as to determine the day-to-day variability of the semidiurnal tide.

4.1 Mean winds

Fig. 1 shows the time variation of the zonal and meridional winds at the three locations Andenes, Juliusruh and Tavistock, from hourly meteor radar observations (left column), and the corresponding 3-hourly NAVGEM analyzed winds (center column) for the same location and each latitude as zonal mean values (right column). Daily mean winds are calculated and small scale variations such as tides and gravity waves are removed by the adaptive spectral filter and planetary waves are effectively filtered using a 30-day running median. The climatologies are based on the same time periods for MR winds and NAVGEM-HA and include December 2009 until December 2010 with periodic boundary conditions. In general, there is a good agreement of the seasonal wind pattern between the meteor radar wind observations and the NAVGEM-HA data. At all three locations, the zonal wind observations show the typical eastward ~~directed~~ winds in winter and the prominent wind reversal in spring. In particular, the seasonal asymmetry of the spring transition as well as the the gradual change of the summer wind reversal altitude seen in the meteor radar winds is well-reproduced in the NAVGEM-HA analyses.

During summer, a strong transition between westward and eastward winds occurs between 80 and 90 km altitude. The transition height decreases from high to midlatitudes. Above 90 km altitude, the eastward jet reaches wind velocities of about 40 m/s for all stations. The meridional winds during winter are typically northward, while they are southward during the summer. Similar behavior is seen in the NAVGEM-HA analysis data, but here the magnitude of the winds is to some extent larger compared to the meteor radar observations. Although the general morphology of the seasonal pattern is well captured in NAVGEM-HA, there are some differences in the wind reversal altitudes in summer in both wind components, which would affect the gravity wave breaking altitudes and, hence, the altitude of the resulting momentum deposition.

Furthermore, the altitude where the zonal wind reverses during summer decreases not as much with latitude as indicated from the meteor radar observations for the different locations. Some differences occur between the NAVGEM-HA locally analyzed winds compared to the zonal averaged NAVGEM-HA analyzed winds for each latitude of the meteor radar stations. Short-term

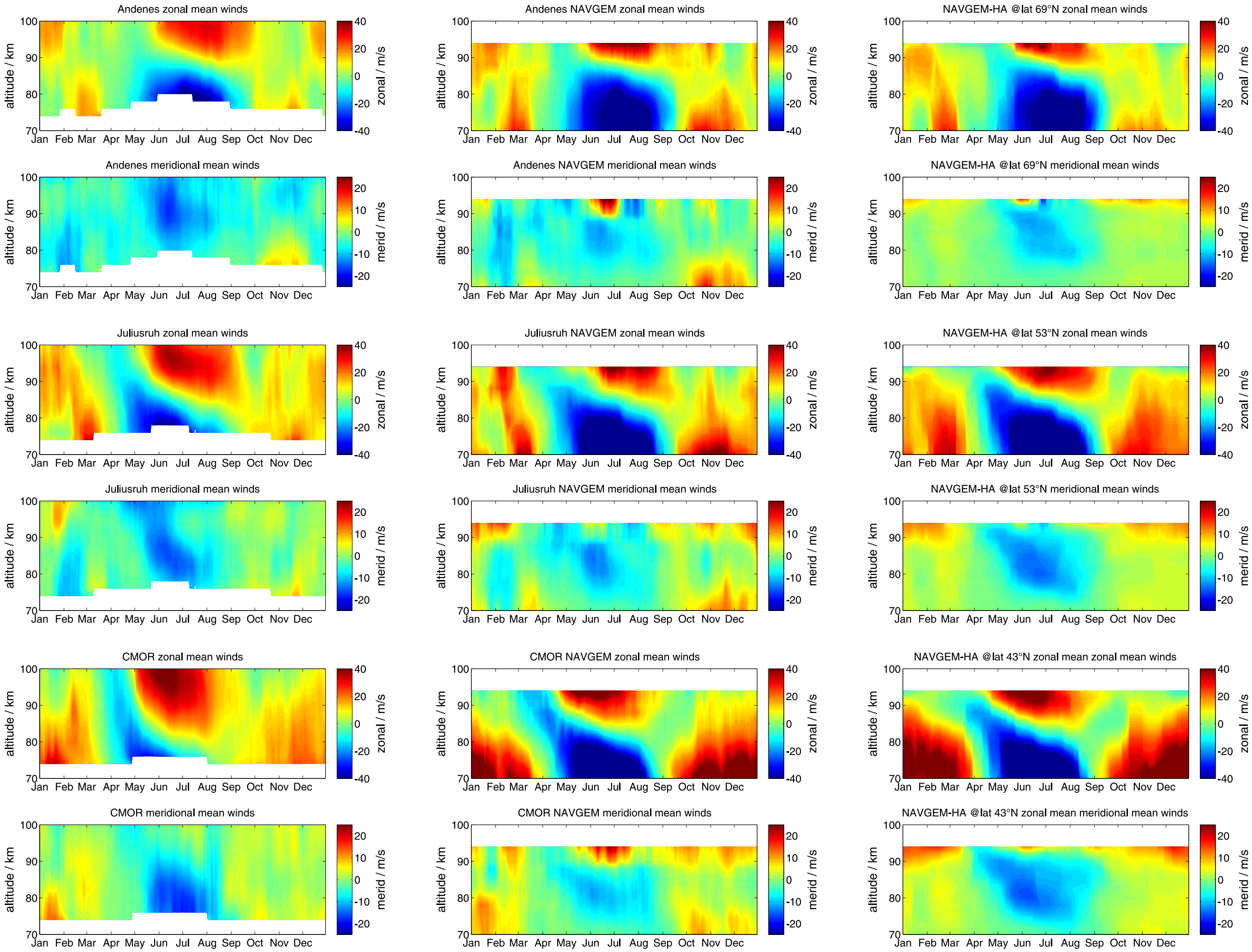
Andenes zonal mean winds

Andenes NAVGEM zonal mean winds

NAVGEM-HA @lat 69°N zonal mean winds

Andenes meridional mean winds

Andenes NAVGEM meridional mean winds

NAVGEM-HA @lat 69°N meridional mean winds

Juliusruh zonal mean winds

Juliusruh NAVGEM zonal mean winds

NAVGEM-HA @lat 53°N zonal mean winds

Juliusruh meridional mean winds

Juliusruh NAVGEM meridional mean winds

NAVGEM-HA @lat 53°N meridional mean winds

CMOR zonal mean winds

CMOR NAVGEM zonal mean winds

NAVGEM-HA @lat 43°N zonal mean zonal mean winds

CMOR meridional mean winds

CMOR NAVGEM meridional mean winds

NAVGEM-HA @lat 43°N zonal mean meridional mean winds

Figure 1. Comparison of mean winds above Andenes, Juliusruh and Tavistock (CMOR) using a 30-day running median with periodic boundary condition using the same dates for NAVGEM-HA and the meteor radar observations. The left panel shows the meteor radar observations. The central panel shows the NAVGEM-HA analysis fields for the same locations and periods. The right panel displays the zonal mean zonal and meridional winds for each latitude.

variations during winter are much more visible in the locally analyzed winds, this is especially true for the meridional wind ~~the~~ case.

4.2 Mean temperatures

~~A similar comparison to the~~ Until now, only NAVGEM-HA wind products have been extensively validated with independent ground-based measurements. To extend this validation to MLT temperatures, we next perform a similar comparison using

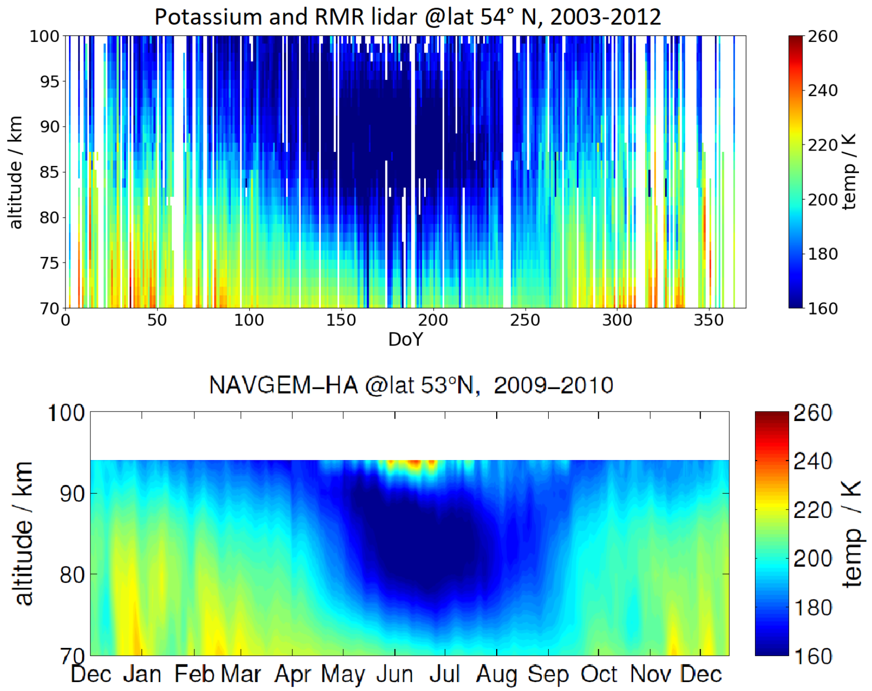
Potassium and RMR lidar @lat 54° N, 2003-2012

NAVGEM–HA @lat 53°N, 2009–2010

Figure 2. Comparison of mean temperatures above Kühlungsborn. The upper panel shows the temperatures derived from the potassium lidar. The lower panel shows the NAVGEM-HA analysis field for the same location.

NAVGEM-HA temperature ~~field is done using~~ analyses and a co-located potassium lidar instrument at Kühlungsborn. The composite daily mean lidar temperatures over the ~~years~~ period 2003-2012 ~~from the lidar~~ are shown in Fig. 2 together with the NAVGEM-HA analyzed temperatures between 2009 and 2010. Both data sets show the same seasonal temperature pattern with the lowest temperatures during summer. The mesopause, where the lowest temperatures occur during the year, is estimated from the lidar data ~~at~~ and found around 88 km in summer and just above 100 km in winter. For the NAVGEM-HA analyzed temperatures the altitude of the mesopause is in nearly the same altitude range. ~~Even the magnitude of both temperatures is~~ In general, the temperature values are in very good agreement with each other~~. Only~~, although we note that the temperatures observed by lidar ~~around~~ near 70 km are ~~higher compared to~~ larger than the NAVGEM-HA ~~data~~temperature. At the upper edge of the NAVGEM-HA data, there is also a temperature enhancement during summer, which is not seen in the lidar data.

4.3 Semidiurnal tides

In this section, we investigate the seasonal variation of the semidiurnal wind tide based on the calculation with the adaptive spectral filter. This component is the most dominant tidal component ~~seen in the MLT region~~ at the MLT and the latitudes analyzed herein (Chapman and Lindzen, 1970). The results for the semidiurnal tidal amplitude and phase for the stations at

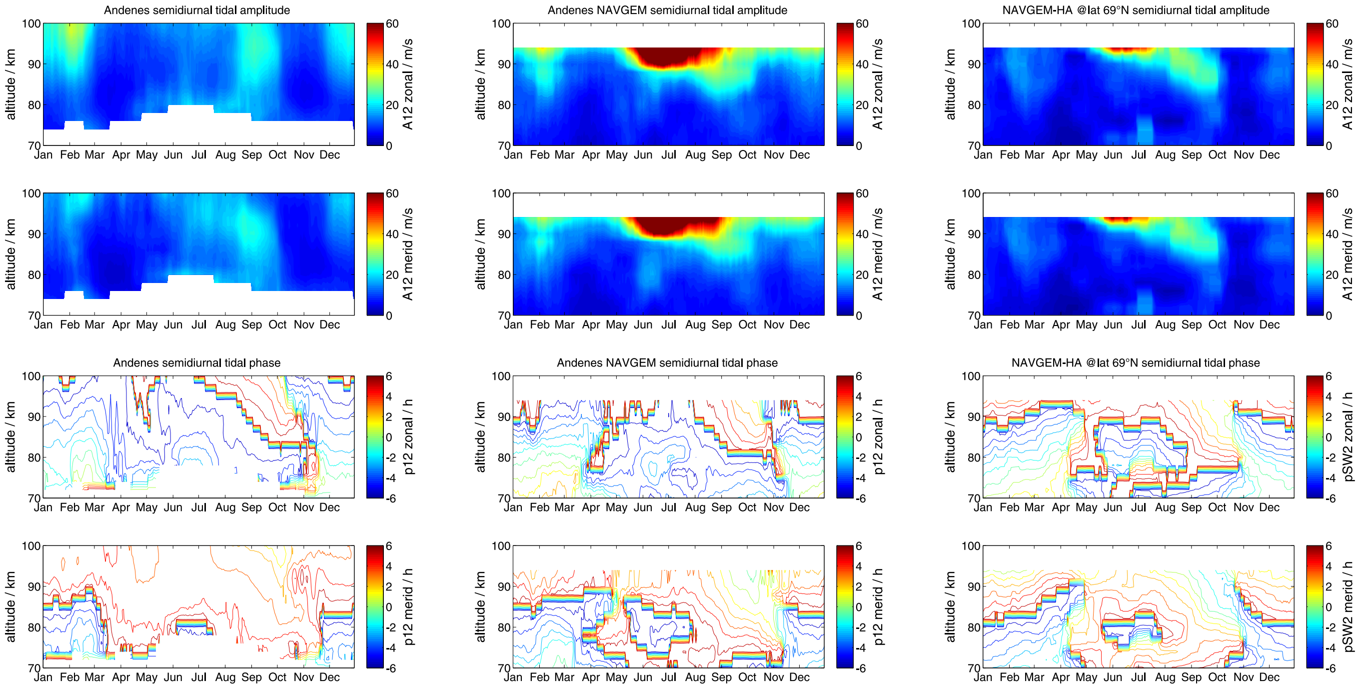

Figure 3. Comparison of semidiurnal seasonal zonal and meridional amplitude (upper two rows) and phase (lower two rows) tidal climatology using a 30-day running median with periodic boundary condition. The left panels show the meteor radar observations above Andenes (69° N, 11° E). The central panels show the NAVGEM-HA analysis fields for the same period. The right panels visualize the zonal mean tidal amplitude and phase of the SW2. The label A12 and p12 corresponds to the semidiurnal amplitude and phase using the local diagnostic.

Andenes, Juliusruh and Tavistock are shown in Fig. 3, 4, and 5, respectively. Every data set is compared to the NAVGEM analyzed tidal fields from a local as well as from a global perspective as already done for the mean winds and temperatures.

The observations from all stations indicate a clear winter amplitude maximum. A ~~further maximum is~~ second maximum is also evident during September. The amplitudes are smallest during November ~~as well as during April. The latter point is not visible above Tavistock~~ and April. Only Tavistock exhibits a significant semidiurnal tidal amplitude for April compared to the ~~other locations. In general,~~ meteor radars at higher latitudes, and we note that the tidal amplitudes above Tavistock are also even stronger during fall than during winter. Compared to the other locations the winter maximum above Tavistock is less pronounced. In general, the amplitudes during winter are strongest for midlatitudes (Juliusruh).

The NAVGEM-HA analyzed amplitudes reveal the same temporal variability over the year as from the observations. Above an altitude of 90 km, the amplitudes from NAVGEM-HA show a significant increase which is not seen in the observations. This was also visible in the temperature data of NAVGEM-HA compared to the lidar data.

In addition to the amplitudes of the semidiurnal tides, the annual phase ~~bahaviour~~ behavior of those tides was also calculated using the spectral adaptive filter. ~~.~~In general, for every location, the phase of the semidiurnal tide is ~~slowly drifting~~ drifting and variable over the year. During winter the phases are ~~quite stable~~continuously changing, at the beginning of March, the phase

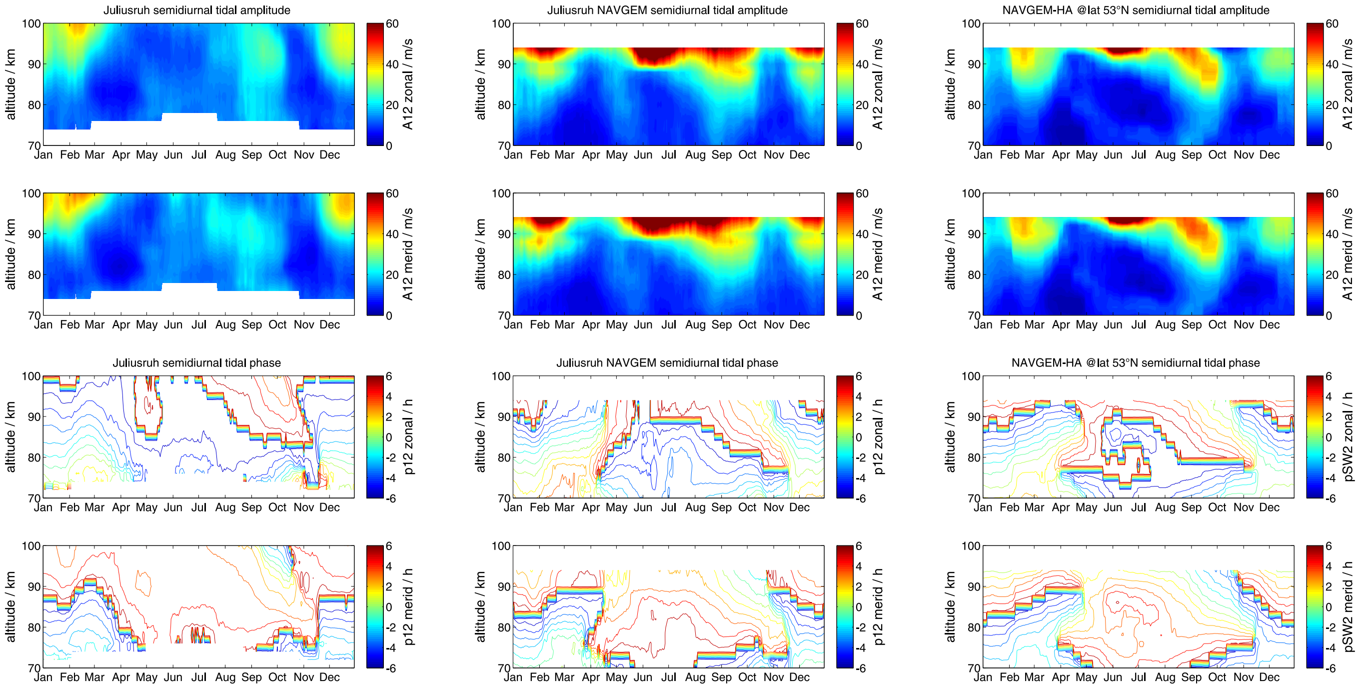

Figure 4. ~~Comparison of semidiurnal seasonal zonal and meridional amplitude (upper two rows) and phase (lower two rows) tidal climatology using a 30-day running median with periodic boundary condition~~Same as Fig.~~The left panels show the meteor radar observations above Juliusruh (54.3° N~~ 3, ~~13° E). The central panels show the NAVGEM-HA analysis fields~~ but for ~~the same period~~Juliusruh.~~The right panels visualize the zonal mean tidal amplitude and phase of the SW2. The label A12 and p12 corresponds to the semidiurnal amplitude and phase using the local diagnostic.~~

shows a sudden ~~increase~~jump, which is evident in every location ~~as well as in~~ of the observations and the meteorological analysis~~data~~. This behavior reverses during October/November, exactly when the ~~atmosphere is changing~~ atmospheric circulation reverses again from summer to winter conditions~~and vice versa~~. A similar phase progression is visible from the NAVGEM-HA locally analyzed data as well as from the global fields. ~~There is a tendency that the global fields show larger differences to the observations during summer which is due to the coarser temporal resolution of the global data .~~

4.4 Day-to-day variability during a sudden stratospheric warming

~~The~~ Having established that NAVGEM-HA wind and temperature analyses capture many of the salient features in the seasonal variation of both meteor radar wind and lidar temperature observations, we now examine the shorter-term variations in both data sets. Specifically, we examine the day-to-day variability of the mean winds, the semidiurnal tidal amplitudes and phases ~~are investigated~~ from the meteor radar winds during the sudden stratospheric warming (SSW) that took place in 2010 and 2013 in comparison to NAVGEM-HA analyzed data from a local perspective as well as from a global view. ~~The analysis is done~~

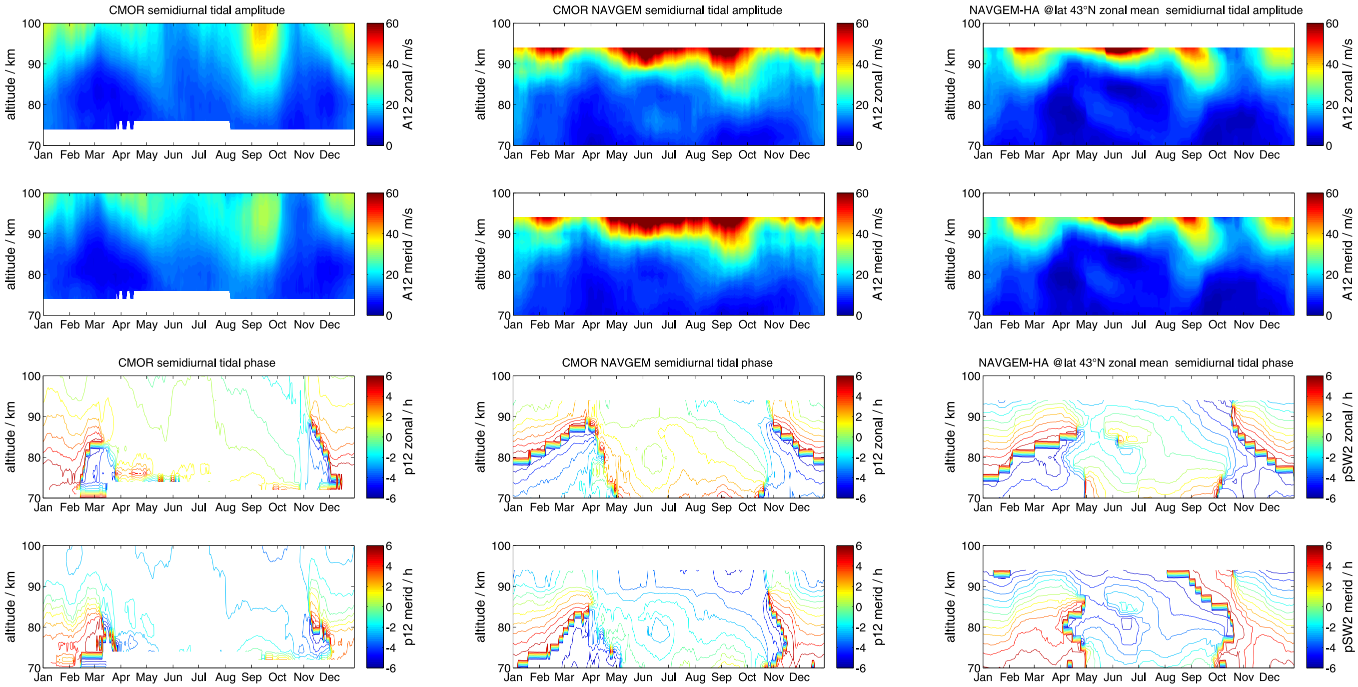

Figure 5. ~~Comparison of semidiurnal seasonal zonal and meridional amplitude (upper two rows) and phase (lower two rows) amplitude and phase tidal climatology using a 30-day running median with periodic boundary condition~~Same as Fig.~~The left panels show the meteor radar observations above Tavistock (43.2° N~~ 3, ~~80.7° W). The central panels show the NAVGEM-HA analysis fields~~ but for ~~the same period~~CMOR.~~The right panels visualize the zonal mean tidal amplitude and phase of the SW2. The label A12 and p12 corresponds to the semidiurnal amplitude and phase using the local diagnostic.~~

~~for high latitudes~~ To do so, we apply the same ASF analysis procedure to both meteor radar and NAVGEM-HA data at a high latitude (Andenes) and ~~midlatitudes~~ midlatitude (Juliusruh) ~~in the same way~~location.

4.4.1 Winter season 2009/2010

During the winter in 2009/2010, a major sudden stratospheric warming occurred at the end of January when the polar vortex was markedly displaced from the pole (Stober et al., 2012) and ~~afterward showed an eventual break up into two unequal strong lobes (e.g. Dörnbrack et al., 2012; Jones Jr. et al., 2018)~~then separated into two unequally strong lobes (e.g., Dörnbrack et al., 2012; Jones Jr. et a . Following previous studies involving NAVGEM-HA, we mark the onset of the SSW ~~occurred~~ as occurring on 27th January (McCormack et al., 2017). Mean winds, the semidiurnal tidal amplitude and phase are shown in Fig. 6 from the meteor radar observations above Andenes as well as for the corresponding locally analyzed NAVGEM-HA data. In Fig. 7 the same results are shown for the station at midlatitudes above Juliusruh. Stronger changes in the winds are visible for Juliusruh than for Andenes. Even the semidiurnal amplitudes are stronger at midlatitudes~~. This is in agreement~~ , which agrees with the stronger seasonal variation of the semidiurnal tidal amplitude above Juliusruh. After the onset of the sudden stratospheric warming, the semidiurnal tidal amplitudes show an enhancement at the beginning of February, which is visible at both stations and in both wind components.

The semidiurnal tidal phases show a large day-to-day variability during the winter period, which is in general stronger at high latitudes than at midlatitudes. After the central date of the sudden stratospheric warming, the tidal phase shows a sudden increase which lasts only a few days. After these days, the phase shows a recovery where they become more stable again just as before the sudden stratospheric warming.

The NAVGEM-HA analyzed winds exhibit the same short-term variability during the 2009/2010 winter at both stations for the winds as well as for the semidiurnal tide. Even the phase enhancement after the central date of the SSW is remarkably well reflected by the NAVGEM-HA data. Some differences occur above an altitude of 85 km, where NAVGEM-HA data reveals larger magnitudes in the winds as well as larger amplitudes for the semidiurnal tide as previously seen. Fig. 8 shows global NAVGEM-HA results for both Andenes and Juliusruh station locations. The global analyzed NAVGEM-HA data ~~exhibit~~ indicates much less variability during the winter compared to the locally analyzed data. But the central date of the SSW is ~~better to see~~ more easily identified in the winds than it was the case for the locally analyzed winds. However, the main features for the semidiurnal tide stay the same. The amplitudes show an increase after the central date of the SSW and the phases reveal a change for a few days at both locations. In contrast to the locally analyzed data, the phases from the global NAVGEM-HA fields slowly ~~increase~~ change during the winter. But in general, the agreement with the MR observations is still good.

4.4.2 Winter season 2012/2013

The winter season in 2012/2013 was also characterized by a major sudden stratospheric warming. In this case, the onset of the SSW ~~occured~~ occurred on 7th of January using again the definition presented in ~~McCormack et al. (2017)~~McCormack et al. (2017). During the SSW the vortex was split into two lobes (Coy and Pawson, 2015). Again, mean winds, the semidiurnal tidal amplitudes and phases are shown in Fig. 9 and Fig. 10 for high latitudes and midlatitudes, respectively.

In this winter season, the mean zonal winds at high latitudes are stronger, especially after the SSW, than at midlatitudes, which is opposite to that seen in the winter season 2009/2010. The mean meridional winds are similar in strength for both stations. Nevertheless, the semidiurnal tide shows again stronger amplitudes at the midlatitude station than at high latitudes. At Andenes, we see a distinct increase of the amplitudes after the SSW, which was already seen in the winter season 2009/2010, while in general at Juliusruh a larger tidal activity is visible. Here, before and during the central date of the SSW the tidal amplitudes decrease in the first place due to the strong changing winds. Afterward, the semidiurnal tidal amplitudes increase again stronger than during the whole winter.

The semidiurnal tidal phases show again a large variability during the whole time. A few days after the central date of the sudden stratospheric warming a sudden increase of the phase is visible in the same way as for the winter 2009/2010. The locally analyzed NAVGEM-HA data reveal structures during this winter period similar to those from the observations. Evident from every data set, the mean winds, as well as the amplitudes, are slightly overestimated in NAVGEM-HA. The NAVGEM-HA

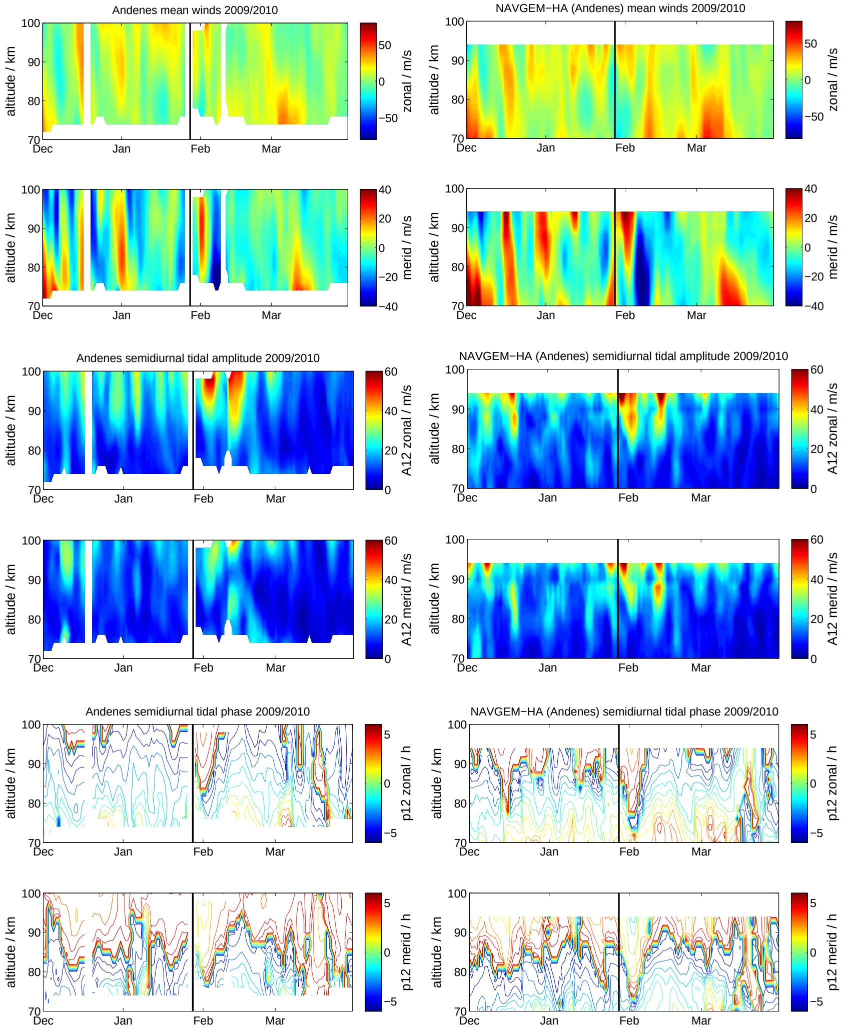

Figure 6. Comparison of meteor radar observations and NAVGEM-HA above Andenes during the winter 2009/10 for daily mean zonal and meridional winds (upper two panels), semidiurnal tidal zonal and meridional amplitude (middle panels) and semidiurnal tidal phases (lower two panels). The label A12 and p12 corresponds to the semidiurnal amplitude and phase using the local diagnostic.

analyzed tidal phases exhibit also a sudden change after the SSW, but not as strong as from the observations, but this might be due to a general more disturbed winter period compared to the year 2009/2010. The globally analyzed data from NAVGEM-HA are shown in Fig. 11. As was the case for the 2009/2010 winter, in this winter season the winds from a global perspective are

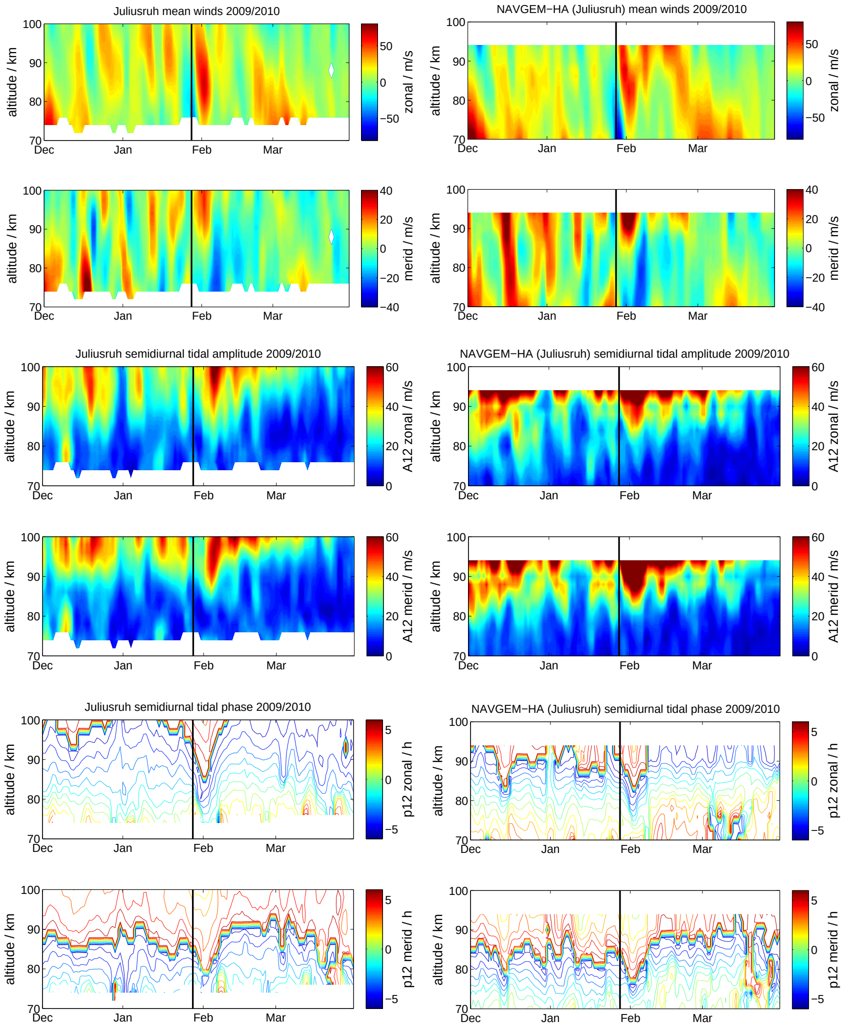

Figure 7. ~~Comparison of meteor radar observations and NAVGEM-HA above Juliusruh during the winter 2009/10 for daily mean zonal and meridional winds (upper two panels), semidiurnal tidal zonal and meridional amplitude (middle panels) and semidiurnal tidal phases (lower two panels).~~ The ~~label A12 and p12 corresponds to the semidiurnal amplitude and phase using the local diagnostic~~same as Fig. 6, but for Juliusruh.

much stronger and uniformly distributed over the winter months, except for the wind reversal during the SSW, which is visible at the beginning of January.

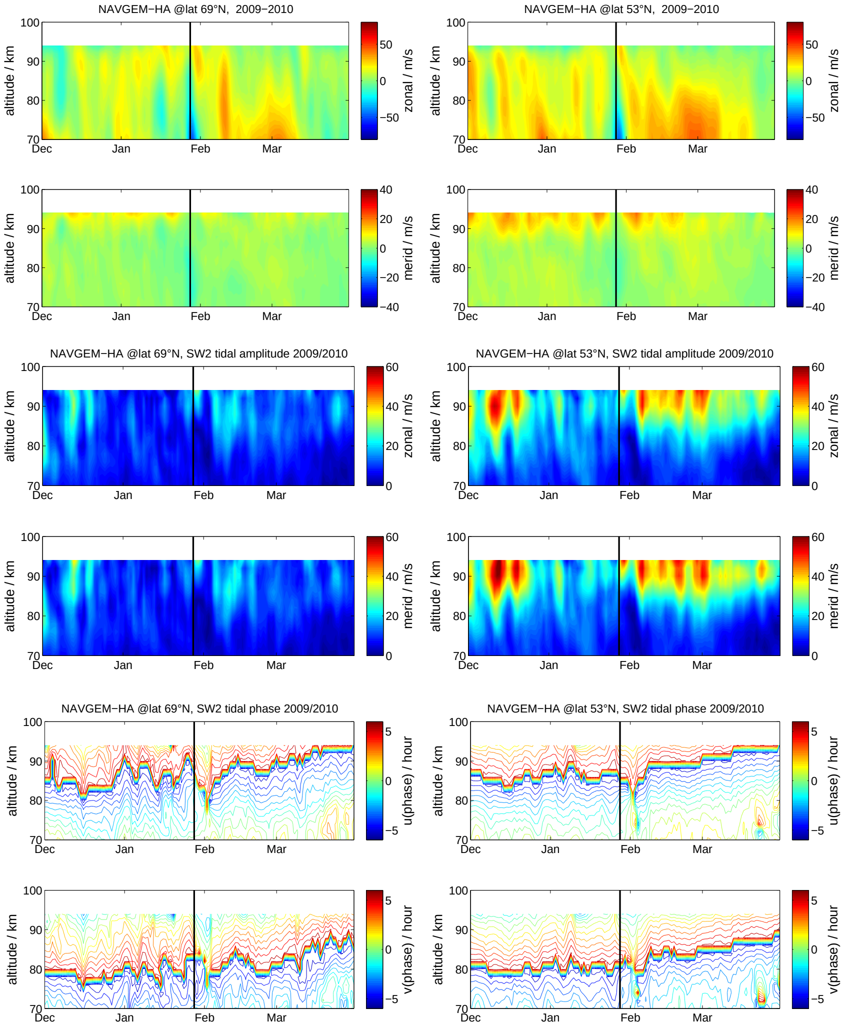

Figure 8. Comparison of global NAVGEM-HA above Andenes and Juliusruh during the winter 2009/10 for daily zonal mean zonal and meridional winds (upper two panels), zonal mean semidiurnal tidal zonal and meridional amplitude (middle panels) and zonal mean semidiurnal tidal phases (lower two panels).

5 Discussion

5.1 ~~Implications of the ASF constraint by the vertical wavelength~~

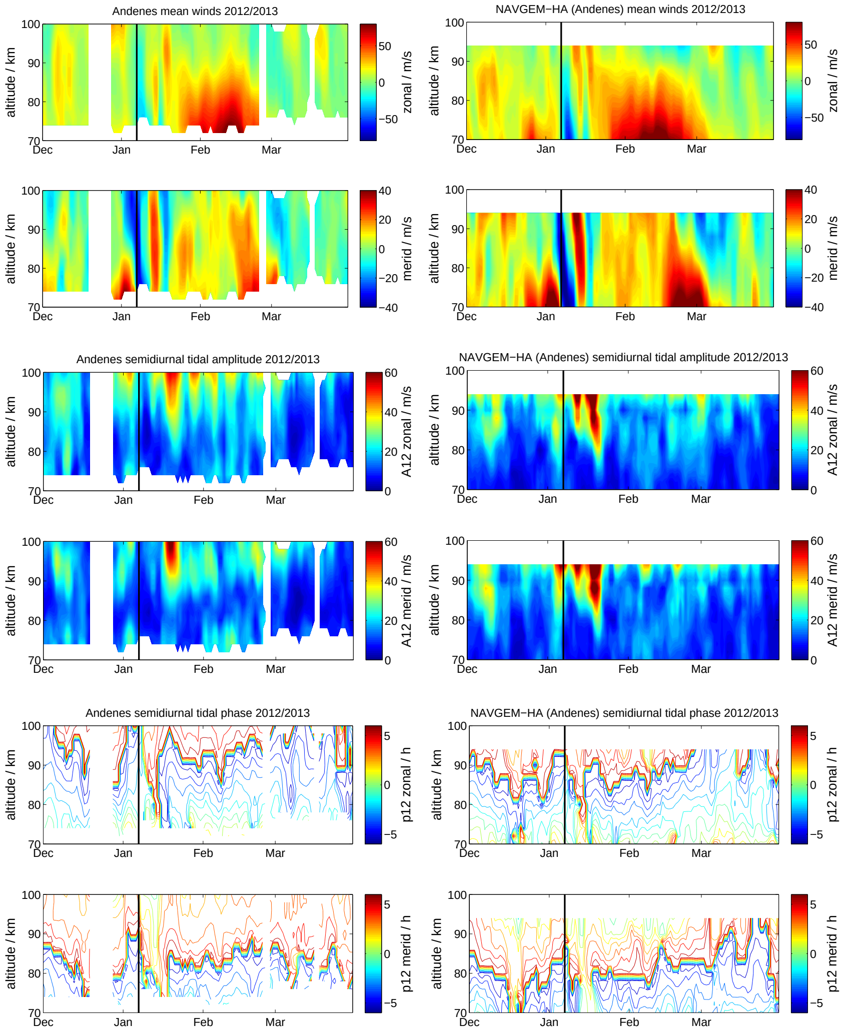

Figure 9. Comparison of meteor radar observations and NAVGEM-HA above Andenes during the winter 2012/13 for daily mean zonal and meridional winds (upper two panels), semidiurnal tidal zonal and meridional amplitude (middle panels) and semidiurnal tidal phases (lower two panels).The label A12 and p12 corresponds to the semidiurnal amplitude and phase using the local diagnostic.

~~Due to the nature of the Fourier transform and the sampling, there are some drawbacks due to the short window length required to assess the short term tidal variability. The frequency bandwidth around each tidal frequency is rather wide. The contamination due to other waves falling into these windows, (for instance gravity waves), is minimized by the vertical regularization of the tidal vertical wavelength, which turns out to be a key element of the ASF.The vertical regularization was implemented~~

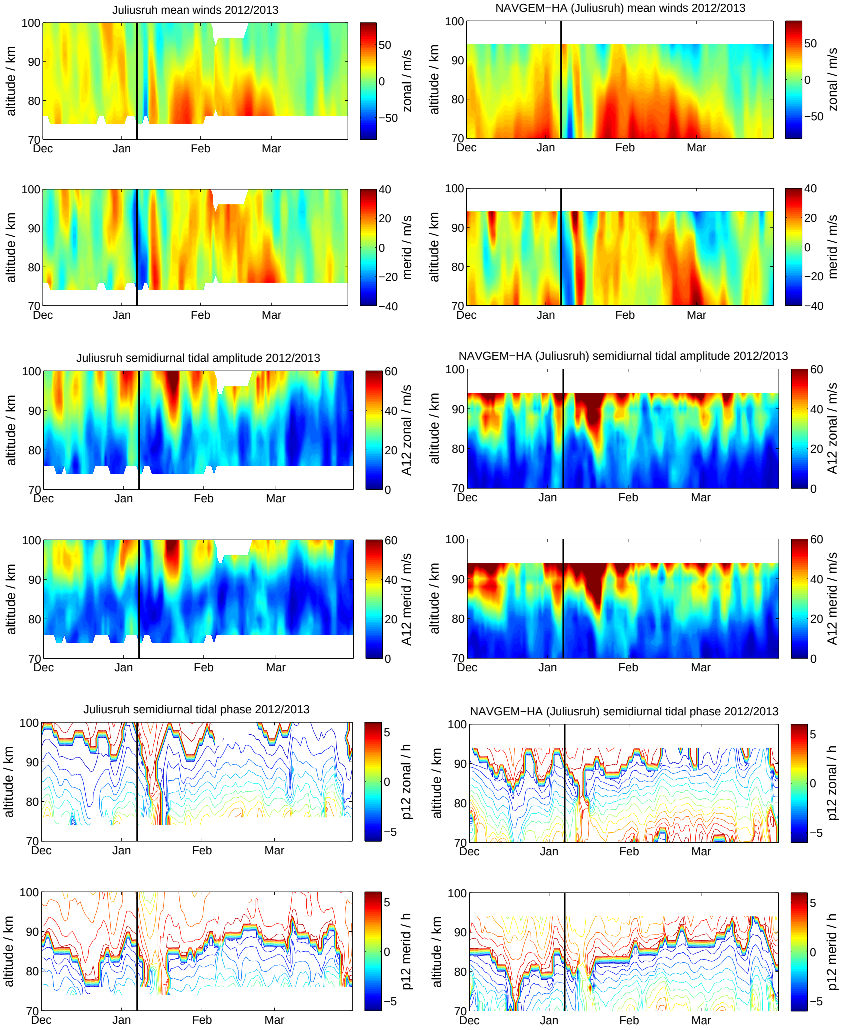

Figure 10. ~~Comparison of meteor radar observations and NAVGEM-HA above Juliusruh during the winter 2012/13 for daily mean zonal and meridional winds (upper two panels), semidiurnal tidal zonal and meridional amplitude (middle panels) and semidiurnal tidal phases (lower two panels).~~The ~~label A12 and p12 corresponds to the semidiurnal amplitude and phase using the local diagnostic~~same as Fig. 9, but for Juliusruh.

~~by allowing gradual changes with altitude for each of the derived wind components. The mean winds are regularized using a 10 km vertical retrieval kernel, the diurnal and semidiurnal tides are retrieved applying a 16 km vertical retrieval kernel. We optimized these vertical wavelength values considering the results of previous studies using meteor radars investigating~~

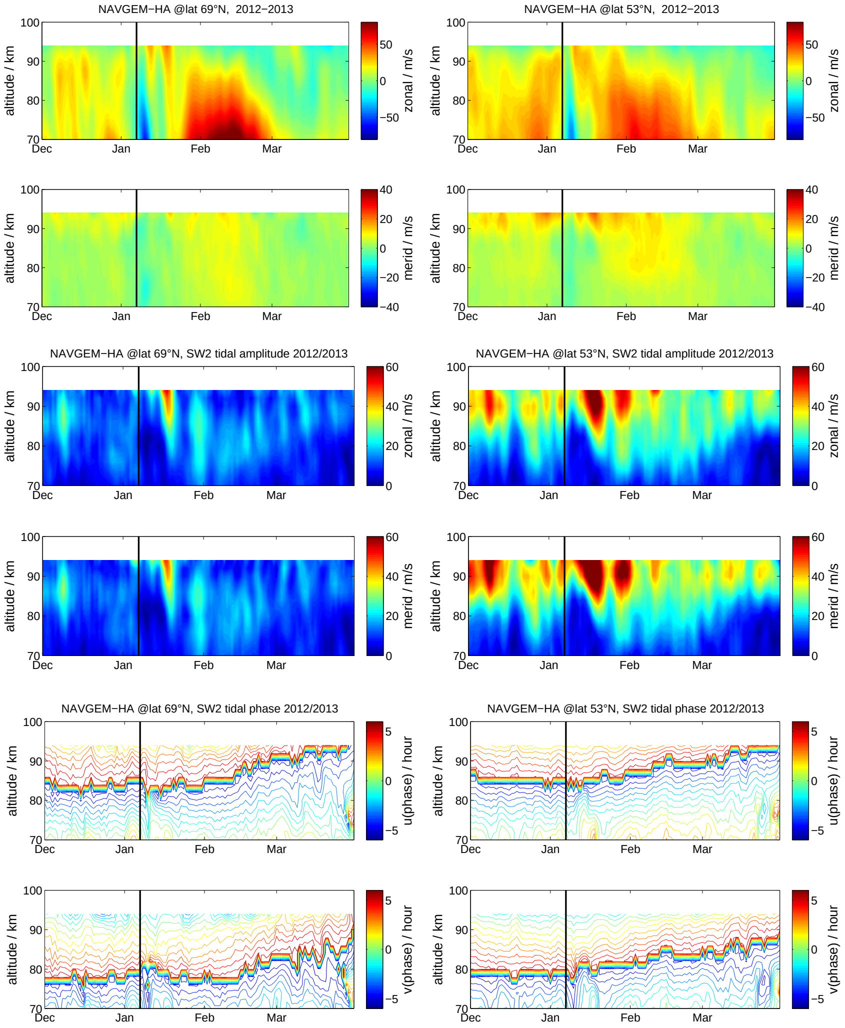

Figure 11. Comparison of global NAVGEM-HA above Juliusruh (left column) and Andenes (right column) during the winter 2012/13 for daily zonal mean zonal and meridional winds (upper two panels), zonal mean semidiurnal tidal zonal and meridional amplitude (middle panels) and zonal mean semidiurnal tidal phases (lower two panels).

~~the vertical wavelengths of tides (Yu et al., 2013; Davis et al., 2013; Fritts et al., 2019). These earlier studies showed that the vertical wavelengths for most of the tidal modes are much larger than >25 km. Only Yu et al. (2013) found for some Hough modes vertical wavelengths shorter than <25 km. To avoid potential contamination of shorter tidal wavelengths in our vertical retrieval kernel, we did not implement a hard cut off vertical wavelength. Instead, we just constrain the smoothness of the~~

~~vertical tidal phase within the averaging kernel and even allow a gradual change.The vertical regularization constraint is an essential feature of the ASF compared to many other diagnostic techniques based on wavelet or Fourier methods. Previous studies based on lidar observations (e.g., Ehard et al., 2015; Baumgarten et al., 2017, and reference therin) already investigated how the potential gravity wave energy changes with the applied filtering. Temporal filters tend to underestimate inertia gravity waves due to their long periods combined with short vertical wavelengths, whereas vertical filters are designed to eliminate the tidal contribution due to their large vertical wavelengths. As a consequence, this filter underestimates gravity waves with comparatively large vertical wavelengths. The ASF is much less prone to such biases due to the combination of spatio-temporal information for the specific waves.~~

5.1 NAVGEM-HA and MR mean wind and temperature climatology

The comparison of the NAVGEM-HA mean winds and the meteor radar climatologies at Andenes, Juliusruh and CMOR is remarkable up to an altitude of 94 km. ~~Due to the data assimilation ,~~The assimilation of satellite-based middle atmospheric temperature and constituent observations enables NAVGEM-HA ~~captures~~ to capture the main features of the seasonal wind climatologies such as the weak eastward winds during the winter, the asymmetry of the seasonal pattern between the spring and autumn wind reversals as well as the gradual descent of the summer wind reversal between the mesospheric westward winds and the higher altitude thermospheric eastward jet. ~~The good agreement~~ Our analysis shows that the initial good agreement reported during the winter months ~~was already outlined in McCormack et al. (2017) presenting initial~~ in McCormack et al. (2017) extends to seasonal time scales, and providing further cross-validation of the NAVGEM-HA winds with globally distributed and available meteor radar wind observations.

The MLT mean wind climatology is still afflicted with a high degree of uncertainty when comparing different GCMs, although nudged to the same reanalysis data sets. Pedatella et al. (2014) compared several GCMs and showed that not even the sign of the mean wind seems to agree between the models at the MLT. Further, the seasonal morphology at mid- and high-latitudes was not well-reproduced by some models compared to the climatologies published from meteor radars (Portnyagin et al., 2004; Wilhelm et al., 2019. In particular, the seasonal asymmetry of the zonal wind circulation from the winter to the summer conditions and back to the winter regime seems to be problematic for the GCMs. Comparing the seasonal morphology of the zonal and meridional winds between NAVGEM-HA and other comprehensive GCMs, such as WACCM or SD-WACCM (Smith, 2012; Chandran and Collins, 2014), and the meteor radar and lidar data indicate a ~~slightly~~ much better agreement for the meteorological analysis for altitudes beyond 80 km. Similar results have been found by comparing meteor radar winds to free running mechanistic ~~GCMs Pokhotelov et al. (2018). Smith (2012) performed a detailed assessment of the WACCM model using various~~ GCM (Pokhotelov et al., 2018). Previous studies comparing eCMAM with ground-based meteor radar observations at low latitudes and on seasonal time-scales revealed a similar good agreement for mean winds and diurnal tidal amplitude and phases (Du et al., 2007; Ward et al., 2010). The good agreement between NAVGEM-HA and ~~satellite measurements in the MLT and also noted some discrepancies between the observations and the model fields.~~ ground-based wind observations shown in Section 4 indicate that global data assimilation products in the MLT can provide a valuable benchmark for evaluating the performance of “whole-atmosphere” GCMs extending into the thermosphere. These products could improve understanding of the large discrepancies among different models noted above by offering insight regarding where these models deviate most from a validated high-altitude meteorological analyses.

The general thermal structure and seasonal climatology are also well-reproduced in NAVGEM-HA for the lidar observations presented in Fig. 2 at the mid-latitude station of Kuehlungsborn. The meteorological ~~analysis~~ analyses captures the seasonal course of the altitude variation of the mesopause. Further, we identified a small offset between the lidar and the NAVGEM-HA temperatures. The analysis data has a tendency ~~toward~~ towards slightly warmer temperatures compared to the resonance lidar. These slightly higher temperatures in NAVGEM-HA may also explain the ~~magnitude of the mean winds from the~~ higher wind magnitudes relative to the MR observations.

~~At mesospheric altitudes, NAVGEM-HA assimilates satellite measurements from TIMED and AURA satellites and radiances from the Defense Meteorological Satellite program (DMSP) (Eckermann et al., 2018). Systematic differences between the meteorological analysis and the data herein may have different origins. There could be intrinsic differences due to the model physics leading to such deviations or the assimilated data itself may show some systematic differences in relation to the observations used for the comparison. Further, considering that the *true* state of the atmosphere temperature and winds remains elusive, it is hard to determine which of the observational techniques provides a better representation of this *true* state. Thus, it is essential to assess some of the systematic differences, which can arise due to the methodology employed for the comparison e.g.,does applying different diagnostics or different spatio-temporal sampling of the instruments make a large difference. Validation and assessment of potential biases between the SABER temperatures and ground-based lidar measurements can be found in Xu et al. (2006); Dawkins et al. (2018). A cross comparison of the MLS and SABER temperatures is presented in Schwartz et al. (2008). A detailed description of how the data assimilation in NAVGEM-HA treats the temperature biases between both satellites is given in Eckermann et al. (2018).Another important point affecting the comparison is the availability of the assimilated data. Above 90 km less satellite observations can be assimilated. Further, it has to be noted that the assimilated SABER temperatures show characteristic pattern due to the yaw cycle of the spacecraft, which changes every 60 days the observing geometry providing a variable latitudinal coverage. From 52° S to 52° N the satellite collects constant measurements whereas the higher latitudes depend on the yaw cycle and alternates between up to 82° S or 82° N latitudinal coverage. This yaw cycle pattern affects the data quality of NAVGEM-HA at Juluisruh and Andenes.~~

5.2 NAVGEM-HA and MR mean wind semidiurnal tidal comparison

~~Atmospheric tides are global-scale waves having periods which are an integer fraction of a day. At the MLT height, tides gain huge amplitudes~~ At MLT heights, tidal amplitudes grow large and contribute significantly to the daily variability of the zonal and meridional winds. At mid- and polar latitudes, the semidiurnal tide is the most prominent tidal wave in the MLT that can be observed throughout the course of the year (Portnyagin et al., 2004; Pokhotelov et al., 2018; Wilhelm et al., 2019).

In principle, local observations (single measurements) can not distinguish between migrating and non-migrating tidal components and only observe a total tide. Earlier studies (e.g., Portnyagin et al., 2004) have investigated the global nature of the diurnal and semidiurnal tide at polar latitudes using a chain of radars at approximately 70° N. They found very good agreement between monthly tidal amplitudes and phases for all stations along the latitudinal circle. Recently, there have been some attempts to separate migrating and non-migrating tides using globally distributed chains of meteor radars (He et al., 2018) assuming theoretical tidal wave fields consisting of migrating and non-migrating components. However, due to the small number of meteor radars at the latitudinal circles, the analysis still contains a high degree of ambiguity.

Combining the benefits of high resolution local measurements with global meteorological analysis data solves this problem. The comparison of the semidiurnal tidal climatology reveals that NAVGEM-HA reproduces the seasonal morphology of the tidal ~~magnitudes~~ amplitudes for both wind components up to an altitude of 90 km applying the ASF tidal diagnostic. The local ASF diagnostic shows remarkable agreement between the global tidal analysis of the migrating SW2 tide in magnitude and phase. The non-migrating semidiurnal components show only very small and often negligible amplitudes. The agreement of the phase of the SW2 tide between the global and local measurements seem to be better at lower latitudes of CMOR and Juliusruh compared to Andenes.

? performed a similar validation of the tidal amplitude and phase behavior using the extended Canadian Middle Atmosphere Model (eCMAM) at low latitudes. However, they used much longer windows of 60-days to compute average amplitudes and phases. They also found the seasonal change of the tidal phase and remarkable good agreement between the ground-based lidar and radar data and the model. The comparison of NAVGEM-HA and the meteor radar indicates that tidal phase are variable on the seasonal scale showing already significant shifts and drifts within a week. Previously, for local observations this phase variability was assumed to be the result of a superposition of migrating and non-migrating tidal modes. However, comparing the global tidal fit obtained from NAVGEM-HA of the SW2 tide reflects this behavior as well. These continuous phase changes have severe implications for the analysis of tides at mid- and high latitudes from satellites, which usually requires to average over several weeks to cover all local times.

5.3 NAVGEM-HA and MR winds and tidal day-to-day variability and lunar tides during SSW events

Besides comparing mean winds, we also investigated the day-to-day variability of the semidiurnal tide during two winter seasons with a major SSW event at the mid-latitude location Juliusruh and polar latitudes above Andenes. In 2010 there was a vortex displacement event (e.g., Stober et al., 2012; Matthias et al., 2013), which was already validated by a cross comparison of the mean winds and waves in ~~McCormack et al. (2017)~~ McCormack et al. (2017) using several worldwide-distributed meteor radars. The second SSW event occurred during winter 2012/13 and evolved as a vortex splitting event (e.g., Xu and San Liang, 2017).

Daily mean winds and tidal amplitudes were diagnosed by the ASF. The meteorological analysis of NAVGEM-HA reproduces the general day-to-day variability of winds and even shows a high level of agreement for individual planetary waves passing over the stations. In particular, the timing of the SSW event itself with the zonal wind reversal and the formation of an elevated stratopause is well-captured. Similar to the zonal and meridional wind climatologies, the meteorological analysis tends to show higher magnitudes of the ~~winds~~wind speeds. Previous comparison of wind observations to model data, such as ECMWF or MERRA2, were limited to a maximum altitude of approximately 70-75 km and below (Rüfenacht et al., 2018) and, thus, we omit here any further detailed discussion.

Another very important aspect of this study is the phase variability on a day-to-day basis. The ASF provides information on the phase stability of tides with basically the same resolution as the original measurement time series. Very often tidal phases are assumed to be stable over long periods of up to several months in the analysis. However, for instance, the TIMED satellite requires 60-days to cover all local times due to its orbit geometry (Zhang et al., 2006; Oberheide et al., 2011). Our results indicate that during an SSW the phase of the SW2 tide is significantly altered on a global scale as well as on a regional or local scale as the dynamics of the middle atmosphere change (e.g., Manney et al., 2009; Matthias et al., 2012). ~~Fuller-Rowell et al. (2016)~~ Fuller-Rowell et al. (2016) discussed three possible mechanisms to understand these changes of the tide; ~~Fuller-Rowell et al. (2010); Jin et al. (2012)~~ Fuller-Rowell et al. (2010); Jin et al. (2012) attributed the change of the migrating tidal phase to changes of the mean winds in the middle atmosphere, whereas ~~Pedatella and Forbes (2010)~~ Pedatella and Forbes (201 suggested non-migrating tides as a source of the SW2 phase variability. Other studies favor an amplification of the lunar tide during an SSW (Fejer et al., 2010; Forbes and Zhang, 2012).

We ~~want to disentangle~~ discuss these three aspects using the results obtained from the ASF decomposition of the local and global measurements and meteorological analysis data. ~~Fejer et al. (2010)~~ Fejer et al. (2010) investigated vertical plasma drifts above Jicamarca and found a drift in local time of the semidiurnal oscillation, which was attributed to the lunar tide assuming that all other tidal waves remained stationary and monochromatic. Later ~~Forbes and Zhang (2012)~~ Forbes and Zhang (2012) proposed that the lunar tide enhancement is a result of ~~a shifting of the semidiurnal tide towards the Pekeris resonance and, hence, to~~ the Pekeris resonance effect that is shifted towards the lunar tide period M2 ~~(~~of 12.42 h ~~)~~ due to changes in the mean zonal winds caused by the SSW. They tested the proposed physical mechanism on satellite observations from SABER, CHAMP and GRACE and the steady state Global-Scale-Wave-Model (GSWM) ~~.~~ for a case study and the SSW in 2009. To separate the lunar tide from the semidiurnal SW2 tide, they used a window of ~~24 days~~ 24-days to ensure sufficient frequency resolution and assumed monochromatic and stationary tidal waves within the window. Later, Zhang and Forbes (2014) claimed that the lunar tides seem to enhance during nearly every SSW event arguing that the Pekeris resonance has a rather broad peak and, thus, the resonance conditions are satisfied for all SSW events. Although, Forbes and Zhang (2012) pointed out that a very specific thermal and dynamic structure is required to satisfy the resonance condition.

~~However, our analysis of the~~ In the following, we investigate the phase variability of the semidurnal tide introducing a holographic analysis for the SSW 2012/13 and discuss a potential connection to the Pekeris resonance (Zhang and Forbes, 2014) . The day-to-day variability, obtained from the ASF, indicates that the tidal phase are not stable with time and show significant interday variability, which appears to be related to changes in the zonal wind in the middle atmosphere driven by the polar vortex and planetary waves. Considering that a time dependent phase corresponds to a frequency shift, it is possible to convert this temporal phase variability into a ~~frequency shift~~ period change and, hence, to estimate the spectral line shape of the tide or to derive a holographic representation of the temporal evolution on a day to day basis.

The hologram is derived considering that the tide can be represented by a cosine wave with amplitude A (e.g., semidiurnal tide), a mean frequency w and a time dependent phase $\phi(t)$;

$$A(t) = A\cos(wt + \phi(t)) \quad . \tag{3}$$

Although the true functional form of the time dependent phase might be unknown, we can express this function as a Taylor series at a certain point in time t;

$$\phi(t) = \phi_0 + \frac{d\phi}{dt} \cdot t + ... \tag{4}$$

Truncating the Taylor series at the first order and inserting them in eq. 3 leads to;

$$A(t) = A\cos(wt + \phi_0 + \frac{d\phi}{dt} \cdot t) \ \ . \tag{5}$$

Rearranging the terms according to their time dependence leads to;

$$A(t) = A\cos((w + \frac{d\phi}{dt}) \cdot t + \phi_0) \ \ . \tag{6}$$

It is now straight forward to numerically obtain the time dependent phase change $d\phi/dt$ using a central differences approach in the complex domain.

In Fig. 12 we show a holographic reconstruction based on the ASF decomposition of the semidiurnal tide. This technique only assumes monochromaticity within the adopted window length (less than a day for the semidiurnal tide) and, thus, captures non-stationary processes on an interday basis. The hologram shows that during the SSW event in 2012/13 the phase behavior of the semidiurnal tide itself is shifted to the period range that is expected for the lunar tide M2 (solid white line) and N2 (dashed white line). Further, we overlayed the lunar orbit as elevation angle for the geographic location of Juliusruh to search for a potential connection of the semidiurnal phase variability and the moon position on the sky. The hologram for the global diagnostic is shown in Fig. 13. The main differences in the holograms between the local MR observations and the global tidal fields from NAVGEM-HA are attributed to the decomposition of the global fields into migrating and non-migrating tides. As shown in the appendix B there is an excitation of the non-migrating tides SW1 and SW3, which leads to the differences in the holographic reconstruction. The local diagnostic shows the superposition of all tidal components. However, the global diagnostic also indicates the frequency shifts of the SW2 tide to periods that can match the predicted Pekeris lunar tide resonances. However, as indicated by the white lines, these phase shifts happen frequently during a winter season and are neither correlated to the lunar orbit nor accompanied by a tide enhancement. The effect of the SSW is visible in both holograms up to 10 days after the onset of the SSW, which is also the time delay corresponding to the amplification of the semidiurnal tide after the SSW.

~~Moreover, Forbes and Zhang (2012)~~ Moreover, Forbes and Zhang (2012) reported a delay of ~~5~~ 5-7 days between the occurrence of the lunar tide amplification and the central day of the SSW event. This delay of approx. ~~5~~ 5-7 days is consistent with the holographic analysis, which also shows that the frequency/period shift towards the lunar tide frequency/period (M2 and N2) occurs after the SSW event (central day), at the beginning of the formation of an elevated stratopause or when the polar vortex begins to restore~~.~~, however, well before the semidiurnal tide enhancement. This time span also corresponds to the response time of the semidiurnal tide to a transient forcing, which was estimated to be between 6-10 days (Vial et al., 1991) for comparisons to steady state models. An SSW is also associated by a large exchange of air masses between mid- and polar

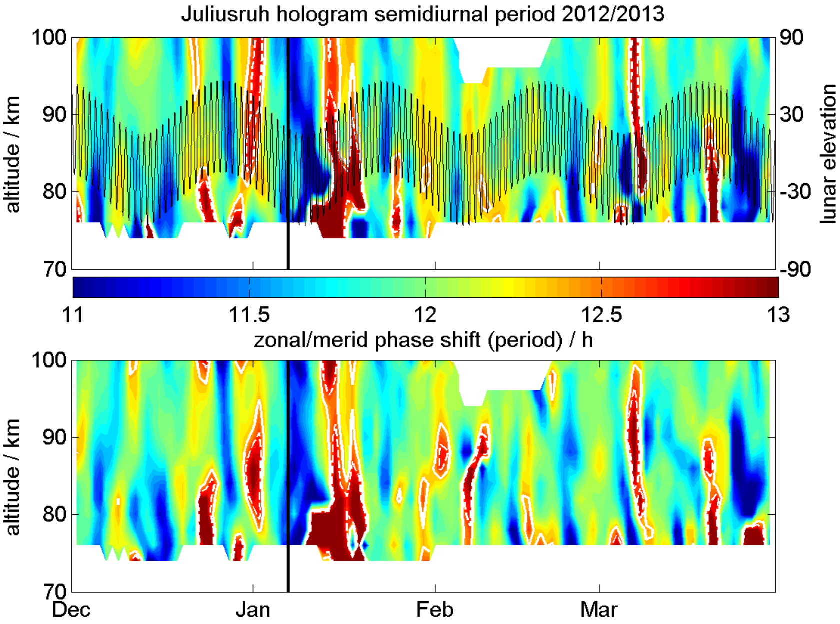

Figure 12. Holographic reconstruction of the semidiurnal tidal phase variability. The hologram shows the periods using a time variable phase, which is equivalent to a frequency shift or change in period. The white contour lines indicate the lunar tide M2 (12.42 h) (solid line) and N2 (12.66 h) (dashed line). The lunar orbit as elevation angle (-90° to 90°) for Juliusruh is plotted as black solid line.

latitudes, which leads to a significant enhancement of the ozone volume mixing ratio inside the polar cap (Schranz et al., 2019), and, thus, provides a potential source to increase the tidal forcing of the semidiurnal tide. Further, this strong meridional coupling also provides a sufficient strong response to explain the low latitude response to the SSW.

Many ~~publications investigating lunar tides use~~ recent studies have investigated lunar tides with window lengths that are long enough to ensure an unambiguous frequency resolution to separate the lunar tide from the semidiurnal tide, which requires at least 21-days or more (e.g., Forbes and Zhang, 2012; Chau et al., 2015; Conte et al., 2017; He et al., 2018; Siddiqui et al., 2018, and reference therein). The ASF analysis indicates that there is a considerable interday tidal variability in amplitude and phase, which poses a challenge to the signal processing. Such intermittent behavior suggests that long windows (longer than even a day) might lead to spurious results, and do not allow a separation of the different waves from each other. The zonal wind reversal and accompanied cooling at the MLT during a SSW last only for a few days (much shorter than the typical window length used for the lunar tides) and cause significant changes in zonal mean wind at mid- and polar latitudes altering the propagation conditions for the tides. As a consequence, such a long window would not allow one to capture SSW effects, which themselves cause changes in the semidiurnal tide. Thus, if one does not notice that an SSW occurred, one cannot know whether the 12.42 h tide is lunar or a semidiurnal tide that was altered by the SSW.

These shortcomings are also mentioned and discussed in (Forbes and Zhang, 2012; Zhang and Forbes, 2014). They fitted the

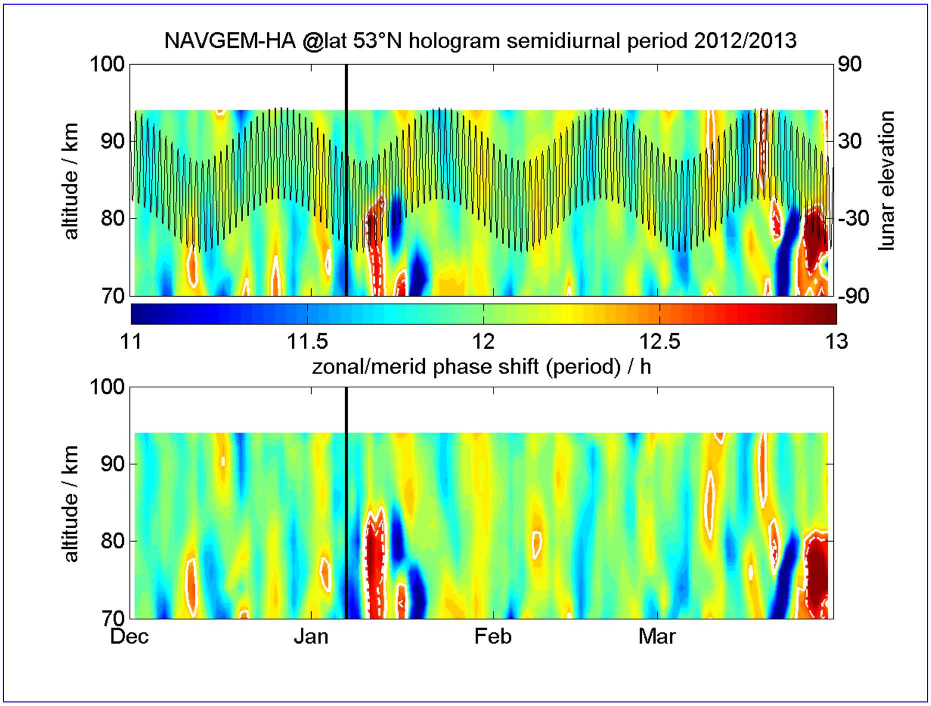

Figure 13. ~~Holographic reconstruction of~~ The same as Fig. 12, but for the ~~SW2 tidal phase variability from the~~ global ~~diagnostic~~ tidal analysis of ~~NAVGEM-HA. The hologram shows~~ the ~~periods using a time variable phase, which is equivalent to a frequency shift or change in period. The white contour lines indicate the lunar tide M2 (12.42 h) (solid line) and N2 (12.66 h) (dashed line).~~ SW2.

lunar tide, for instance, on the residuals of SABER measurements after removing the semidiurnal tide by a 12-day running mean, which still is too long given the huge phase variability of the tide. The caveats of the steady state model GSWM are also discussed in Forbes and Zhang (2012). In particular, the steady state assumption seems to be not fully met during an SSW recalling the results from Vial et al. (1991) as the whole event lasts only 3-4 days at the MLT. We also investigated the non-migrating tidal components (see appendix B) ~~from the~~ derived from NAVGEM-HA winds. It appears that only the SW1 and SW3 tides show a response to the SSW event depending on the latitude and how the SSW evolved. This is consistent with previous studies ~~(Liu et al., 2010). The SW3,~~ (Du et al., 2007; Liu et al., 2010). The SE1, SE2, SE3 and S0 semidiurnal tides show much smaller amplitudes and are negligible compared to the SW2 tide, in particular, at polar latitudes. Another interesting aspect when comparing the migrating and non-migrating tides from NAVGEM-HA is the winter seasonal phase behavior of the SW2 tide. The phase of the tide drifts by several hours between December to March, which correlates to the mean wind morphology. Apparently, the change of the phase of the semidiurnal tide ~~is not explainable~~ may not be explained by a superposition of migrating and non-migrating tides. However, this needs to be examined in more detail and is beyond the scope of this paper.

~~Based on the present analysis , there was no amplification of the lunar tide at mid- and high-latitudes during the two examined~~

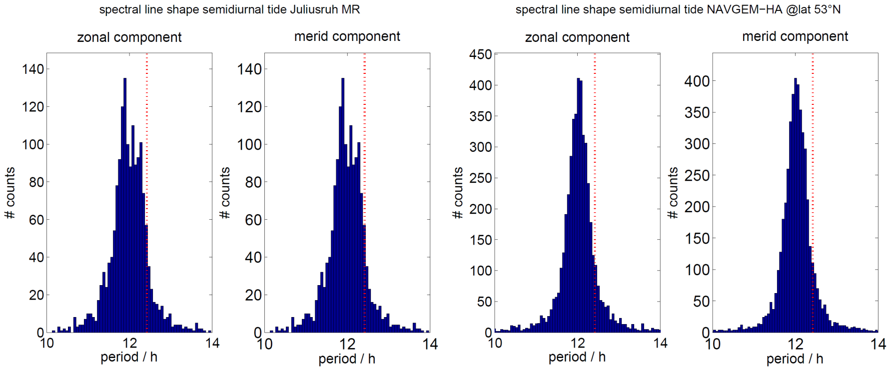

Figure 14. Histograms for the zonal and meridional frequency shift due to a temporal variable phase derived from the holograms. The left two panels show the local meteor radar observations at Juliusruh and the right two panels the global diagnostic inferred from NAVGEM-HA.

~~SSW events.~~ The next aspect we did investigate is a potential correlation between the phase shifts from the holographic analysis and the lunar orbit. Thus, the lunar azimuth, elevation and lunar distance was checked, whether there exists a connection with the SSW events. Holographic analysis of the S2 phase shifts shows frequently periods close to the the M2 tide, indicated by the white contour lines, but no obvious correlation to the lunar position or the other orbital parameters. This behavior is also found for the global hologram.

Finally, we examined the properties of the semidiurnal tide with respect to the frequency and vertical wavelength at the MLT before and during the SSW as well as during the amplitude enhancement after the SSW. The vertical wavelength of the semidiurnal tide was about 50-60 km before the SSW at altitudes between 74-100 km. The same vertical wavelength was observed during the tide enhancement. During the SSW event the vertical wavelength suddenly increased to 150-600 km at Juliusruh and then decreased just as suddenly after the wind reversal, but before the tide enhancement. The global zonal mean diagnostic exhibit similar vertical wavelengths before and after the SSW, but the sudden response in vertical wavelength due to the SSW was less pronounced. However, the hologram also shows that the mean period of the S2/SW2 tide before the SSW and during the tide enhancement is centered around 12.0 h. This does not indicate a lunar tide enhancement, which would require a 12.42 h period. Only during the SSW event itself do the increase in vertical wavelength and the shift of the period towards the M2 period together point to a lunar tide signature that could be interpreted as Pekeris resonance. However, this needs to be investigated with comprehensive models to account for the complex dynamics associated with a SSW.

Previous analysis of the lunar tide facilitating multi-year observations from meteor radars by ~~Sandford et al. (2006)~~ Sandford et al. (2006 showed that the signal is much weaker compared to the total S2 tide. Their spectral analysis also confirms that tides show some spectral broadening. Such a line broadening is also found in our holographic analysis.

Fig. 14 shows the histograms of the frequency distributions obtained from the holograms. The left two panels are computed from the meteor radar observations at Juliusruh (zonal and meridional) and the right two panels from the global diagnostic using NAVGEM-HA at the same latitude (zonal and meridional, respectively). The spectral line shape seems to agree from their general morphology, in particular, the line width. The vertical dashed line denotes the period of the ~~Pekeris resonance~~lunar tide M2, which lies in the natural line width of the SW2 tide. However, the peak of the spectral line obtained from the meteor radar observations at Juliusruh shows two side peaks that can be associated to the vortex splitting event and are related to the planetary wave activity during the winter 2012/13. Due to instrumental effects the number of measurements is not equally distributed over the winter season leading to an apparent double peak structure. The same plot obtained from NAVGEM-HA at the Juliusruh location shows a fully symmetric spectral line shape similar to the global diagnostic. During the vortex displacement event in the winter season 2009/10 the spectral line at Juliusruh is entirely symmetric similar to the global diagnostic for both cases. The global diagnostic is not prone to this type of effect as all longitudes are included in the analysis and, hence, these particularities average out. In the case of lunar tide amplification the global diagnostic should reveal a shoulder at the ~~Pekeris resonance~~ M2 period or asymmetry around the dashed vertical line, which ~~is~~ seems to be not present.~~In principle, it is possible to separate the lunar tide from the semidiurnal tide by modeling the line shape of the S2 tide.~~

Similar to previous studies (Fuller-Rowell et al., 2010, 2016), we attribute the day-to-day variability of the semidiurnal tidal amplitudes and phases to changes of the zonal winds in the middle atmosphere altering the vertical propagation conditions. Although atmospheric tides are global scale waves, their vertical propagation depends on the regional meteorological situation. As a consequence, the observed period or phase at the MLT can be altered. Due to the long horizontal wavelength of the semidiurnal tide, a change in the wind pattern in the middle atmosphere manifests as changes in phase for a single station measurement accompanied by a change of the vertical wavelength of the tide. The holographic reconstruction shows that the day-to-day variability of phase is equivalent to a Doppler shifting of the intrinsic tidal frequency, which causes the line broadening at the MLT.

6 Conclusions

In this study, we cross-validate ~~the meteorological analysis model~~ NAVGEM-HA meteorological analyses with ground-based meteor radar and lidar observations at mid- and high latitudes. For the validation, we performed a detailed analysis of mean winds and temperatures and atmospheric tides using a recently developed tool called adaptive spectral filter (ASF), which is designed to capture the intermittent tidal behavior and provide vector information for mean winds and tides for climatologies. We present a ~~climatological~~ comparison of mean winds, temperatures and the semidiurnal wind tide and its phase behavior ~~. We also presented~~ and a detailed discussion of the day-to-day variability of the semidiurnal tide during two SSW events in 2009/10 and 2012/13 combining global and local diagnostics. We discussed our results in the context of previous studies, in particular, on the lunar tide amplification during SSWs and have outlined potential issues due to the day-to-day semidiurnal tidal variability. ~~Our main conclusions are:~~ The agreement between MR/lidar climatologies and NAVGEM-HA analysis data is remarkably good compared to the seasonal wind and temperature pattern of comprehensive models. NAVGEM-HA tends to show slightly higher ~~winds~~ wind speeds and temperatures compared to the ground-based instruments.

NAVGEM-HA reproduces the seasonal asymmetry of the zonal wind at mid- and high latitudes. The temperature and wind fields in NAVGEM-HA are realistic compared to ground-based sensors up to an altitude of 90 km (geometric altitude). However, our comparison also confirms that the availability of satellites observations for the data assimilation in NAVGEM-HA has an impact on the overall agreement. Further, the meteorological analysis reflects the seasonal phase behavior of the semidiurnal tide, which is constantly changing. These continuous phase changes are important and need to be considered when analyzing satellite observations or spectral analysis using long windows.

NAVGEM-HA reflects the day-to-day variability of the wind and semidiurnal tide amplitude and phase behavior during SSW events.

The combination of NAVGEM-HA meteorological analysis data and ground-based observations allowed us to develop new diagnostics to retrieve atmospheric information and to investigate physical processes. The cross-validation suggests that the global fields of NAVGEM-HA ~~can be used to~~ provide a realistic ~~nudging for~~ boundary to nudge other GCMs coupling the middle atmosphere to the upper atmosphere. In particular, the good agreement of the tidal phases ~~provides~~ is an essential quality benchmark for the lower forcing of the thermosphere and ionosphere through atmospheric tides.

~~The ASF diagnostic allows us to capture the intermittent tidal behavior on a~~ The day-to-day ~~basis and is applicable to different data sets.~~

~~The semidiurnal tidal phase shows a significant variation over the year. This is highly relevant for the extraction of tides from satellite measurements or for the determination of the lunar M2 tide .~~

tidal variability (amplitude and phase) of the semidiurnal tide is associated to changes in the wind pattern in the middle atmosphere altering the vertical propagation conditions of the tide. This is in agreement with previous studies by Fuller-Rowell et al. (2010); . Further, we did investigate a potential lunar tide amplification through the Pekeris resonance effect as proposed by Forbes and Zhang (2012 . The ASF and holographic analysis ~~provides no signature of a lunar tide amplification during SSWevents at mid- and high latitudes as reported by Forbes and Zhang (2012); Conte et al. (2017); He et al. (2018). However, we confirmed that the SSW event causes a~~ permit to determine the different phases of the SSW 2012/13 and the tidal response in much more detail with respect to the timing. The tidal enhancement after the SSW, which was in many previous studies termed to be a lunar tidal enhancement, shows essentially a period around 12.0 h (see holograms) and has the same vertical wavelength of about 50-60 km than the semidiurnal tide before the SSW. The global diagnostic also confirms a wavenumber 2 structure. Further, there are no signs of a coupling and phase relation to the lunar orbit during this time. However, during the SSW there occurs a phase shift of the semidiurnal tide towards the ~~Pekeris resonance, which occurs~~ 12.42 h period and the dynamical and thermal structure could be suitable to shift the Pekeris resonance towards a period of 12.42 h as well, as outlined in Forbes and Zhang (2012); Zhang and Forbes (2014). The increased vertical wavelength of about 150-400 km and the time span of 3-5 days ~~after the SSW .~~

~~The day-to-day tidal variability~~ during this phase of the SSW might be the result of the resonance and may indicate the presence of a lunar tidal mode, but this needs to be confirmed by tidal modelling and is beyond the discussion herein. However, the amplitude of this tidal mode is still much smaller than a typical semidiurnal tide, but might be larger than the average lunar amplitude of about 1-4 m/s (Sandford et al., 2006). Holographic analysis provide a new method to investigate the frequency behavior using short windows in the time domain, but keeping a localized measurement of the frequency resolution. Further, we were able to provide a quantitative spectral measurement of the spectral variability for the semidiurnal tide, which pointed out that the lunar tide (M2) lies well withing the spectral line shape. This has now some implications for epoch analysis of the lunar tide from local observations. The holograms show that there are frequently shifts of the semidiurnal tide towards the M2 (~~amplitude and phase) of~~ 12.42 h) that are disconnected to the ~~semidiurnal tide is attributed to changes in the wind pattern in the middle atmosphere altering the vertical propagation conditions of the tide. This is in agreement with previous studies by Fuller-Rowell et al. (2010); Jin et al. (2012); Fuller-Rowell et al. (2016).~~

lunar orbit, which means the lunar tide can hardly be inferred from such an analysis without additional information, for instance, the vertical wavelength of the lunar tide. In this work we ~~demonstrate~~ have demonstrated the value of meteorological analysis data from NAVGEM-HA to investigate the day-to-day variability of tides in a global context and for local meteor radar observations. Such data sets are essential for nudging thermospheric and ionospheric models for space weather applications. Further, we emphasized that new analysis techniques are required to infer the tidal variability or to separate lunar tides from the semidiurnal tide. Holographic reconstructions and spectral line models for atmospheric tides might be part of such a solution.

Data availability. The meteor radar can be obtained from Gunter Stober upon request from the Leibniz-Institute for Atmospheric Physics. The NAVGEM-HA data used in this study can be obtained from (https://map.nrl.navy.mil/map/pub/nrl/navgem/iap). The lidar observations are available upon request from Kathrin Baumgarten.

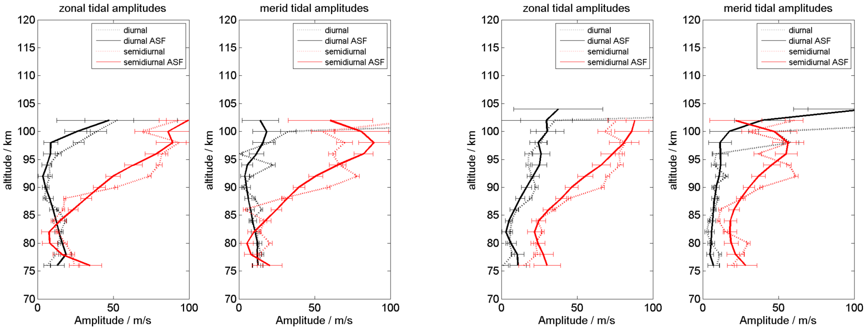

Figure A1. Here we show observations from 1st February 2010 and the Juliusruh meteor radar. The dashed lines indicate the tidal solution applying only temporal fitting and solid line shows the ASF solution with vertical regularization for the diurnal and semidiurnal tide.

Appendix A: Comparison of ASF with and without vertical regularization

Here we provide two examples comparing a tidal amplitude fit for the zonal and meridional component using the 1D ASF and the 2D ASF with vertical regularization to demonstrate how a potential contamination of gravity waves with short vertical wavelengths is reduced. The time difference between the left two panels and the right two panels is 6 hours.

Appendix B: Tidal components from global NAVGEM-HA analyzed winds

In addition to the semidiurnal tide locally observed from the meteor radar as well as from NAVGEM analyzed winds here we provide the results for the westward- and eastward-propagating non-migrating semidiurnal tidal components (SW1, SW3, SE1, SE2, SE3) as well as for the stationary semidiurnal tide (S0) during the winter 2009/2010 and 2012/2013 for the stations at Andenes and Juliusruh from the global fields of NAVGEM-HA.

Appendix C: Vertical wavelength from MR and NAVGEM-HA

Vertical wavelengths were derived from the vertical profiles of the phases of the semidiurnal tidal fit for every day. In the case of the meteor radar the fit is performed at altitudes between 74-100 km. The NAVGEM-HA data was analyzed in the altitude range from 70-90 km. However, as we estimate the vertical wavelengths from a rather thin atmospheric layer at the MLT, the uncertainty of the obtained wavelengths scales with the wavelength itself. There is a tendency that the uncertainties are larger for wavelengths beyond 250 km.

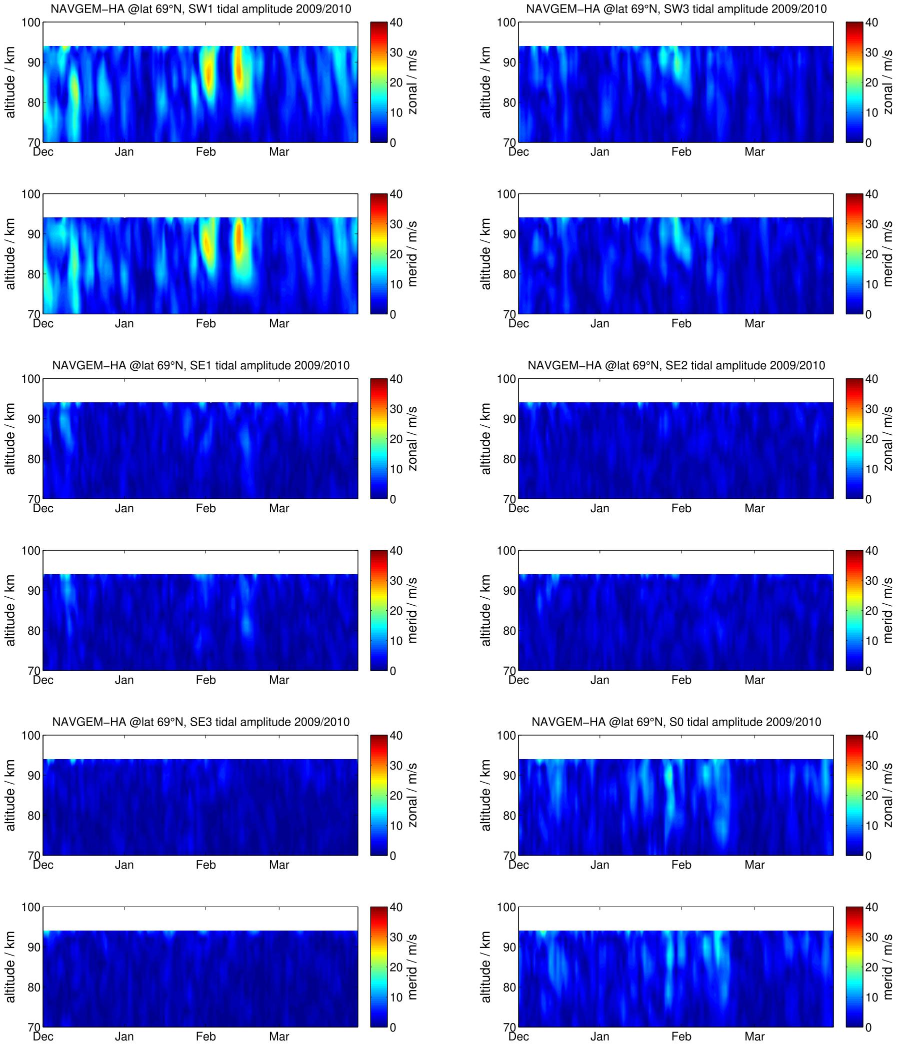

Figure B1. Non-migrating tides derived from global NAVGEM-HA winds above Andenes during the winter 2009/10 for SW1 and SW3 (upper two panels), SE1 and SE2 (middle panels), and SE3 and S0 (lower two panels) tidal components.

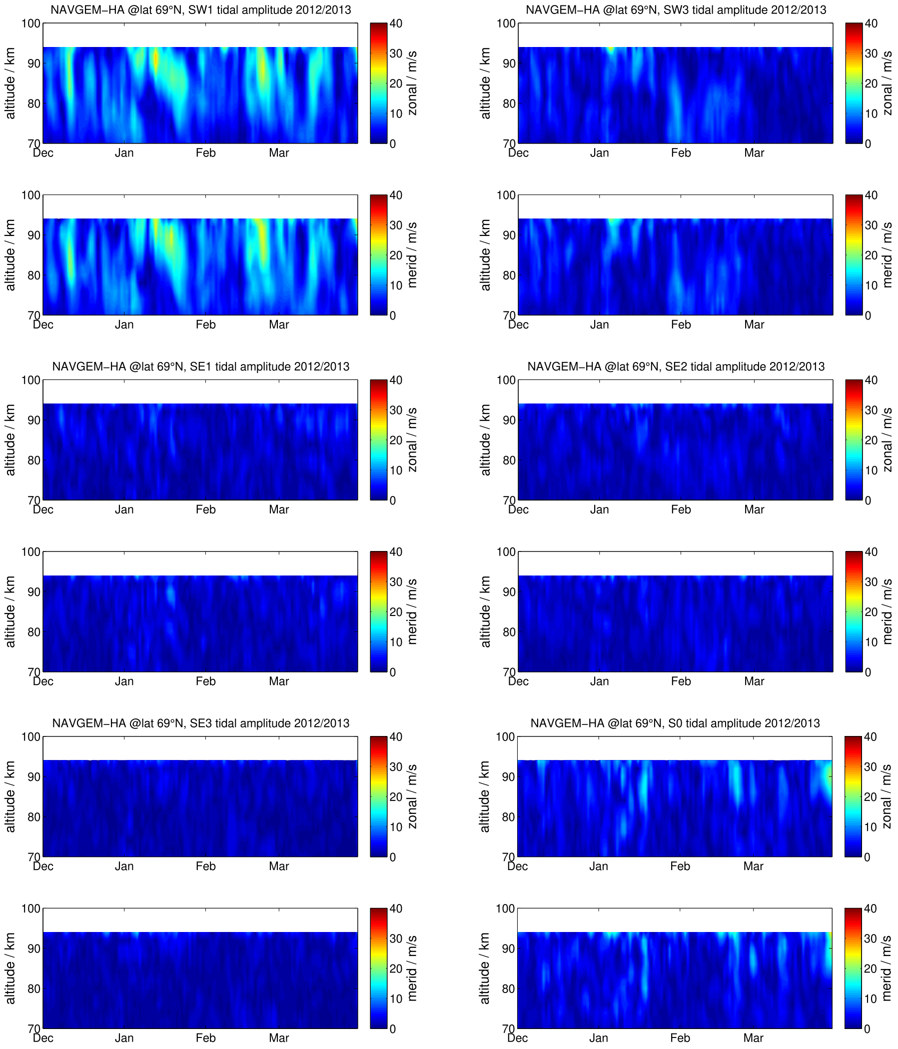

Figure B2. The same as Fig. 13 but for the winter 2012/2013.

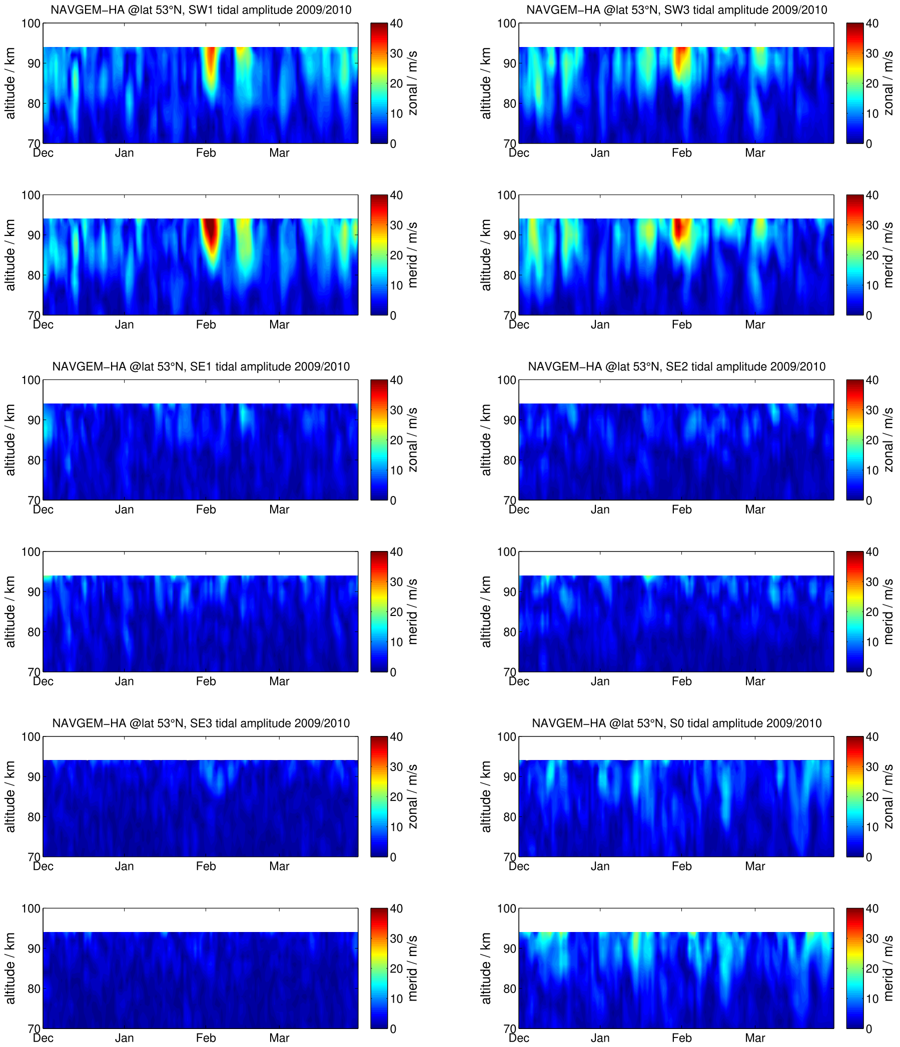

Figure B3. The same as Fig. 13 but above Juliusruh and for the winter 2009/2010.

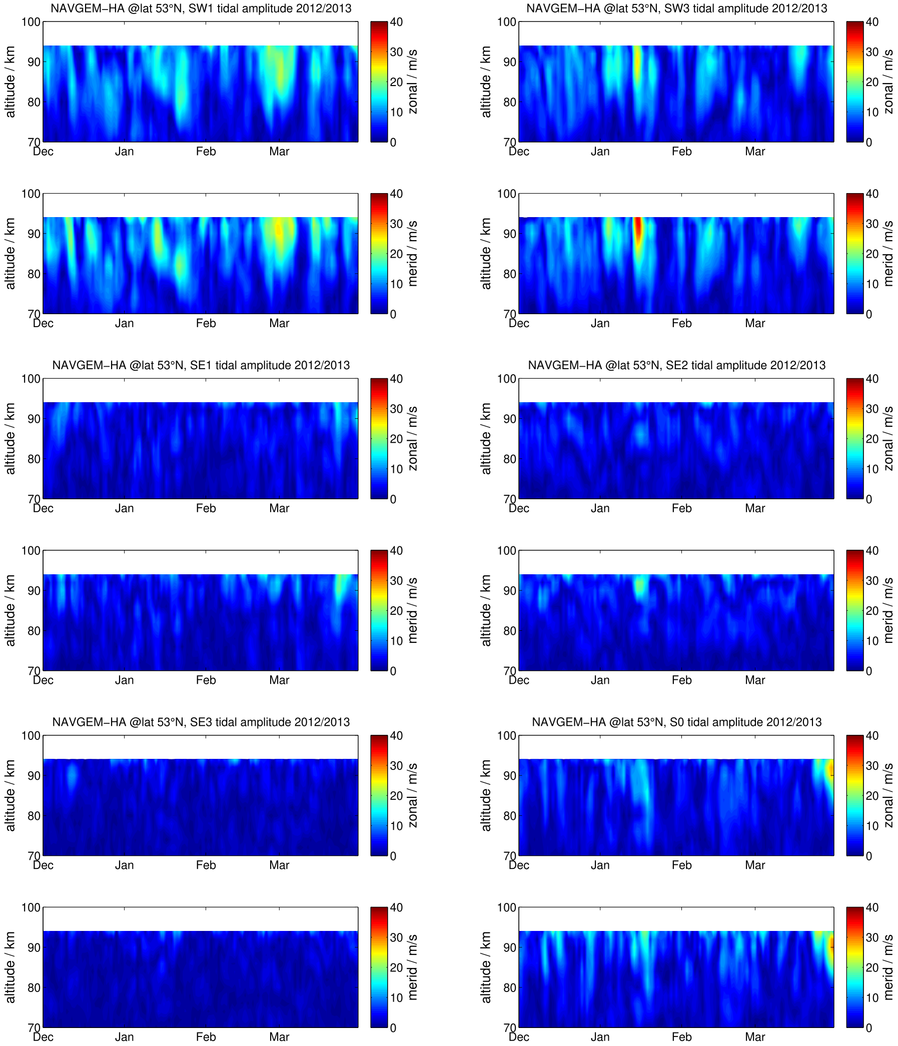

NAVGEM–HA @lat 53°N, SW1 tidal amplitude 2012/2013

NAVGEM–HA @lat 53°N, SW3 tidal amplitude 2012/2013

NAVGEM–HA @lat 53°N, SE1 tidal amplitude 2012/2013

NAVGEM–HA @lat 53°N, SE2 tidal amplitude 2012/2013

NAVGEM–HA @lat 53°N, SE3 tidal amplitude 2012/2013

NAVGEM–HA @lat 53°N, S0 tidal amplitude 2012/2013

Figure B4. The same as Fig. 13 but above Juliusruh and for the winter 2012/2013.

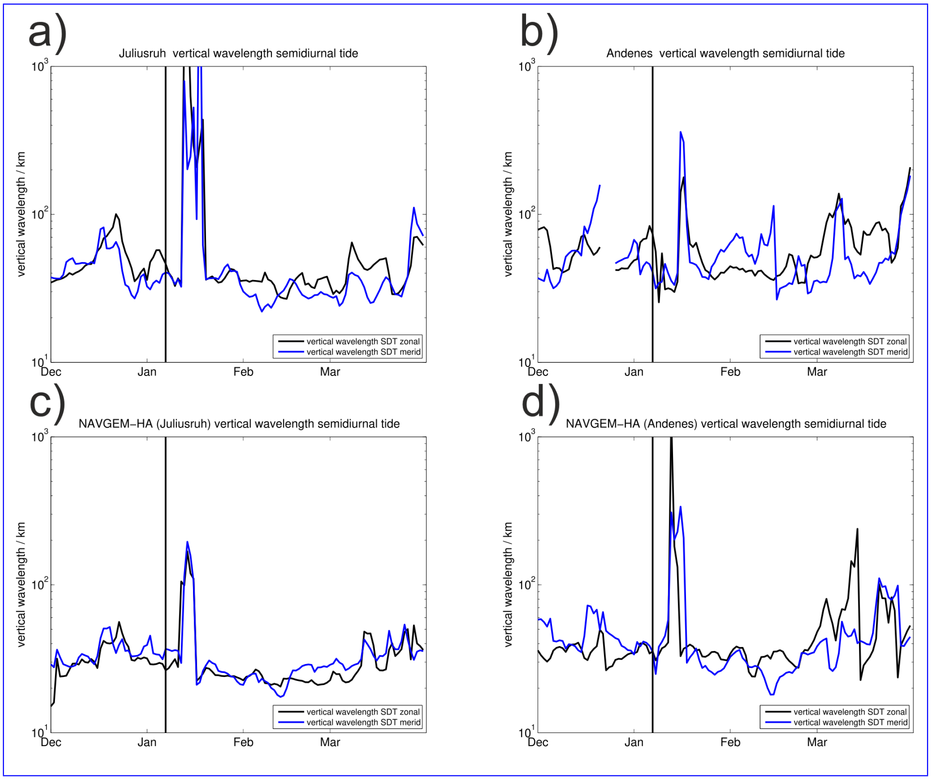

Figure C1. Time series of the vertical wavelength of the semidiurnal tide at Juliusruh and Andenes. The upper two panels a) and b) denote the meteor radar observations for both locations. The lower panels c) and d) are obtained from NAVGEM-HA.

Author contributions. The manuscript is edited and discussed with all authors. The conceptual idea of the manuscript was developed by Gunter Stober, Kathrin Baumgarten and John McCormack. The meteor radar data analysis is performed by Gunter Stober. Kathrin Baumgarten computed partly the lidar temperatures and analyzed both lidar data sets. Peter Brown contributed with the CMOR radar data, read and edited the manuscript and helped with the discussions. Jerry Czarnecki provided support in the data analysis and helped discussing the results.

Acknowledgements. This work is supported by the University of Bern Institute of Applied Physics and the Oeschger Center for Climate Change Research. Kathrin Baumgarten is supported by the Deutsche Forschungsgemeinschaft (DFG; German Research Foundation) under project LU1174/8-1 (PACOG) of the research unit FOR1898 within the Research Unit MS-GWaves. The work at the Naval Research Laboratory was supported by the Chief of Naval research and by a grant of computer time from the High Performance Computing Modernization Program. We gratefully acknowledge Michael Gerding, Michael Priester and Torsten Köpnick for the maintenance and operation of the lidar systems at IAP as well as all students for helping in lidar operation. We appreciate the support from Josef Höffner in computing the resonance lidar temperatures. We acknowledge the technical support of the IAP technicians in the operation of the meteor radars.

References

Akmaev, R. A.: WHOLE ATMOSPHERE MODELING: CONNECTING TERRESTRIAL AND SPACE WEATHER, Reviews of Geophysics, 49, https://doi.org/10.1029/2011RG000364, https://agupubs.onlinelibrary.wiley.com/doi/abs/10.1029/2011RG000364, 2011.

Alpers, M., Eixmann, R., Fricke-Begemann, C., Gerding, M., and Höffner, J.: Temperature lidar measurements from 1 to 105 km altitude using resonance, Rayleigh, and rotational Raman scattering, Atmos. Chem. Phys., 4, 793–800, 2004.

Andrews, D., Holton, J., and Leovy, C.: Middle Atmosphere Dynamics, International Geophysics, Elsevier Science, https://books.google.de/books?id=N1oNurYZefAC, 1987.

Baumgarten, K. and Stober, G.: On the evaluation of the phase relation between temperature and wind tides based on ground-based measurements and reanalysis data in the middle atmosphere, Annales Geophysicae, 37, 581–602, https://doi.org/10.5194/angeo-37-581-2019, https://www.ann-geophys.net/37/581/2019/, 2019.

Baumgarten, K., Gerding, M., and Lübken, F.-J.: Seasonal variation of gravity wave parameters using different filter methods with daylight lidar measurements at midlatitudes, Journal of Geophysical Research: Atmospheres, 122, 2683–2695, https://doi.org/10.1002/2016JD025916, https://agupubs.onlinelibrary.wiley.com/doi/abs/10.1002/2016JD025916, 2017.

Baumgarten, K., Gerding, M., Baumgarten, G., and Lübken, F.-J.: Temporal variability of tidal and gravity waves during a record long 10-day continuous lidar sounding, Atmospheric Chemistry and Physics, 18, 371–384, https://doi.org/10.5194/acp-18-371-2018, https://www.atmos-chem-phys.net/18/371/2018/, 2018.

Becker, E.: Dynamical Control of the Middle Atmosphere, Space Science Reviews, 168, 283–314, https://doi.org/10.1007/s11214-011-9841-5, http://dx.doi.org/10.1007/s11214-011-9841-5, 2012.

Becker, E.: Mean-Flow Effects of Thermal Tides in the Mesosphere and Lower Thermosphere, Journal of the Atmospheric Sciences, 74, 2043–2063, https://doi.org/10.1175/JAS-D-16-0194.1, https://doi.org/10.1175/JAS-D-16-0194.1, 2017.

Brown, P., Weryk, R., Wong, D., and Jones, J.: A meteoroid stream survey using the Canadian Meteor Orbit Radar: I. Methodology and radiant catalogue, Icarus, 195, 317–339, https://doi.org/https://doi.org/10.1016/j.icarus.2007.12.002, http://www.sciencedirect.com/science/article/pii/S0019103507005994, 2008.

Chandran, A. and Collins, R. L.: Stratospheric sudden warming effects on winds and temperature in the middle atmosphere at middle and low latitudes: a study using WACCM, Annales Geophysicae, 32, 859–874, https://doi.org/10.5194/angeo-32-859-2014, https://www.ann-geophys.net/32/859/2014/, 2014.

Chandran, A., Collins, R., and Harvey, V.: Stratosphere-mesosphere coupling during stratospheric sudden warming events, Advances in Space Research, 53, 1265–1289, https://doi.org/https://doi.org/10.1016/j.asr.2014.02.005, http://www.sciencedirect.com/science/article/pii/S0273117714000933, 2014.

Chapman, S. and Lindzen, R.: Atmospheric Tides: Thermal and Gravitational, Gordon and Breach, https://books.google.de/books?id=9kSRJaLJ9EEC, 1970.

Chau, J. L., Hoffmann, P., Pedatella, N. M., Matthias, V., and Stober, G.: Upper mesospheric lunar tides over middle and high latitudes during sudden stratospheric warming events, Journal of Geophysical Research: Space Physics, 120, 3084–3096, https://doi.org/10.1002/2015JA020998, https://agupubs.onlinelibrary.wiley.com/doi/abs/10.1002/2015JA020998, 2015.

Chen, C., Chu, X., McDonald, A. J., Vadas, S. L., Yu, Z., Fong, W., and Lu, X.: Inertia-gravity waves in Antarctica: A case study using simultaneous lidar and radar measurements at McMurdo/Scott Base (77.8°S, 166.7°E), Journal of Geophysical Research: Atmospheres, 118, 2794–2808, https://doi.org/10.1002/jgrd.50318, https://agupubs.onlinelibrary.wiley.com/doi/abs/10.1002/jgrd.50318, 2013.

Conte, J. F., Chau, J. L., Stober, G., Pedatella, N., Maute, A., Hoffmann, P., Janches, D., Fritts, D., and Murphy, D. J.: Climatology of semidiurnal lunar and solar tides at middle and high latitudes: Interhemispheric comparison, Journal of Geophysical Research: Space Physics, 122, 7750–7760, https://doi.org/10.1002/2017JA024396, https://agupubs.onlinelibrary.wiley.com/doi/abs/10.1002/2017JA024396, 2017.

Coy, L. and Pawson, S.: The Major Stratospheric Sudden Warming of January 2013: Analyses and Forecasts in the GEOS-5 Data Assimilation System, Monthly Weather Review, 143, 491–510, https://doi.org/10.1175/MWR-D-14-00023.1, https://doi.org/10.1175/MWR-D-14-00023.1, 2015.

Davis, R. N., Du, J., Smith, A. K., Ward, W. E., and Mitchell, N. J.: The diurnal and semidiurnal tides over Ascension Island (8° S, 14° W) and their interaction with the stratospheric quasi-biennial oscillation: studies with meteor radar, eCMAM and WACCM, Atmospheric Chemistry and Physics, 13, 9543–9564, https://doi.org/10.5194/acp-13-9543-2013, https://www.atmos-chem-phys.net/13/9543/2013/, 2013.

Dawkins, E. C. M., Feofilov, A., Rezac, L., Kutepov, A. A., Janches, D., Hoeffner, J., Chu, X., Lu, X., Mlynczak, M. G., and Russell, J.: Validation of SABER v2.0 Operational Temperature Data With Ground-Based Lidars in the Mesosphere-Lower Thermosphere Region (75-105 km), Journal of Geophysical Research: Atmospheres, 123, 9916–9934, https://doi.org/10.1029/2018JD028742, https://doi.org/10.1029/2018JD028742, 2018.

Dhadly, M. S., Emmert, J. T., Drob, D. P., McCormack, J. P., and Niciejewski, R. J.: Short-Term and Interannual Variations of Migrating Diurnal and Semidiurnal Tides in the Mesosphere and Lower Thermosphere, Journal of Geophysical Research: Space Physics, 123, 7106–7123, https://doi.org/10.1029/2018JA025748, https://agupubs.onlinelibrary.wiley.com/doi/abs/10.1029/2018JA025748, 2018.

Dörnbrack, A., Pitts, M. C., Poole, L. R., Orsolini, Y. J., Nishii, K., and Nakamura, H.: The 2009–2010 Arctic stratospheric winter – general evolution, mountain waves and predictability of an operational weather forecast model, Atmospheric Chemistry and Physics, 12, 3659–3675, https://doi.org/10.5194/acp-12-3659-2012, https://www.atmos-chem-phys.net/12/3659/2012/, 2012.

Du, J., Ward, W., Oberheide, J., Nakamura, T., and Tsuda, T.: Semidiurnal tides from the extended Canadian Middle Atmosphere Model (CMAM) and comparisons with TIMED Doppler interferometer (TIDI) and meteor radar observations, Journal of Atmospheric and Solar-Terrestrial Physics, 69, 2159 – 2202, https://doi.org/https://doi.org/10.1016/j.jastp.2007.07.014, http://www.sciencedirect.com/science/article/pii/S1364682607002234, vertical Coupling in the Atmosphere/Ionosphere System, 2007.

Eckermann, S. D., Hoppel, K. W., Coy, L., McCormack, J. P., Siskind, D. E., Nielsen, K., Kochenash, A., Stevens, M. H., Englert, C. R., Singer, W., and Hervig, M.: High-altitude data assimilation system experiments for the northern summer mesosphere season of 2007, Journal of Atmospheric and Solar-Terrestrial Physics, 71, 531 – 551, https://doi.org/https://doi.org/10.1016/j.jastp.2008.09.036, http://www.sciencedirect.com/science/article/pii/S1364682608002575, global Perspectives on the Aeronomy of the Summer Mesopause Region, 2009.

Eckermann, S. D., Ma, J., Hoppel, K. W., Kuhl, D. D., Allen, D. R., Doyle, J. A., Viner, K. C., Ruston, B. C., Baker, N. L., Swadley, S. D., Whitcomb, T. R., Reynolds, C. A., Xu, L., Kaifler, N., Kaifler, B., Reid, I. M., Murphy, D. J., and Love, P. T.: High-Altitude (0-100 km) Global Atmospheric Reanalysis System: Description and Application to the 2014 Austral Winter of the Deep Propagating Gravity Wave Experiment (DEEPWAVE), Monthly Weather Review, 146, 2639–2666, https://doi.org/10.1175/MWR-D-17-0386.1, https://doi.org/10.1175/MWR-D-17-0386.1, 2018.

Ehard, B., Kaifler, B., Kaifler, N., and Rapp, M.: Evaluation of methods for gravity wave extraction from middle-atmospheric lidar temperature measurements, Atmospheric Measurement Techniques, 8, 4645–4655, https://doi.org/10.5194/amt-8-4645-2015, https://www.atmos-meas-tech.net/8/4645/2015/, 2015.

Fejer, B. G., Olson, M. E., Chau, J. L., Stolle, C., Lühr, H., Goncharenko, L. P., Yumoto, K., and Nagatsuma, T.: Lunar-dependent equatorial ionospheric electrodynamic effects during sudden stratospheric warmings, Journal of Geophysical Research: Space Physics, 115, https://doi.org/10.1029/2010JA015273, https://agupubs.onlinelibrary.wiley.com/doi/abs/10.1029/2010JA015273, 2010.

Forbes, J. M.: Atmospheric tides: 1. Model description and results for the solar diurnal component, Journal of Geophysical Research: Space Physics, 87, 5222–5240, https://doi.org/10.1029/JA087iA07p05222, https://agupubs.onlinelibrary.wiley.com/doi/abs/10.1029/JA087iA07p05222, 1982.

Forbes, J. M. and Zhang, X.: Lunar tide amplification during the January 2009 stratosphere warming event: Observations and theory, Journal of Geophysical Research: Space Physics, 117, https://doi.org/10.1029/2012JA017963, https://agupubs.onlinelibrary.wiley.com/doi/abs/10.1029/2012JA017963, 2012.

Forbes, J. M., Zhang, X., Palo, S., Russell, J., Mertens, C. J., and Mlynczak, M.: Tidal variability in the ionospheric dynamo region, Journal of Geophysical Research: Space Physics, 113, https://doi.org/10.1029/2007JA012737, https://agupubs.onlinelibrary.wiley.com/doi/abs/10.1029/2007JA012737, 2008.

Fricke-Begemann, C., Alpers, M., and Höffner, J.: Daylight rejection with a new receiver for potassium resonance temperature lidars, Opt. Lett., 27, 1932–1934, https://doi.org/10.1364/OL.27.001932, http://ol.osa.org/abstract.cfm?URI=ol-27-21-1932, 2002.

Fritts, D. C., Miller, A. D., Kjellstrand, C. B., Geach, C., Williams, B. P., Kaifler, B., Kaifler, N., Jones, G., Rapp, M., Limon, M., Reimuller, J., Wang, L., Hanany, S., Gisinger, S., Zhao, Y., Stober, G., and Randall, C. E.: PMC Turbo: Studying Gravity Wave and Instability Dynamics in the Summer Mesosphere Using Polar Mesospheric Cloud Imaging and Profiling From a Stratospheric Balloon, Journal of Geophysical Research: Atmospheres, 124, 6423–6443, https://doi.org/10.1029/2019JD030298, https://agupubs.onlinelibrary.wiley.com/doi/abs/10.1029/2019JD030298, 2019.

Fuller-Rowell, T., Wu, F., Akmaev, R., Fang, T.-W., and Araujo-Pradere, E.: A whole atmosphere model simulation of the impact of a sudden stratospheric warming on thermosphere dynamics and electrodynamics, Journal of Geophysical Research: Space Physics, 115, https://doi.org/10.1029/2010JA015524, https://agupubs.onlinelibrary.wiley.com/doi/abs/10.1029/2010JA015524, 2010.

Fuller-Rowell, T. J., Fang, T.-W., Wang, H., Matthias, V., Hoffmann, P., Hocke, K., and Studer, S.: Impact of Migrating Tides on Electrodynamics During the January 2009 Sudden Stratospheric Warming, chap. 14, pp. 163–174, American Geophysical Union (AGU), https://doi.org/10.1002/9781118929216.ch14, https://agupubs.onlinelibrary.wiley.com/doi/abs/10.1002/9781118929216.ch14, 2016.

Gerding, M., Höffner, J., Lautenbach, J., Rauthe, M., and Lübken, F.-J.: Seasonal variation of nocturnal temperatures between 1 and 105 km altitude at 54° N observed by lidar, Atmospheric Chemistry and Physics, 8, 7465–7482, https://doi.org/10.5194/acp-8-7465-2008, https://www.atmos-chem-phys.net/8/7465/2008/, 2008.

Hauchecorne, A. and Chanin, M. L.: Density and Temperature Profiles obtained by Lidar between 35 and 70 km, Geophys. Res. Lett., 7, 565–568, 1980.

He, M., Chau, J. L., Stober, G., Li, G., Ning, B., and Hoffmann, P.: Relations Between Semidiurnal Tidal Variants Through Diagnosing the Zonal Wavenumber Using a Phase Differencing Technique Based on Two Ground-Based Detectors, Journal of Geophysical Research: Atmospheres, 123, 4015–4026, https://doi.org/10.1002/2018JD028400, https://agupubs.onlinelibrary.wiley.com/doi/abs/10.1002/2018JD028400, 2018.

Hocking, W., Fuller, B., and Vandepeer, B.: Real-time determination of meteor-related parameters utilizing modern digital technology, Journal of Atmospheric and Solar-Terrestrial Physics, 63, 155 – 169, https://doi.org/http://dx.doi.org/10.1016/S1364-6826(00)00138-3, http://www.sciencedirect.com/science/article/pii/S1364682600001383, radar applications for atmosphere and ionosphere research - PIERS 1999, 2001.

Hogan, T. F., Liu, M., Ridout, J. A., Peng, M. S., Whitcomb, T. R., Ruston, B. C., Reynolds, C. A., Eckermann, S. D., Moskaitis, J. R., Baker, N. L., McCormack, J. P., Viner, K. C., McLay, J. G., Flatau, M. K., Xu, L., Chen, C., and Chang, S. W.: The Navy Global Environmental Model, Oceanography, 27, https://doi.org/10.5670/oceanog.2014.73, 2014.

Jacobi, C., Hoffmann, P., and Kürschner, D.: Trends in MLT region winds and planetary waves, Collm (52° N, 15° E), Annales Geophysicae, 26, 1221–1232, https://doi.org/10.5194/angeo-26-1221-2008, https://www.ann-geophys.net/26/1221/2008/, 2008.

Jin, H., Miyoshi, Y., Pancheva, D., Mukhtarov, P., Fujiwara, H., and Shinagawa, H.: Response of migrating tides to the stratospheric sudden warming in 2009 and their effects on the ionosphere studied by a whole atmosphere-ionosphere model GAIA with COSMIC and TIMED/SABER observations, Journal of Geophysical Research: Space Physics, 117, https://doi.org/10.1029/2012JA017650, https://agupubs.onlinelibrary.wiley.com/doi/abs/10.1029/2012JA017650, 2012.

Jones Jr., M., Drob, D. P., Siskind, D. E., McCormack, J. P., Maute, A., McDonald, S. E., and Dymond, K. F.: Evaluating Different Techniques for Constraining Lower Atmospheric Variability in an Upper Atmosphere General Circulation Model: A Case Study During the 2010 Sudden Stratospheric Warming, Journal of Advances in Modeling Earth Systems, 10, 3076–3102, https://doi.org/10.1029/2018MS001440, https://agupubs.onlinelibrary.wiley.com/doi/abs/10.1029/2018MS001440, 2018.

Kuhl, D., Rosmond, T., Bishop, C., McLay, J., and Baker, N.: Comparison of hybrid ensemble/4DVar and 4DVar within the NAVDAS-AR data assimilation framework, Mon. Wea. Rev., 141, 2740–2758, https://doi.org/10.1175/MWR-D-12-00182.1, 2013.

Laskar, F. I., McCormack, J. P., Chau, J. L., Pallamraju, D., Hoffmann, P., and Singh, R. P.: Interhemispheric Meridional Circulation During Sudden Stratospheric Warming, Journal of Geophysical Research: Space Physics, 124, 7112–7122, https://doi.org/10.1029/2018JA026424, https://agupubs.onlinelibrary.wiley.com/doi/abs/10.1029/2018JA026424, 2019.

Lima, L. M., Paulino, A. R. S., Medeiros, A. F., Buriti, R. A., Batista, P. P., Clemesha, B. R., and Takahashi, H.: First observation of the diurnal and semidiurnal ocillation in the mesospheric winds over São João do Cariri-PB, Brazil, Revista Brasileira de Geofísica, 25, 35–41, http://www.scielo.br/scielo.php?script=sci_arttext&pid=S0102-261X2007000600005&nrm=iso, 2007.

Limpasuvan, V., Orsolini, Y. J., Chandran, A., Garcia, R. R., and Smith, A. K.: On the composite response of the MLT to major sudden stratospheric warming events with elevated stratopause, Journal of Geophysical Research: Atmospheres, 121, 4518–4537, https://doi.org/10.1002/2015JD024401, https://agupubs.onlinelibrary.wiley.com/doi/abs/10.1002/2015JD024401, 2016.

Lindzen, R. S.: Atmospheric Tides, Annual Review of Earth and Planetary Sciences, 7, 199–225, https://doi.org/10.1146/annurev.ea.07.050179.001215, https://doi.org/10.1146/annurev.ea.07.050179.001215, 1979.

Liu, H., Miyoshi, Y., Miyahara, S., Jin, H., Fujiwara, H., and Shinagawa, H.: Thermal and dynamical changes of the zonal mean state of the thermosphere during the 2009 SSW: GAIA simulations, Journal of Geophysical Research: Space Physics, 119, 6784–6791, https://doi.org/10.1002/2014JA020222, https://agupubs.onlinelibrary.wiley.com/doi/abs/10.1002/2014JA020222, 2014.

Liu, H.-L.: Variability and predictability of the space environment as related to lower atmosphere forcing, Space Weather, 14, 634–658, https://doi.org/10.1002/2016SW001450, https://agupubs.onlinelibrary.wiley.com/doi/abs/10.1002/2016SW001450, 2016.

Liu, H.-L., Wang, W., Richmond, A. D., and Roble, R. G.: Ionospheric variability due to planetary waves and tides for solar minimum conditions, Journal of Geophysical Research: Space Physics, 115, https://doi.org/10.1029/2009JA015188, https://agupubs.onlinelibrary.wiley.com/doi/abs/10.1029/2009JA015188, 2010.

Lomb, N. R.: Least-squares frequency analysis of unequally spaced data, Astrophysics and Space Science, 39, 447–462, https://doi.org/10.1007/BF00648343, http://dx.doi.org/10.1007/BF00648343, 1976.

Manney, G. L., Krüger, K., Pawson, S., Minschwaner, K., Schwartz, M. J., Daffer, W. H., Livesey, N. J., Mlynczak, M. G., Remsberg, E. E., Russell III, J. M., and Waters, J. W.: The evolution of the stratopause during the 2006 major warming: Satellite data and assimilated meteorological analyses, Journal of Geophysical Research: Atmospheres, 113, https://doi.org/10.1029/2007JD009097, https://agupubs.onlinelibrary.wiley.com/doi/abs/10.1029/2007JD009097, 2008.

Manney, G. L., Schwartz, M. J., Krüger, K., Santee, M. L., Pawson, S., Lee, J. N., Daffer, W. H., Fuller, R. A., and Livesey, N. J.: Aura Microwave Limb Sounder observations of dynamics and transport during the record-breaking 2009 Arctic stratospheric major warming, Geophysical Research Letters, 36, https://doi.org/10.1029/2009GL038586, https://agupubs.onlinelibrary.wiley.com/doi/abs/10.1029/2009GL038586, 2009.

Marsh, D. R.: Chemical–Dynamical Coupling in the Mesosphere and Lower Thermosphere, pp. 3–17, Springer Netherlands, Dordrecht, https://doi.org/10.1007/978-94-007-0326-1_1, https://doi.org/10.1007/978-94-007-0326-1_1, 2011.

Matsuno, T.: A Dynamical Model of the Stratospheric Sudden Warming, Journal of the Atmospheric Sciences, 28, 1479–1494, https://doi.org/10.1175/1520-0469(1971)028<1479:ADMOTS>2.0.CO;2, https://doi.org/10.1175/1520-0469(1971)028<1479:ADMOTS>2.0.CO;2, 1971.

Matthias, V., Hoffmann, P., Rapp, M., and Baumgarten, G.: Composite analysis of the temporal development of waves in the polar {MLT} region during stratospheric warmings, Journal of Atmospheric and Solar-Terrestrial Physics, 90 - 91, 86 – 96, https://doi.org/http://dx.doi.org/10.1016/j.jastp.2012.04.004, recent Progress in the Vertical Coupling in the Atmosphere-Ionosphere System, 2012.

Matthias, V., Hoffmann, P., Manson, A., Meek, C., Stober, G., Brown, P., and Rapp, M.: The impact of planetary waves on the latitudinal displacement of sudden stratospheric warmings, Annales Geophysicae, 31, 1397–1415, https://doi.org/10.5194/angeo-31-1397-2013, http://www.ann-geophys.net/31/1397/2013/, 2013.

McCormack, J., Hoppel, K., Kuhl, D., de Wit, R., Stober, G., Espy, P., Baker, N., Brown, P., Fritts, D., Jacobi, C., Janches, D., Mitchell, N., Ruston, B., Swadley, S., Viner, K., Whitcomb, T., and Hibbins, R.: Comparison of mesospheric winds from a high-altitude meteorological analysis system and meteor radar observations during the boreal winters of 2009-2010 and 2012-2013, Journal of Atmospheric and Solar-Terrestrial Physics, 154, 132 – 166, https://doi.org/http://dx.doi.org/10.1016/j.jastp.2016.12.007, http://www.sciencedirect.com/science/article/pii/S1364682616303182, 2017.

McCormack, J. P., Eckermann, S. D., and Hogan, T. F.: Generation of a Quasi-Biennial Oscillation in an NWP Model Using a Stochastic Gravity Wave Drag Parameterization, Monthly Weather Review, 143, 2121–2147, https://doi.org/10.1175/MWR-D-14-00208.1, https://doi.org/10.1175/MWR-D-14-00208.1, 2015.

Merzlyakov, E., Jacobi, C., Portnyagin, Y., and Solovjova, T.: Structural changes in trend parameters of the MLT winds based on wind measurements at Obninsk (55°N, 37°E) and Collm (52°N, 15°E), J. of Atmospheric and Solar-Terrestrial Physics, 71, 1547–1557, https://doi.org/https://doi.org/10.1016/j.jastp.2009.05.013, http://www.sciencedirect.com/science/article/pii/S1364682609001461, long-Term Changes and Trends in the Atmosphere-Ionosphere System, 2009.

Miyoshi, Y., Pancheva, D., Mukhtarov, P., Jin, H., Fujiwara, H., and Shinagawa, H.: Excitation mechanism of non-migrating tides, J. of Atmospheric and Solar-Terrestrial Physics, 156, 24–36, https://doi.org/https://doi.org/10.1016/j.jastp.2017.02.012, http://www.sciencedirect.com/science/article/pii/S1364682616302711, 2017.

Oberheide, J., Forbes, J. M., Häusler, K., Wu, Q., and Bruinsma, S. L.: Tropospheric tides from 80 to 400 km: Propagation, interannual variability, and solar cycle effects, Journal of Geophysical Research: Atmospheres, 114, https://doi.org/10.1029/2009JD012388, https://agupubs.onlinelibrary.wiley.com/doi/abs/10.1029/2009JD012388, 2009.

Oberheide, J., Forbes, J. M., Zhang, X., and Bruinsma, S. L.: Climatology of upward propagating diurnal and semidiurnal tides in the thermosphere, Journal of Geophysical Research: Space Physics, 116, https://doi.org/10.1029/2011JA016784, https://agupubs.onlinelibrary.wiley.com/doi/abs/10.1029/2011JA016784, 2011.

Pedatella, N. M. and Forbes, J. M.: Evidence for stratosphere sudden warming-ionosphere coupling due to vertically propagating tides, Geophysical Research Letters, 37, https://doi.org/10.1029/2010GL043560, https://agupubs.onlinelibrary.wiley.com/doi/abs/10.1029/2010GL043560, 2010.

Pedatella, N. M. and Maute, A.: Impact of the semidiurnal lunar tide on the midlatitude thermospheric wind and ionosphere during sudden stratosphere warmings, Journal of Geophysical Research: Space Physics, 120, 10,740–10,753, https://doi.org/10.1002/2015JA021986, https://agupubs.onlinelibrary.wiley.com/doi/abs/10.1002/2015JA021986, 2015.

Pedatella, N. M., Liu, H.-L., and Richmond, A. D.: Atmospheric semidiurnal lunar tide climatology simulated by the Whole Atmosphere Community Climate Model, Journal of Geophysical Research: Space Physics, 117, https://doi.org/10.1029/2012JA017792, https://agupubs.onlinelibrary.wiley.com/doi/abs/10.1029/2012JA017792, 2012.

Pedatella, N. M., Fuller-Rowell, T., Wang, H., Jin, H., Miyoshi, Y., Fujiwara, H., Shinagawa, H., Liu, H.-L., Sassi, F., Schmidt, H., Matthias, V., and Goncharenko, L.: The neutral dynamics during the 2009 sudden stratosphere warming simulated by different whole atmosphere models, Journal of Geophysical Research: Space Physics, 119, 1306–1324, https://doi.org/10.1002/2013JA019421, https://agupubs.onlinelibrary.wiley.com/doi/abs/10.1002/2013JA019421, 2014.

Pokhotelov, D., Becker, E., Stober, G., and Chau, J. L.: Seasonal variability of atmospheric tides in the mesosphere and lower thermosphere: meteor radar data and simulations, Annales Geophysicae, 36, 825–830, https://doi.org/10.5194/angeo-36-825-2018, https://www.ann-geophys.net/36/825/2018/, 2018.

Portnyagin, Y., Forbes, J., Fraser, G., Vlncent, R., Avery, S., Lysenko, I., and Makarov, N.: Dynamics of the Antarctic and Arctic mesosphere and lower thermosphere regions II. The semidiurnal tide, J. of Atmospheric and Terrestrial Physics, 55, 843–855, https://doi.org/https://doi.org/10.1016/0021-9169(93)90025-T, http://www.sciencedirect.com/science/article/pii/002191699390025T, 1993.

Portnyagin, Y. I., Solovjova, T. V., Makarov, N. A., Merzlyakov, E. G., Manson, A. H., Meek, C. E., Hocking, W., Mitchell, N., Pancheva, D., Hoffmann, P., Singer, W., Murayama, Y., Igarashi, K., Forbes, J. M., Palo, S., Hall, C., and Nozawa, S.: Monthly mean climatology of the prevailing winds and tides in the Arctic mesosphere/lower thermosphere, Annales Geophysicae, 22, 3395–3410, https://doi.org/10.5194/angeo-22-3395-2004, https://www.ann-geophys.net/22/3395/2004/, 2004.

Rüfenacht, R., Baumgarten, G., Hildebrand, J., Schranz, F., Matthias, V., Stober, G., Lübken, F.-J., and Kämpfer, N.: Intercomparison of middle-atmospheric wind in observations and models, Atmospheric Measurement Techniques, 11, 1971–1987, https://doi.org/10.5194/amt-11-1971-2018, https://www.atmos-meas-tech.net/11/1971/2018/, 2018.

Sandford, D. J., Muller, H. G., and Mitchell, N. J.: Observations of lunar tides in the mesosphere and lower thermosphere at Arctic and middle latitudes, Atmospheric Chemistry and Physics, 6, 4117–4127, https://doi.org/10.5194/acp-6-4117-2006, https://www.atmos-chem-phys.net/6/4117/2006/, 2006.

Scargle, J. D.: Studies in astronomical time series analysis. II - Statistical aspects of spectral analysis of unevenly spaced data, Astrophysical Journal, 263, 835–853, 1982.

Schranz, F., Hagen, J., Stober, G., Hocke, K., Murk, A., and Kämpfer, N.: Small-scale variability of stratospheric ozone during the SSW 2018/2019 observed at Ny-Ålesund, Svalbard, Atmospheric Chemistry and Physics Discussions, 2019, 1–25, https://doi.org/10.5194/acp-2019-1093, https://www.atmos-chem-phys-discuss.net/acp-2019-1093/, 2019.

Schwartz, M., Lambert, A., Manney, G., Read, W., Livesey, N., Froidevaux, L., Ao, C., Bernath, P., Boone, C., Cofield, R., Daffer, W., Drouin, B., Fetzer, E., Fuller, R., Jarnot, R., Jiang, J., Jiang, Y., Knosp, B. W., Krüger, K., Li, J.-L., Mlynczak, M., Pawson, S., Russell, J., Santee, M., Snyder, W., Stek, P., Thurstans, R., Tompkins, A., Wagner, P., Walker, K., Waters, J. W., and Wu, D. L.: Validation of the Aura Microwave Limb Sounder temperature and geopotential height measurements, Journal of Geophysical Research: Atmospheres, 113, https://doi.org/10.1029/2007JD008783, http://dx.doi.org/10.1029/2007JD008783, d15S11, 2008.

Shibuya, R., Sato, K., Tsutsumi, M., Sato, T., Tomikawa, Y., Nishimura, K., and Kohma, M.: Quasi-12 h inertia–gravity waves in the lower mesosphere observed by the PANSY radar at Syowa Station (39.6° E, 69.0° S), Atmospheric Chemistry and Physics, 17, 6455–6476, https://doi.org/10.5194/acp-17-6455-2017, https://www.atmos-chem-phys.net/17/6455/2017/, 2017.

Siddiqui, T. A., Yamazaki, Y., Stolle, C., Lühr, H., Matzka, J., Maute, A., and Pedatella, N.: Dependence of Lunar Tide of the Equatorial Electrojet on the Wintertime Polar Vortex, Solar Flux, and QBO, Geophysical Research Letters, 45, 3801–3810, https://doi.org/10.1029/2018GL077510, https://agupubs.onlinelibrary.wiley.com/doi/abs/10.1029/2018GL077510, 2018.

Smith, A. K.: Global Dynamics of the MLT, Surveys in Geophysics, 33, 1177–1230, https://doi.org/10.1007/s10712-012-9196-9, https://doi.org/10.1007/s10712-012-9196-9, 2012.

Stober, G., Latteck, R., Rapp, M., Singer, W., and Zecha, M.: MAARSY - the new MST radar on Andøya: first results of spaced antenna and Doppler measurements of atmospheric winds in the troposphere and mesosphere using a partial array, Advances in Radio Science, 10, 291–298, https://doi.org/10.5194/ars-10-291-2012, http://www.adv-radio-sci.net/10/291/2012/, 2012.

Stober, G., Matthias, V., Jacobi, C., Wilhelm, S., Höffner, J., and Chau, J. L.: Exceptionally strong summer-like zonal wind reversal in the upper mesosphere during winter 2015/16, Annales Geophysicae, 35, 711–720, https://doi.org/10.5194/angeo-35-711-2017, https://www.ann-geophys.net/35/711/2017/, 2017.

Stober, G., Chau, J. L., Vierinen, J., Jacobi, C., and Wilhelm, S.: Retrieving horizontally resolved wind fields using multi-static meteor radar observations, Atmospheric Measurement Techniques, 11, 4891–4907, https://doi.org/10.5194/amt-11-4891-2018, https://www.atmos-meas-tech.net/11/4891/2018/, 2018.

Stockwell, R. G., Mansinha, L., and Lowe, R. P.: Localization of the complex spectrum: the S transform, IEEE Transactions on Signal Processing, 44, 998–1001, https://doi.org/10.1109/78.492555, 1996.

Stray, N. H., Orsolini, Y. J., Espy, P. J., Limpasuvan, V., and Hibbins, R. E.: Observations of planetary waves in the mesosphere-lower thermosphere during stratospheric warming events, Atmospheric Chemistry and Physics, 15, 4997–5005, https://doi.org/10.5194/acp-15-4997-2015, https://www.atmos-chem-phys.net/15/4997/2015/, 2015.

Torrence, C. and Compo, G. P.: A Practical Guide to Wavelet Analysis, Bull. Amer. Meteor. Soc., 79, 61–78, 1998.

Vial, F., Forbes, J. M., and Miyahara, S.: Some transient aspects of tidal propagation, Journal of Geophysical Research: Space Physics, 96, 1215–1224, https://doi.org/10.1029/90JA02181, https://agupubs.onlinelibrary.wiley.com/doi/abs/10.1029/90JA02181, 1991.

von Zahn, U. and Höffner, J.: Mesopause temperature profiling by potassium lidar, Geophysical Research Letters, 23, 141–144, https://doi.org/10.1029/95GL03688, https://agupubs.onlinelibrary.wiley.com/doi/abs/10.1029/95GL03688, 1996.

Wang, H., Boyd, J. P., and Akmaev, R. A.: On computation of Hough functions, Geoscientific Model Development, 9, 1477–1488, https://doi.org/10.5194/gmd-9-1477-2016, https://www.geosci-model-dev.net/9/1477/2016/, 2016.

Ward, W. E., Oberheide, J., Goncharenko, L. P., Nakamura, T., Hoffmann, P., Singer, W., Chang, L. C., Du, J., Wang, D.-Y., Batista, P., Clemesha, B., Manson, A. H., Riggin, D. M., She, C.-Y., Tsuda, T., and Yuan, T.: On the consistency of model, ground-based, and satellite observations of tidal signatures: Initial results from the CAWSES tidal campaigns, Journal of Geophysical Research: Atmospheres, 115, https://doi.org/10.1029/2009JD012593, https://agupubs.onlinelibrary.wiley.com/doi/abs/10.1029/2009JD012593, 2010.

Wilhelm, S., Stober, G., and Chau, J. L.: A comparison of 11-year mesospheric and lower thermospheric winds determined by meteor and MF radar at 69° N, Annales Geophysicae, 35, 893–906, https://doi.org/10.5194/angeo-35-893-2017, https://www.ann-geophys.net/35/893/2017/, 2017.

Wilhelm, S., Stober, G., and Brown, P.: Climatologies and long-term changes in mesospheric wind and wave measurements based on radar observations at high and mid latitudes, Annales Geophysicae, 37, 851–875, https://doi.org/10.5194/angeo-37-851-2019, https://www.ann-geophys.net/37/851/2019/, 2019.

Xu, F. and San Liang, X.: On the Generation and Maintenance of the 2012/13 Sudden Stratospheric Warming, Journal of the Atmospheric Sciences, 74, 3209–3228, https://doi.org/10.1175/JAS-D-17-0002.1, https://doi.org/10.1175/JAS-D-17-0002.1, 2017.

Xu, J., She, C. Y., Yuan, W., Mertens, C., Mlynczak, M., and Russell, J.: Comparison between the temperature measurements by TIMED/SABER and lidar in the midlatitude, Journal of Geophysical Research: Space Physics (1978–2012), 111, https://doi.org/10.1029/2005JA011439, https://doi.org/10.1029/2005JA011439, 2006.

Yu, Y., Wan, W., Ning, B., Liu, L., Wang, Z., Hu, L., and Ren, Z.: Tidal wind mapping from observations of a meteor radar chain in December 2011, Journal of Geophysical Research: Space Physics, 118, 2321–2332, https://doi.org/10.1029/2012JA017976, https://agupubs.onlinelibrary.wiley.com/doi/abs/10.1029/2012JA017976, 2013.

Zhang, X. and Forbes, J. M.: Lunar tide in the thermosphere and weakening of the northern polar vortex, Geophysical Research Letters, 41, 8201–8207, https://doi.org/10.1002/2014GL062103, https://agupubs.onlinelibrary.wiley.com/doi/abs/10.1002/2014GL062103, 2014.

Zhang, X., Forbes, J. M., Hagan, M. E., Russell III, J. M., Palo, S. E., Mertens, C. J., and Mlynczak, M. G.: Monthly tidal temperatures 20–120 km from TIMED/SABER, Journal of Geophysical Research: Space Physics, 111, https://doi.org/10.1029/2005JA011504, https://agupubs.onlinelibrary.wiley.com/doi/abs/10.1029/2005JA011504, 2006.

Zülicke, C., Becker, E., Matthias, V., Peters, D. H. W., Schmidt, H., Liu, H.-L., Ramos, L. d. l. T., and Mitchell, D. M.: Coupling of Stratospheric Warmings with Mesospheric Coolings in Observations and Simulations, Journal of Climate, 31, 1107–1133, https://doi.org/10.1175/JCLI-D-17-0047.1, https://doi.org/10.1175/JCLI-D-17-0047.1, 2018.